THE VARIABILITY IN THE FLUXES AND VIABILITY OF MICROBES LIBERATED IN SUPRAGLACIAL STREAM RUNOFF

Jennifer Laura McGowan

160021833

Department of Geography and Earth Sciences

The Institute of Biological, Environmental and Rural Sciences

Aberystwyth University

Thesis submitted for the degree of Master of Philosophy (F9352S)

30th March 2022

DECLARATION AND STATEMENTS

Word count of thesis:	46,984 (excluding references and appendices)
DECLARATION: This work has not previously been accepted in substance for any degree and is not being concurrently submitted in candidature for any degree.	
Candidate name:	Jennifer Laura McGowan
Signature:	
Date:	30 / 03 / 2022

STATEMENT 1

This thesis is the result of my own investigations, except where otherwise stated. Where *__correction services__ have been used, the extent and nature of the correction is clearly marked in a footnote(s).

Other sources are acknowledged by footnotes giving explicit references. A bibliography is appended.

Signature:	
Date:	30 / 03 / 2022

[*this refers to the extent to which the text has been corrected by others]

STATEMENT 2

I hereby give consent for my thesis, if accepted, to be available for photocopying and for inter-library loan, and for the title and summary to be made available to outside organisations.

Signature:	
Date:	30 / 03 / 2022

ABSTRACT

Supraglacial ecosystems harbour diverse microbial communities. However, the reaction of such microbes to evident climatic global warming and longer summer ablation is still unconstrained. Assessments of microbial fluxes through supraglacial streams, with such microbes ultimately liberated from the ice surface by melt, are sparce. Here, the microbial abundance found on the surface of Storglaciären, Sweden, and within supraglacial streams on Fountain Glacier, Canadian Arctic and the high-Arctic glaciers of Midtre Lovénbreen and Foxfonna, Svalbard, were quantified. Using flow cytometric protocols, mean microbe abundances were found between 1.47 to 10.78 × 10^4 cells mL^{-1} for different ice types on Storglaciären, with superimposed ice harbouring the highest mean microbial abundance. Supraglacial streams on Fountain and Foxfonna Glacier revealed estimated mean microbial fluxes of 5.46 × 10^{11} cells h^{-1} and 4.81 × 10^{12} cells h^{-1}, respectively. The mechanism for superimposed ice formation and melt presents a likely process for cell liberation at the glacier surface, but with the environmental variables of short-wave incident solar radiation, melt, discharge and EC, found to significantly associate with microbial abundances found within supraglacial streams. Here, the first viability determination of cells within supraglacial stream samples has been carried out using the dual-staining combination of PI and TO. An estimated 54.65 % of the cells exported through the Foxfonna supraglacial stream per hour were revealed as 'live', holding the potential to interact with the eco-hydrology of glacier-fed environments. However, unexpected shifts in TO fluorescence in the presence of glutaraldehyde necessitate further exploration into viability staining of supraglacial samples.

AKNOWLEDGEMENTS

Throughout the course of my MPhil, I have been fortunate to receive guidance, expertise and support from many people during my time as an MPhil research student. Such an experience as this has motivated me to achieve my full potential throughout my research degree, and going forward with my future research career.

Firstly, I would like to extend my thanks to my supervisor Dr Tristram Irvine-Fynn who also supervised my Undergraduate dissertation, and has helped me to become a well-rounded, independent and confident researcher. Thanks also go to Dr Arwyn Edwards for his support with my MPhil as my second supervisor, and in the editing of my first academic paper alongside Tris. Also, thanks are owed to Dr Andy Mitchell for stepping in and offering his support with my MPhil project. It has been pivotal to have had Tris, Arwyn and Andy's support throughout the outbreak of the COVID-19 pandemic which took place during the depths of my MPhil degree; an uncertain time that presented challenges for myself as a research student and personally. The additional adaptation, flexibility and development to my project as a result of these unprecedented times was achieved with the guidance of my supervisors. I am also incredibly grateful for the support received from Dr Ian Saunders during my time in the C66 laboratory carrying out my sample analyses and maintenance of the BD Accuri C6 Plus flow cytometer. Furthermore, I have a great appreciation for the knowledge and support received by Professor Hazel Davey in all manner of cell viability and flow cytometry; her time taken to offer me useful guidance has been valuable. I appreciate the timely and clear advice from team members Elena, Maritza, Nicholas, and Rose from BD Technical Support during the final year of my MPhil, their guidance and help on the Accuri C6 Plus flow cytometer has been paramount. Special thanks are also owed to Dr Ian Stevens who has been invaluable, patient and clear when answering my many, many random email queries regarding flow cytometry. I would like to thank fellow research students, and my dear friends, Eleanor Furness and Sarah Easter who have shared their wisdom and support with me right from the outset of my MPhil, and helped me with my transition from Undergraduate to Postgraduate Research.

As a result of the COVID-19 pandemic, opportunities for fieldwork during this project were curtailed. However, a large amount of archived field samples and hydrometeorological data previously collected from different glacier locations, were supplied to me for processing for my MPhil thesis and FCM analyses. Therefore, thanks are owed to Tristram Irvine-Fynn, Stephen Jennings, Arwyn Edwards and Ottavia Cavelli, supported by EU FP7 InterAct grant awarded to Tris and Arwyn, for the Storglaciären sample collection. Additionally, for the Fountain Glacier sample collection, appreciation goes to Tris and Brian Moorman, supported by the NERC project awarded to Tris and NSERC, and PCSP funding to Brian. For Midtre Lovénbreen, Tris, Jon Telling and Jon Hawkins, supported by the NERC project awarded to Andy Hodson and Alex Anesio; and finally, for Foxfonna Glacier, thanks are owed to Tris

and Arwyn, supported by Andy Hodson and UNIS. Also, it is important to express my thanks to Arwyn and Dr Jarishma Gokul for providing me with glacial *Janthinobacterium* sp. (JG1) which they isolated from alpine cryoconite, thus allowing me to use the dual-staining protocol on this glacial isolate in the first instance and so create my live, dead, and injured gates in FCM for my viability determination on the archived Midtre Lovénbreen and Foxfonna field samples.

I have become a very independent and resilient research student throughout the course of my MPhil with the many challenges I have faced, and I couldn't have done it without the help of my consistent support bubble. Therefore, I would like to whole heartedly thank my friends and family for their continued support, love and reassurance. In particular, I wish to thank my Mum and sister Hannah who are constant rocks and best friends in my life, and have provided me with nothing but encouragement and support throughout my lifetime and my degrees. My Mum has inspired me to achieve my best for me, and to never have any limiting beliefs despite what obstacles may be thrown my way.

TABLE OF CONTENTS

LIST OF FIGURES

LIST OF TABLES

1 INTRODUCTION

1.1 Context

With continued global climatic warming, many mountain glaciers worldwide are expected to recede and disappear by 2100, regardless of the emission scenario (IPCC, 2019). It is forecast that between 2015-2100, projected ice mass losses from polar regions will be 9-23 % for conservative (RCP 2.6) and 22-44 % for severe (RCP 8.5) climate warming scenarios (IPCC, 2019). From mountain glacier regions, ice mass loss is projected to be 22-44 % for RCP 2.6 and 37-57 % for RCP 8.5 (IPCC, 2019). Rapidly shrinking glaciers will impact on meltwater runoff and downstream ecosystems including glacier forefields, freshwater proglacial streams, and ultimately the oceans. Glacial melt alters the hydrological regimes, sediment and contaminant fluxes, biogeochemical processing, and biodiversity in downstream ecosystems; but also at a regional scale, the ecosystem services in which human populations consume such meltwater for their livelihoods (Milner et al., 2017). Melting glacier ice surfaces also present supraglacial habitats in which active microbes can colonize, survive and thrive (Hodson et al., 2008). Consequently, now more than ever in this present era of continued climate change, it is important to better understand and contribute to current knowledge of the eco-hydrology of declining valley and Arctic glaciers.

The melting glacier ice surface develops a weathering crust (Müller and Keeler, 1969), a shallow porous blanket of ice at the ice-atmosphere interface that is constrained by a thermal or hydrological limit, overlying impermeable glacier ice. The weathering crust is hydrologically active, but delays runoff by storing meltwater and creating a lag between meltwater and discharge into near-by supraglacial channels (Munro, 2011). However, the weathering crust has been referred to as a photic zone (Irvine-Fynn and Edwards, 2014), and an active ecosystem in its own right (Christner et al., 2018). Yet, observations have also suggested the inefficient transport of cells and particles through this supraglacial ecosystem, instead retaining them within its porous matrix (Irvine-Fynn et al., 2012). Consequently, questions remain over the flux of microbes in supraglacial streams and what this implies about the liberation of microbes from the weathering crust, with its apparent hydrological properties in the regulation of microbe delivery to supraglacial streams.

Microorganisms found on the surface of glaciers are cold-adapted, but other microbes can also arrive to the glacier ice surface from external sources too (Franzetti et al., 2017), and such microbes are able to carry out varying roles in the supraglacial ecosystem. Here, they carry out particular biogeochemical interactions and feedbacks within their physical and chemical environment, such as carbon and nutrient cycling (Anesio et al., 2017). Such active microbes found at the surface and/or in glacial ice masses are important to understand due to previously acknowledged viable, and even ancient, organisms being liberated in periods of thaw and so transported in meltwater on glacier ice surfaces, such as in the Arctic

environment, thus allowing such microbes to culture at distance (Dancer et al., 1997). Therefore, surface ablation liberates microbes, nutrients and associated biogeochemical products, releasing them to supraglacial channels that drain to downstream ecosystems. Viable, and even non-viable microbes, liberated from glacier surfaces hold the potential to influence the microbial ecology of downstream aquatic ecosystems (Hotaling et al., 2017), and their food webs, but the viability of microbes released from glacier surfaces and into downstream systems is unknown. However, microbial viability is a difficult physiological state to define and equally difficult to measure (Davey and Guyot, 2020). Cells can be at various stages of viability which makes it difficult to simply state cells as either 'live' or 'dead', but cytochemical analyses for viability determination is an approach which could provide a generalised estimate of the proportion of 'live/dead' cells found within environmental samples.

1.2 Research Aim and Objectives

Many studies have investigated supraglacial hydrology (e.g. Yang et al., 2018; Pitcher and Smith, 2019), but only a few studies have intrinsically investigated the biogeochemical and eco-hydrological characteristics of supraglacial streams (Scott et al., 2010; Irvine-Fynn et al., 2012; Foreman et al., 2013). Therefore, further investigation is necessary into the fluxes and viability of supraglacial microbes transported from glacier surfaces and into downstream ecosystems. Understanding these aspects of eco-hydrology will help future research predict microbe fluxes, and the variations thereof, from declining mountain and Arctic glaciers, thus serving to improve predictions of how connected ecosystems may respond to the decline of glaciers in climatic global warming, as well as the potential controlling factors of microbe fluxes and viability. Therefore, the research aim for this investigation is to assess the variability in the abundance of microbes liberated in supraglacial stream fluxes, and their viability status, using previously archived meltwater samples drawn from four Arctic valley glacier environments.

The statements hypothesised below will be investigated and such findings used to either support or reject the below statements in the context of this study's stated research aim:

1) Optimising a flow cytometric standard operating procedure (SOP) will improve the reliability in microbial enumerations of previously archived supraglacial meltwater samples from Storglaciären, Sweden; Midtre Lovénbreen and Foxfonna Glacier, Svalbard, and Fountain Glacier, Canada.
2) Flow cytometry (FCM) can be used to reliably assess the viability of cells within non-fixed supraglacial samples using the LIVE/DEAD BD Cell Viability dual-staining kit, thus allowing for a determination of the proportion of expected live and dead cells.
3) Statistically significant associations will be present for microbe abundance and viability status against key hydrometeorological conditions, such as melt.

1.3 Thesis Structure

This research thesis is presented in eight chapters with Chapter 2 presenting an insight into the background literature surrounding the research topic in question. Chapter 3 then outlines the steps taken for flow cytometric SOP refinement and the staining protocols used for this thesis investigation, with such protocols then applied for the enumeration of microbes in Chapters 4 and 5, and for viability determination in Chapter 6. Chapter 4 explores the microbe abundance within various ice type samples from the weathering crust of Storglaciären, with a discussion of the results. Chapter 5 explores the microbe abundances in supraglacial stream runoff from Fountain Glacier, Canada, and Foxfonna Glacier and Midtre Lovénbreen, Svalbard, with a discussion of the results here. Chapter 6 is an exploratory chapter presenting a brief review on the definition of viability in microbes and the different viability staining approaches available, but then progresses on to assess the results of viability determination carried out on supraglacial microbes from Midtre Lovénbreen and Foxfonna Glacier. Finally, Chapter 7 synthesises and concludes the key findings of this research thesis from Chapters 3 to 6, and presents potential directions for future research.

2 REVIEW OF SUPRAGLACIAL HYDROLOGY AND MICROBIOLOGY

2.1 Introduction

The supraglacial ecosystem, which includes the near-surface components of the weathering crust and supraglacial channels, is assured to expand in extent as the global temperature continues to rise (Christner et al., 2018), as well as during summer in which the seasonal snowpack is eliminated over glacier ablation areas. The exposed glacier ice surface melts and results in the increased presence of hydrological networks, and this suite of supraglacial channels and rills may transport a wealth of impurities from dusts to microbes to downstream ecosystems. Surface meltwater runoff may enter the supraglacial channel networks directly, however glacial meltwater also flows through the porous near-surface ice that is known as the weathering crust (Müller and Keeler, 1969; Stevens et al., 2020) and with it, the microbial cells, nutrients and other particles, regulated and liberated from this ice medium (Irvine-Fynn et al., 2012). Quantifying and understanding microbe fluxes in supraglacial channels that are inevitably transported to downstream freshwater, terrestrial, and/or marine ecosystems, is important, especially in the wider context of biodiversity change as a result of glacier recession, and how glacially discharged microbes impact on the biogeochemical nature of downstream ecosystems (Cauvy-Fraunié and Dangles, 2019). However, it is also important to consider not only the impact on downstream glacier-adjacent ecosystems to microbial fluxes released with glacial meltwater and recession, but also the impact microbe fluxes and their activity will have within the supraglacial ecosystem itself in response to glacier recession with climate warming (Stibal et al., 2020). This chapter provides a detailed overview of the supraglacial ecosystem including the thermal and melt regimes of glaciers, and the supraglacial hydrology and associated microbiology of these cryospheric systems.

2.2 Glaciers and their Thermal Regime

Glaciers form in cold locations where precipitated snow accumulates and becomes compact over time, but such an ice mass is then consequently lost due to summer season ablation. However, it is the net long-term heat energy balance which influences a glacier's thermal regime (Irvine-Fynn et al., 2011). Thermal regimes can be complicated by glacier dynamics and motion, as well as their environmental setting (Wilson et al., 2013) such as latitude, altitude, topography and local climate. Equally the thermal regimes of glaciers significantly influence the hydrological configuration of such ice masses (Irvine-Fynn et al., 2011). Glaciers can be classified as cold-based, temperate or polythermal; however thermal regime can vary in space and time in response to medium- to longer-term changes in ice geometry and climate. Climatically sensitive valley glaciers are an example of polythermal ice masses and can be found in various regions worldwide, such as the European Alps and the Arctic. Subsequently, such valley glaciers have experienced rapid net surface mass losses between 1960 and 2010, with accelerations in surface mass balance loss occurring often after the year 2000 (Van den Broeke and Giesen, 2021).

A combination of internal and external factors control the heat energy balance of a glacier and affect the conduction, advection and latent heat transfers of that particular glacier system, resulting in the various thermal regimes (Paterson, 1994; Irvine-Fynn et al., 2011). At the glacier surface, external penetrating radiative and turbulent energy fluxes are present, but internally at the ice-bedrock interface, friction from basal sliding occurs and the presence of geothermal heat from the native bedrock, as well as the latent heat released during the refreezing of meltwater and interstitial meltwater flow likewise transferring heat within a glacier mass (Paterson, 1994). Where there is more heat energy on or in a glacier mass, temperate ice is apparent and has been described as a heat-conducting mixture of water and ice, that is at the local pressure melting point of pure ice (Figure 2.1a) (Pettersson and Jansson, 2004). However, cold-based glaciers (Figure 2.1b) which are found to be below the pressure melting point, exhibit negligible water content within interstitial spaces (Irvine-Fynn et al., 2011). Comparatively, glaciers of a polythermal regime (Figure 2.1c to i) occur where a mixture of temperate and cold ice co-exists; separated by the cold-temperate transition surface (CTS) where interstitial water content changes from zero (cold ice), to a positive (temperate ice) value (Blatter and Hutter, 1991). However, despite the array of thermal regimes, most if not all glaciers exhibit a shallow transient temperate surface in the ablation zone which is subject to seasonal changes.

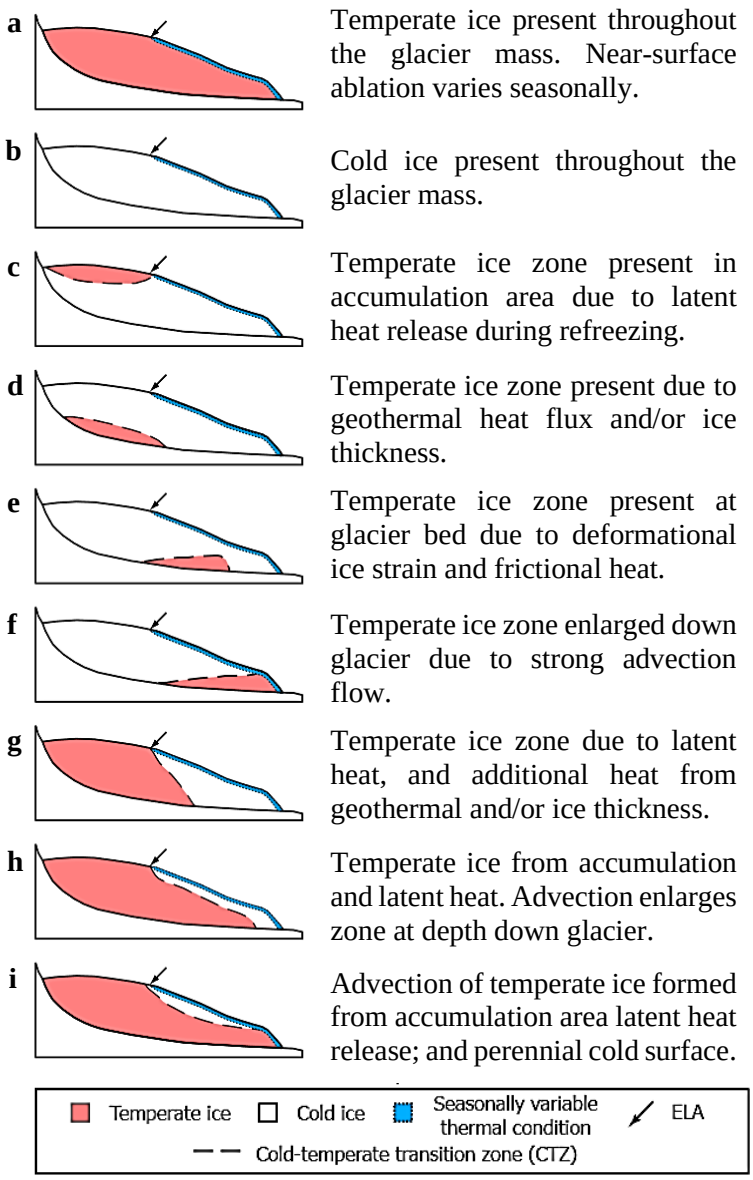

Figure 2.1. Illustration of the various glacier thermal regime scenarios. Schematics taken and descriptions adapted from Irvine-Fynn et al. (2011): **(a)** temperate glacier; **(b)** cold-based glacier; **(c-i)** polythermal glaciers with varying CTS location.

During winter a cold wave approaches which penetrates down from the surface of the glacier and results in an ice surface which is below the pressure melting point, but conversely remains at the pressure melting point during spring and summer seasons (Paterson, 1994; Irvine-Fynn et al., 2011). Despite the presence of snow on the surface of a glacier, cold wave penetration can still occur which over the long-term, affects the thermal regime of glaciers. However, lower elevation glaciers experience seasonal snow removal by melting thus resulting in this subsequent transient temperate thermal surface. Previous studies by Sobota (2009) have measured the temperature of this transient surface, such as on Waldemarbreen- a high-latitude, polythermal glacier located in Svalbard, whereby the ice temperature 10 m from the surface remained at approximately -2.5 °C, fluctuating by less than 1 °C, compared to ice

1 m from the surface which fluctuated more sensitively between the temperatures of 0 °C (surface pressure melting point; summer months) and -8 °C (winter months). Additionally, some polythermal and temperate glaciers have been suggested as indistinguishable (Irvine-Fynn et al., 2011) as solely temperate glaciers are a rare phenomenon due to winter cold and decadal climate cycles, which result in cold zones being apparent in thermal regimes, even in Alpine glaciers. Therefore, spatial diversity of a glacier's thermal structure is common, particularly the comparison between the transient surface which occupies differing temperatures to that of the main glacier body. The transient thermal ice surface is dependent on the seasons and associated external meteorological factors, such as radiative thermal energy from the sun, turbulent energy fluxes, and in many places, positive air temperatures, which results in a hydraulically active glacier surface; a meltwater-rich environment that creates a perfect microbial habitat.

2.3 Supraglacial Hydrology Overview

2.3.1 Surface Energy Balance

Glacier ice provides a freshwater asset that accounts for approximately 70 % of the Earth's freshwater resources (Shiklomanov, 1998), but resulting energy balances at glacier surfaces controlled by meteorological conditions, decide on how much of this asset is lost as ice melt. Meltwater produced from snow has been reviewed in previous literature (e.g. DeWalle and Rango, 2008), but melt produced from the transient temperate surface in the ablation zone of exposed glacier ice will be of focus here. The energy balance at the glacier surface-atmosphere interface determines glacier melt, runoff and so the hydrology (Hock, 2005). The sum of all energy fluxes at the surface of a glacier (Equation 2.1) influences its energy balance, with the energy available for melt (Q_M) given as:

$$Q_M = (1 - \alpha)SWRG_{in} + LWR_{in} + LWRT_{in} + LWR_{out} + Q_S + Q_L + Q_P + Q_C \qquad \text{[Equation 2.1]}$$

For which α is ice surface albedo ($0 \leq \alpha \leq 1$); $SWRG_{in}$ is global short-wave radiation (includes direct solar radiation, diffuse sky radiation, and radiation reflected from the surrounding terrain); LWR_{in} is incoming long-wave sky radiation; $LWRT_{in}$ is incoming long-wave radiation from surrounding terrain; LWR_{out} is outgoing long-wave radiation; Q_S is sensible heat flux; Q_L is latent heat flux (Q_S and Q_L are denoted as the turbulent heat fluxes); Q_P is the heat flux from precipitation, and Q_C is the subsurface conductive heat energy flux needed to overcome the cold content (Hock, 2005). Here, the surplus energy known as the cold content is necessary in order to bring the surface ice to the pressure melting point temperature of 0 °C to allow surface ablation to occur (Hock, 2005). Furthermore, it is common for energy inputs to be reported as positive and outputs negative. During summer months, typically $SWRG_{in}$, LWR_{in} and Q_S increase resulting in ablation, and are collectively greater than the energy lost to or by the glacier in the form of LWR_{out}, Q_L and Q_C (Irvine-Fynn and Hubbard, 2017). Alternatively, the short-term surface energy balance, that of which is predominant in the summer months in Alpine and Arctic

settings, results in the elimination and so melt of any winter snow and exposes the glacier ice surface; it is therefore the surface energy balance that is able to dictate melt and the hydrology on the glacier surface.

When calculating surface energy balance models, a component that can often be overlooked is that of the cold content (Q_C). A zero-degree assumption when calculating ablation can be present in many models whereby temperatures of glacier surface ice are assumed to already be at the 0 °C pressure melting point. However, this is certainly not the case at night, or more critically on cold-based ice, high elevation, and polythermal glaciers with transient ice surfaces which are sensitive to their immediate external atmospheric temperatures. Such a zero-degree assumption results in modelled melt exceeding the observed ablation as the subsurface conductive heat flux energy has not been considered as a separate component which brings the glacier surface to the pressure melting point first (Pellicciotti et al., 2009), but is instead included by models as energy for melt. In reality, cold-based glaciers for example will lose more energy to the cold content in order to raise the surface temperature to 0 °C before being able to melt and so less energy into ablation itself. Therefore, the subsurface conductive heat energy flux, or cold content, is an important component to include in surface energy balance models when modelling melt and surface runoff, to avoid overestimation in melt.

Albedo varies on glaciers both spatially and temporally and so is a key parameter in the surface energy balance of a glacier and resulting meltwater production (Hock, 2005). High albedo can be seen where there is a reflection of a large fraction of incoming short-wave radiation, usually when fresh snow is present, meaning less energy is available for melt, compared to bare ice which reduces the albedo. Impurities such as anthropogenic black carbon, fine mineral, and biogenic dust particles, also reduce the albedo of ice surfaces (e.g. Goelles and Bøggild, 2017; Oerlemans et al., 2009), and even microbes. However, cloud cover can restrict such incoming energy fluxes available to the glacier surface. For example, clouds can limit incoming short-wave radiation in overcast conditions, whilst increasing incoming long-wave radiation, compared to more energy for melt provided in clear-sky conditions (Lund et al., 2017). However, clear-sky energy fluxes result in positive surface energy balances occurring on bare ice surfaces of glaciers and so the increased ablation of the surface, and subsequent formation of a porous ice surface matrix, thus increasing the meltwater production and associated development of complex hydrological channel systems.

2.3.2 Formation and Variation of Weathering Crusts

The near-surface of glacier ice masses presents an important hydrological, ecological and biogeochemical role in the supraglacial system, with the identity given as the weathering crust and has previously been recognised as an ecosystem in its own right (e.g. Christner et al., 2018). This porous ice develops on the glacier surface during periods of clear sky whereby solar radiative energy is at its highest

and able to penetrate the glacier surface, thus causing subsurface melt along ice crystal boundaries, enlargement of interstitial pores, subsequent ice crystal disaggregation and so the formation of a weathering crust (Müller and Keeler, 1969) (Figure 2.2). In contrast, during periods of overcast, high winds and rainfall (turbulent energy fluxes), the weathering crust depletes and is ablated away leaving the ice surface glazed and hard (Müller and Keeler, 1969), and so ice of a greater density. The weathering crust itself is less dense and more porous as it has greater intergranular pore space, compared to glacier ice at depth which has a greater bulk ice density. However, during conditions were air temperatures fall and short-wave radiation receipt is reduced, a cold wave can propagate down through the weathering crust and so any interstitial meltwater present in this near-surface ice matrix loses thermal energy to the atmospheric cold air and results in the refreezing of such meltwater. However, below this surface ice is a water table where the weathering crust here is highly saturated; with impermeable glacier ice at the base of this saturated weathering crust medium.

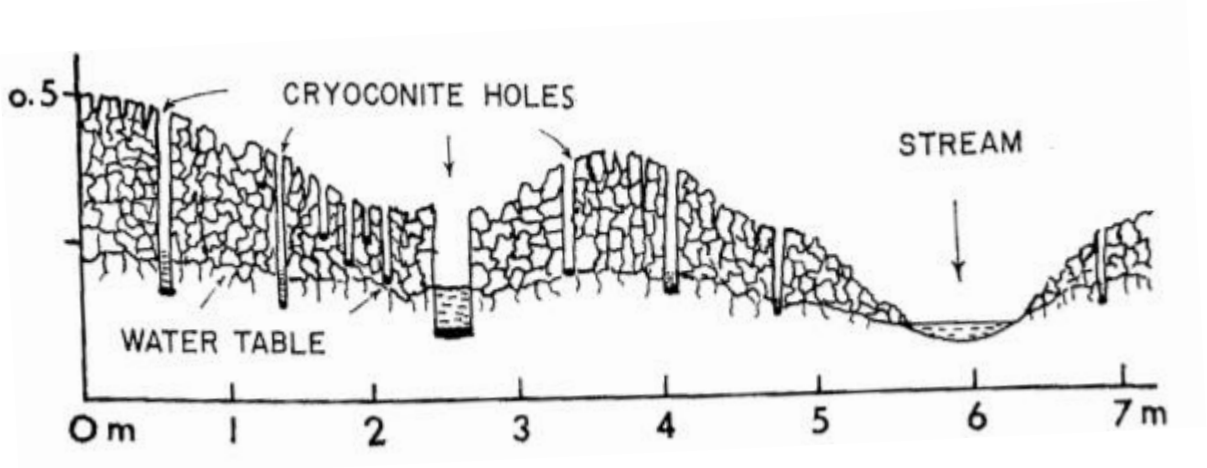

Figure 2.2. Schematic model of the weathering crust ice matrix on the surface of glaciers, but can vary in depth. Taken from Müller and Keeler (1969).

Darcy's Law has previously been applied to describe the permeability and flow of water through the weathering crust due to its porous medium properties (e.g. Stevens, 2019); a law with an associated equation commonly used with respect to aquifers and reservoir rocks (Darcy, 1856). The flow rate (Q) within such a porous medium as the weathering crust (Equation 2.2) is given as:

$$Q = KiA \qquad \text{[Equation 2.2]}$$

For which K is the hydraulic conductivity of the porous medium, i is the hydraulic gradient, and A is the cross-sectional area of the media through which flow occurs. Previous work carried out by Stevens et al. (2018) on the hydraulic conductivity of the weathering crust, states that Darcy's Law can be applied to weathering crust hydrology as the flow through such a porous medium appears to be homogenous at the synoptic scale. However, progressive changes in the near-surface ice matrix are not uniform due to

such an ablating surface experiencing significant local variations in development as a result of small differences in the physical properties of the weathering crust (Müller and Keeler, 1969). Therefore, variations in the development and so depths of weathering crusts, and the associated hydraulic conductivity, is not uncommon, especially as a result of influences from diurnal and seasonal variability.

The weathering crusts of ice masses have been seen to vary in depth depending on geographical location, the local environmental setting of the glacier, and the morphological structure of the ice mass itself. Weathering crust formation and so development in depth, in middle and high latitude settings, can be influenced by solar geometry, the slope of the surface, and glacier orientation (Stevens et al., 2018). Diurnally, the weathering crust will vary, such as overnight when the ice matrix will drain resulting in reduced hydraulic conductivity due to limited meltwater input from the lack of solar irradiance, and refreeze in lower air temperatures. In the daylight hours however, short-wave radiation flux is dominant and resets and extends the depth of the weathering crust as a result of such subsurface melt. Seasonally, the weathering crust is apparent on ablating glacier ice surfaces during the summer melt season in which short-wave radiation receipt is at its highest as well as air temperatures, compared to the winter whereby the weathering crust can disappear in some cryospheric settings altogether. Essentially the weathering crust can be described as the transient thermal surface ice as described in Section 2.2. For example, Hoffman et al. (2014) explored modelling the near-surface ice densities on Antarctic Dry Valley glaciers and identified an annual cycle formation of weathering crust in the summer ablation season, but then a removal of this near-surface crust during the winter due to sublimation, with a duration of 10 months. Additionally, the weathering crust can be seen to range in thickness of centimetres, such as in central-western Svalbard, but the depth of the weathering crust rarely exceeds 1 m (Sobota, 2009; Irvine-Fynn et al., 2012).

Weathering crust formation depends on the optical properties of ice and short-wave incident radiation. Beer's Law can be applied here to explain how optically clear blue ice has the potential to extend solar radiation to greater depths in weathering crust formation, due to the exponential decay of solar irradiance with distance through ice (Oke, 1987; Cook et al., 2016a). High latitudes experience less short-wave incident radiation, but because long-wave radiation, sensible heat and latent heat are also less, the ice surface is ablated away slowly and so the weathering crust is more developed. Comparatively, lower latitudes experience more short-wave incident radiation and so it would be assumed that the weathering crust would therefore be deep, however because long-wave radiation, sensible heat and latent heat are also higher in such settings, the ice surface ablates more rapidly and so a weathering crust does not attain much depth. Clearly, blue glacier ice will allow a deeper penetration of short-wave incident radiation compared to other glacier surfaces types thus suggesting the potential for a weathering crust of greater depth. However, a study carried out by Christner et al. (2018) found that even for the temperate Matanuska Glacier, south-central Alaska, a weathering crust aquifer with a maximum depth of

approximately 2 m during the melt season was observed, thus showing how weathering crust depths can vary spatially and temporally. At synoptic and seasonal timescales, variations in the thickness and porosity of weathering crusts will likely result in spatial and temporal variability in the hydraulic permeability, conductivity, and storage potential of meltwater at the near-surface (Stevens et al., 2018). Therefore, such variability in weathering crusts is an important concept to understand as such a phenomena may influence the accuracy of predictive meltwater runoff modelling. This is increasingly important as the weathering crust has been described as having properties for potential storage of meltwater and presents a hydrologically inefficient, perched aquifer at the glacier surface (e.g. Irvine-Fynn et al., 2012; Stevens et al., 2018). Therefore, the weathering crust has an impact on the supraglacial hydrological system by mediating the meltwater that flows through its porous medium and on it as surface runoff (see Figure 2.3), thus influencing the supraglacial drainage and formation of hydrological channel networks on glacier surfaces.

Figure 2.3. Photo exemplifying the clean ice weathering crust environment of Midtre Lovénbreen, Svalbard. Surface complexity of this small scale topography is presented by the disaggregated glacier ice surface and so weathering crust, as opposed to a glossy, blue ice surface where the weathering crust has depleted. Linear channels are apparent on the glacier ice surface with the potential to funnel preferential meltwater down-glacier. Photo provided by T. Irvine-Fynn.

2.3.3 Supraglacial Drainage and Channel Formation

The volume of meltwater runoff produced by a glacier is a function of the surface area and ablation rate of that particular ice mass (Irvine-Fynn and Hubbard, 2017). Seasonal and diurnal changes in ablation rate and runoff are the result of increased instances of solar irradiance and air temperatures; the meteorological heat energy fluxes to the surface of glaciers causing positive energy balances. Supraglacial drainage systems become particularly visible during summer melt seasons when the ice surface hydrological networks consisting of river channels, streams, and rills develop and extend up-

glacier following the retreat of the transient snowline (Bingham et al., 2003). Supraglacial channel networks develop as a result of the persistent thermal energy of concentrated meltwater at the ice surface thus initiating downcutting and thermal incision (see Figure 2.4), which is also influenced by the topography of ice masses such as the slope and resulting meltwater flow down such gradients (Mantelli et al., 2015).

Figure 2.4. Example of a supraglacial stream on Fountain Glacier, Canadian Arctic. Photo provided by T. Irvine-Fynn.

Temperate latitude glaciers typically accommodate shallow supraglacial channel depths as the ablation rate of the ice surface and stream incision rates are equivalent, compared to colder climate glaciers which have stream incision rates that are typically an order of magnitude greater than ice surface ablation rates thus forming deeper channels characteristic of canyons (Irvine-Fynn and Hubbard, 2017). Cold-based glaciers occupy internal and surface ice temperatures below the pressure melting point of 0 °C and experience lower air temperatures, and so more energy is used as the cold content to raise the temperature of the ice surface, with less energy available for ice surface ablation. However, frictional heat is present in cold-based supraglacial streams between the ice and meltwater interface, and so results in the deeper incision of such channels into the glacier surface.

Differences between supraglacial rivers and streams have been characterised, but with both formations collectively acknowledged as channels as a generic term. Supraglacial rivers are main-stem networks, perennially occupied, are of a high-stream order, spatially distributed, and run parallel to the direction of ice flow, although have been seen to meander (Pitcher and Smith, 2019). In comparison, supraglacial streams are of a low-stream order, occupy shallower depths, annual in presence, and typically form tributary to the larger supraglacial rivers on the ice surface (Ewing, 1970; Smith et al., 2015; Pitcher and Smith, 2019). Supraglacial channels are activated during summer melt seasons as a result of thermal and frictional energy sources, and are found to terminate in moulins, crevasses, supraglacial meltwater lakes or ponds. However, as well as draining into englacial/subglacial systems, meltwater may also directly

be discharged to the proglacial aquatic environment, either freshwater or marine, thus making meltwater fluxes from supraglacial systems an important concept to understand, particularly when microbial cells and other impurities are present in such meltwaters.

2.4 Supraglacial Microbiology Overview

2.4.1 Microbial Habitats on Glacier Surfaces

Microbiota are able to thrive on the surface, within, or below glacier ice masses. The porous photic zone of glacier ice surfaces, provides plentiful supraglacial habitats for microbes to exist. It has been suggested that globally, excluding Antarctica, between 10^{21} and 10^{26} cells may occupy this zone, and that an estimated 3.15×10^{21} cells are delivered annually from glacier ice to downstream environments; including nutrient fluxes and macromolecules which may be important for locally deglaciating catchments, along with the associated biodiversity already found there (Irvine-Fynn and Edwards, 2014). Microbes can be dispersed to this photic zone on glacier surfaces in various ways including long-range aeolian transport from distal areas; by precipitation from the atmosphere, and short-range transport whereby microbes are recruited from ice-marginal environments and dusts from the surrounding terrain such as moraines, dirt cones, or the glacier forefields themselves, and blown onto the surface of glaciers (Franzetti et al., 2017). Microbes that have been sequestered within the body of a glacier can also re-emerge to the ice surface, along with anthropogenic compounds (Miner et al., 2021), as a result of ablation of internal ice layers. Microbial cells can actively colonize the glacier surfaces from passive dispersal by physical processes including the freezing of source waters where cells subsequently become concentrated, or the deposition of snow in which cells are also present and colonize (Boetius et al., 2015). Microbes can then be further distributed on the glacier surface as a result of meltwater production and runoff, but can be found in distinct supraglacial habitats such as in snowpack, cryoconite holes, supraglacial ponds, rills, supraglacial streams, and the near-surface weathering crust ice.

The surface of glaciers experience seasonal and residual snowpack which provide an important supply of microbes, nutrients, ions, and water which ultimately percolate and cascade through the glacial ecosystem. Worldwide snow on the surface of glaciers has been found to be abundant in microbes such as cyanobacteria and algae (Hodson et al., 2008), including eukaryotic Zygnematales and Chlamydomonadales which are said to dominate ice surfaces and snowpack, respectively (Anesio et al., 2017). The microbiota of snow have been compared to that found on bare ice surfaces of glaciers, a result of the transience of snow lines during summer melt seasons (Hodson et al., 2008). The transience of the equilibrium line altitude (ELA) snow lines and so an up-glacier extension of the supraglacial drainage network, presents an additional source of microbiota from snowmelt on the ablating ice surface and into nearby supraglacial streams in the summer season. Additionally, glacier surfaces equally provide supraglacial habitats for a diverse consortium of micro- and even macro-organisms. For example, ice worms are also commonly found on glacier ice surfaces where they vertically migrate to

the surface, and have been observed to provide a food source for the Gray-crowned Rosy Finch (Hotaling et al., 2020), thus further evidencing the ecological importance of glacier ice surfaces.

Cryoconite holes are examples of depressions found in ice mass surfaces which provide habitable hotspots for diverse microbiota (see Figure 2.5b). Cryoconite holes found in high latitude and high alpine environments develop as a result of aeolian debris, both biological and mineral dust, deposited in depressions on the bare ice surface (Cook et al., 2016b). Here, the dark sediment rich material, cryoconite (see Figure 2.5a), has a low albedo and so initiates melting down into the ice creating a meltwater hole within the ice surface that can further deepen; with ice lids covering the holes in high latitude conditions which can appear due to short-wave energy receipt and air temperatures being lower than in high Alpine settings (MacDonell and Fitzsimons, 2008). Cryoconite holes provide a great diversity of microorganisms and are particularly dominated by filamentous cyanobacteria (Cook et al., 2016b) but also viruses, algae, fungi, and even large tardigrades, rotifers, and nematodes (Hodson et al., 2008); such microbes use the cryoconite granules as their substrate. It is important to note that such cryoconite hole supraglacial hotspots for microbial diversity and activity, have the potential to be unstable and vulnerable to flushing by surface meltwater into nearby supraglacial channels (Hodson et al., 2008), and so sediment and microbial delivery is mediated and distributed further at the ice surface. Thus, microbial communities within such hole habitats can reset, especially during increased meltwater production. Furthermore, a substantial proportion of deposited particles on the surface of glaciers, such as cryoconite forming sediment, can be retained from season to season and so contribute to the thinning of glacier surfaces (Boetius et al., 2015). In terms of the sediment found in cryoconite holes themselves, such holes that are enclosed by ice lids in particular would contribute to the proportion of sediment retained on the ice surface as these holes would not be disturbed by meltwater runoff.

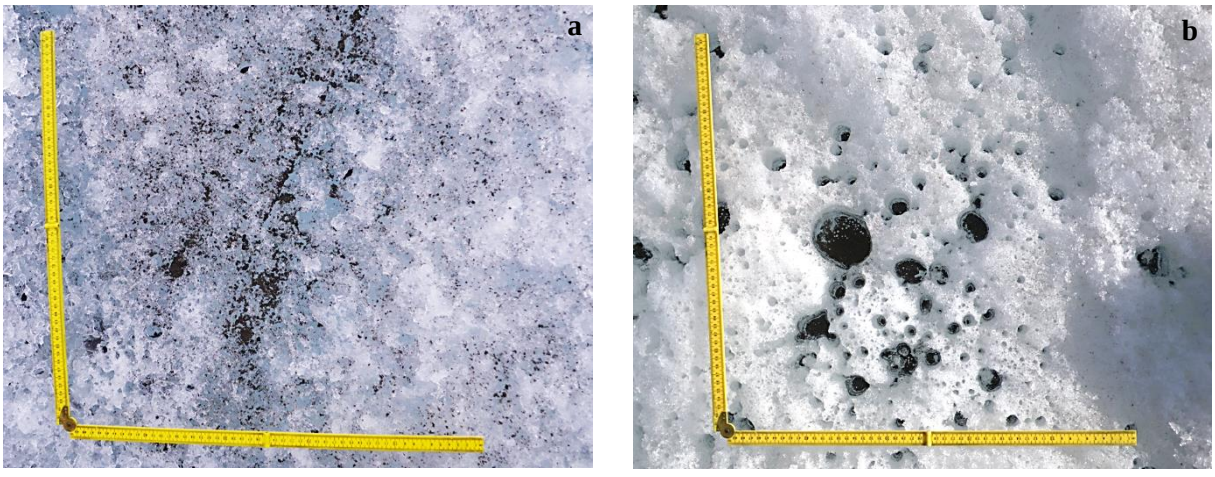

Figure 2.5. Example of the supraglacial environment on Midtre Lovénbreen, Svalbard, with the microbial habitats of cryoconite holes: **(a)** shows the distributed cryoconite material, and **(b)** shows thermally incised cryoconite holes. Photographs provided by T. Irvine-Fynn and present a 50 x 50 cm ruler scale.

Supraglacial streams further provide an aquatic microbial habitat at the glacier surface, as well as the rills creating small tributaries into such stream channels. Crucially, supraglacial streams with longer residence times and an abundance in fine substrate, have been found to experience measurable nitrification and uptake of dissolved organic carbon (DOC) showing the presence of active microbes in this aquatic supraglacial habitat (Scott et al., 2010). The Cotton Glacier of Antarctica also exemplifies a supraglacial stream system that has a microbial rich habitat (Foreman et al., 2013). Here, abundant concentrations of chlorophyll-*a* have been measured suggesting the assemblage of an autotrophic community, with additional counts in bacterial cells including rods, cocci, and filaments, as well as bacteriophages or virus-like particles, but no filamentous fungi or yeasts were found (Foreman et al., 2013). Therefore, it is clear that such cryospheric microorganisms actively occupy their own biogeochemical roles within supraglacial streams and other glacier surface habitats, and so contribute to an active supraglacial ecosystem as a whole.

2.4.2 Microbial Processes on Glacier Surfaces

The supraglacial ecosystem, comprising the near-surface weathering crust, streams, and cryoconite holes, harbour a diverse consortium of microbiota such as bacteria, algae, phytoflagellates, fungi, viruses, rotifers, diatoms, and tardigrades, and are active in carrying out important biogeochemical reactions (Hodson et al., 2008). Roles include the cycling of carbon and nutrients at glacier surfaces, such as the resident primary producers using autochthonous organic carbon and heterotrophs of allochthonous organic carbon (Stibal et al., 2012). Such supraglacial microorganisms carry out their biological activity on the surface of glaciers as they are able to withstand the stressful environmental conditions present here, including periodic freeze-thaw cycles, radiative fluxes, exposure to ultraviolet radiation, desiccation, temperature variations, and more. Microbes on glacier surfaces are also able to function in other ways and exploit mechanisms to survive in such extreme glacial environments, such as in biofilms. Particularly in the supraglacial habitat of cryoconite holes, biofilms formed by the bacterial production of extracellular polymetric substances (EPS) result in the subsequent accumulation of organic matter on the existing cryoconite minerals (Smith et al., 2016). Such a phenomenon is beneficial for the cryospheric microbiota themselves as microbe-substrate and microbe-microbe adhesions occur thus protecting the cells from meltwater erosion, as well as the promotion of enhanced nutrient storage and transfer between microbial community members (Smith et al., 2016). However, the role of such biofilms in the supraglacial ecosystem also results in the lowering of the surface albedo of glaciers due to further aggregation of microbes and organic matter within cryoconite sediment due to the production of EPS, and so additional darkening of glacier surfaces (Cook et al., 2016b).

Nutrient retention in a supraglacial stream on Mendenhall Glacier, south-eastern Alaska, USA, has previously been observed where nitrogen and phosphorous were able to be transported along the stream reach largely uninterrupted, but instead, soluble nitrate ions increased suggesting the presence of

resident nitrifying and heterotrophic bacterial cells (Scott et al., 2010). The roles played by heterotrophic bacteria such as Proteobacteria, which include Alpha- and Beta-Proteobacteria, Actinobacteria, and Bacteroidetes, on supraglacial ecosystems is to cycle nutrients from decaying organic matter (Anesio et al., 2017), which can then be broken down into DOC. However, glacier surfaces can also obtain DOC from a variety of sources which is subsequently biologically cycled, such as from: inorganic atmospheric carbon dioxide which is fixed by photoautotrophic microbes- usually occurs in algal blooms and within cryoconite granules, and so providing autochthonous organic carbon to the cryospheric system; allochthonous organic carbon sourced locally from adjacent deglaciated areas to ice surfaces, and lastly, allochthonous organic carbon, often of anthropogenic origin, sourced from distant locations and in the form of aeolian deposits (Stibal et al., 2012). Any organic matter and carbon provided to the ice surface is utilised by heterotrophic microorganisms as their carbon source allowing for metabolic respiration, which exemplifies why supraglacial ecosystems, particularly bare glacier ice surfaces, have been referred to as carbon sinks and sources (Stibal et al., 2012). Particularly, algae, and cyanobacteria in cryoconite holes, present photosynthetically active primary producers on the surface of glaciers with the role of sequestering inorganic carbon dioxide thus creating a carbon sink in cryospheric systems in this way. Heterotrophs are able to utilise the highly labile organic carbon produced by primary autotrophs, such as the photosynthetic bacteria, within 24 hours thus supporting the demands of bacterial growth (Smith et al., 2017). Phototrophically derived organic carbon is highly bioavailable for supraglacial stream microbial communities (Smith et al., 2017). Previous studies have also stated how glacial organic matter, and microbially-produced organic carbon, have a higher bioavailability than that of terrestrial ecosystems (e.g. Hood et al., 2009; Singer et al., 2012). Consequently, it is important to understand that when such active microbes and biogeochemical products are discharged in meltwater to downstream ecosystems, they have the potential to contribute to the carbon cycling in such terrestrial or marine terminating ecosystems. As Hood et al. (2009, p.1044) states, “glacial runoff is a quantitatively important source of labile reduced carbon to marine ecosystems”, but as glacial melt increases during summer ablation seasons and as a result of climatic global warming, such an input of readily available carbon may put downstream ecosystems into disequilibrium.

Surface ice albedo is reduced as a result of darkening of ice surfaces due to the deposition of light-absorbing impurities such as inorganic dust and black carbon (Tedstone et al., 2017), however glacier algae can also reduce ice surface albedo. Glacier algae on the surface of ice masses, and indeed in the snowpack, are important microorganisms to monitor due to their pigmentation and subsequent biological activity in forming algal blooms. The algae on the supraglacial ice surface produce pigments to shield their photosynthetic apparatus but in doing so reduce surface albedo, thus inducing more meltwater production through such biological darkening (Williamson et al., 2020), or bio-albedo. Algal blooms observed on polar and Alpine glacier surfaces are identified by their brown-grey colouration, but are often mistaken as dirt instead of the algae itself which do also encompass mineral debris and

anthropogenic black carbon deposits (Anesio et al., 2017). A previous study carried out on bare glacier surfaces in Svalbard, found the microalgae *Ancylonema nordenskiöldii* (Zygnematales, Streptophyta) blooming, and so a resulting brown colouration on the glacier surface (Remias et al., 2012). It was further observed that this brownish pigmentation enables *A. nordenskiöldii* to be well adapted to live on the glacier surface as it allows the algae to metabolically and cytologically live in temperatures close to freezing and in conditions were excessive irradiation is present (Remias et al., 2012). Similarly, a study carried out on ablating glacier bare-ice surfaces on Brøggerhalvøya, Svalbard, also found *A. nordenskiöldii*, as well as other diverse green algae such as *Chlamydomonas nivalis* which can be identified by their red pigmentation, usually found on snow surfaces, and also cyanobacteria (Takeuchi et al., 2019). Additionally, the Greenland Ice Sheet has also been found to harbour high glacier algal abundance whereby only ~1 to 2.4 % of the total incident solar energy is captured by the algae for photochemistry, compared to 48 to 65 % of the available irradiance which is not absorbed and instead contributes to ice surface melt (Williamson et al., 2020). This shows the limited irradiance that algal blooms actually use for photochemistry, and instead observe more solar energy being directed to surface melt, whilst the algae themselves also reduce ice surface albedo through their pigmentation and blooms, and further induce melt. However, ice algal communities are affected by the local, specific conditions of the glacier in question, such as the surface hydrology and glacier mineral loading, thus affecting the associated carbon cycling carried out by such microbes (Takeuchi et al., 2019). However, it is clear that the biological darkening of ice and snow is driven by the pigmentations and activity of glacier algae; and with climatic global warming, the meltwater and associated nutrient fluxes present which drive algal blooms increase, and so such blooms will subsequently increase in extent and duration resulting in the reduction of the surface albedo of snow and ice further, and consequently increasing meltwater rates (Anesio et al., 2017).

The role that microbial metabolic activity in glacial habitats may have on the heat budget of glaciers, is a phenomenon that has been touched upon in previous literature, but scarce in nature. However, what is stated is that metabolic heat from respiring microbes may present a source of energy with potential to induce glacier ice melt in supraglacial habitats (Hodson et al., 2008). For example, the heat from microbial metabolic processes may contribute to the thermodynamics of cryoconite holes, perhaps providing as much as 10 % of the heat energy which is used to melt such an icy habitat's walls during the summer season (e.g. McIntyre, 1984; Gerdel and Drouet, 1960). However, the metabolic activity of microbes, and the potential to induce melting in glacial habitats from such activity, needs more direct measurements and assessment, but emphasises how highly active microorganisms carrying out their various ecosystem roles at the supraglacial surface, could indirectly have an impact on the heat budget and associated mass balance of glaciers. If such measurements were to be obtained, and with confidence, a critical understanding might be found with regards to the rate and duration of metabolic activity present in glacial habitats which are near or at freezing point (Hodson et al., 2008).

2.5 Significance of the Supraglacial System

Annual glacier runoff for large-scale glacierized drainage basins has been modelled to 2100 and shows the continued increase in meltwater runoff until a 'peak water' is reached- the maximum meltwater runoff from a glacierized basin (Huss and Hock, 2018). However, after a 'peak water' has been reached, runoff will steadily decline as the glacier mass is being lost (Huss and Hock, 2018). Consequently, the mobilisation and transport of microbes in ice melt may fall if the glaciers are past their 'peak water', or may rise and then fall if the glaciers haven't yet reached their peak melt threshold. However, during increased meltwater runoff with rising snowlines and temporarily expanding supraglacial ablation areas, and so before this peak melt stage has been reached, the mobilisation of microbes and organic materials from glaciers will be increased. The significance of such supraglacial hydrology resulting from ice surface melt on glaciers, and the subsequent export of microbes to downstream ecosystems will be explored in Sections 2.5.1 and 2.5.2.

2.5.1 Hydrology

There is a hydrological assumption that the porous near-surface weathering crust ultimately feeds supraglacial channels with meltwater, however previous studies have stated that the weathering crust has a role in regulating meltwater discharge. A delay between peak melt and supraglacial stream discharge has been stated as typically within < 12 hours (Munro, 2011; Stevens et al., 2018), with findings from Stevens et al. (2018) implying that a meltwater parcel could even be retained within the weathering crust matrix for 34 hours, minimum. Therefore, it is clear that the weathering crust is hydraulically inefficient at draining meltwater, and so meltwater runoff models need to be considerate to this phenomenon in order to avoid overestimation in melt due to the weathering crusts' aquifer storing properties. Additionally, when assessing the hydrological significance of the weathering crust, it is also important to consider the presence of the water table within such an ice matrix which is perched above the impermeable glacier body below, and that of which has been found to affect the hydraulic conductivity. Hydraulic conductivity against water table height has been found to correlate positively meaning the higher the water table, the greater the hydraulic conductivity in the weathering crust and so flow of water through the saturated ice matrix (Stevens et al., 2018) (see Figure 2.6). However, at times when increased meltwater input exceeds the ability of the weathering crust to transport water, the water table of the weathering crust rises into the near-surface ice which becomes increasingly saturated raising the potential sheet flow on the ice surface (Stevens et al., 2018). Meltwater input which does not result in surface runoff and infiltrates the ice medium, increases the water table height but also positively influences the hydraulic conductivity of the saturated ice matrix, thus resulting in the overriding or displacement of old stored or retained meltwater, and associated microbes and particles present (Stevens et al., 2018).

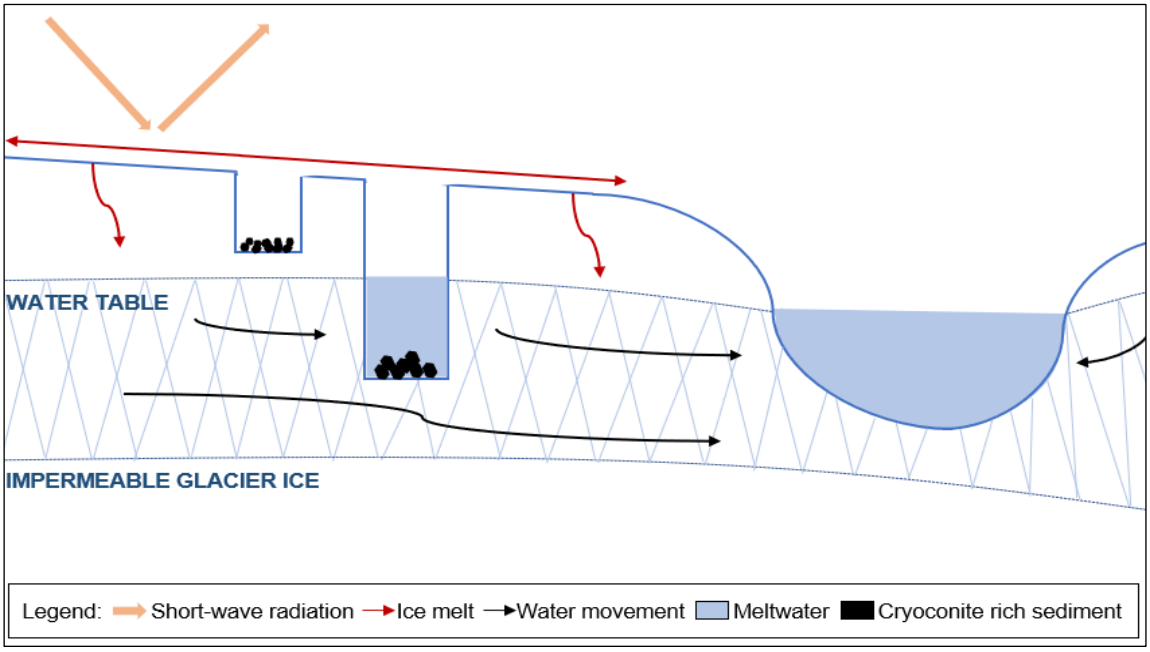

Figure 2.6. Conceptual model illustrating a cross-sectional schematic of the weathering crust ecosystem including a water table influencing the hydraulic conductivity of the glacial meltwater within the porous medium. Glacial meltwater runoff occurs at the ice surface, and through the weathering crust near-surface ecosystem and cryoconite hole habitats, ultimately entering near-by supraglacial channel networks. Figure not constructed to scale; adapted from Müller and Keeler (1969).

Additionally, on debris-covered glacier systems, such high sediment loads also likely influence the hydrology of supraglacial systems, as well as providing a supraglacial habitat for microorganisms. For example, the thickness of debris impacts on the melting below the ice surface, whereby thicker debris coverage found near the terminus of debris-covered glaciers actually lowers the melt rate compared to thinner debris coverage with higher melt rates (Fyffe et al., 2019; Fair et al., 2020); the ice below the thicker debris is insulated meaning less influence by short-wave radiation and so less melt.

2.5.2 Ecology

The porous supraglacial near-surface also has an important ecological significance for which many microorganisms have been found *in situ*. For example, boreholes cut into the weathering crust on the temperate Matanuska Glacier in Alaska found *in situ* microbial populations such as phototrophic taxa-cyanobacteria, and golden and green algae growing in the meltwater recharge percolating through the porous surface ice (Christner et al., 2018). Like with meltwater, the weathering crust ecosystem also has a role in regulating the mobilisation and retention of cells, and associated particles, before being discharged to nearby supraglacial channels. It has previously been recognised that three scenarios can be used to explain the regulation in the mobilisation and retention of cells within the weathering crust matrix, and so the consequent microbial interactions experienced there. A study carried out by Irvine-

Fynn et al. (2012) found that the microbial abundance transported over the observation period of 36 days by a supraglacial stream on Midtre Lovénbreen, Svalbard, was 37 % less than that of the number of cells sourced in the near-surface glacier ice alone, thus demonstrating storage of cells in the weathering crust, or even the destruction/death/lysis of cells. The properties of the weathering crust affects microbial mobilisation in the following ways: as a result of larger interstitial flow paths capturing and reducing water flow from elsewhere in the weathering crust at times when discharge has risen locally, meaning some areas of the weathering crust may experience a decrease in water transfer and associated cell entrainment; the weathering crust becomes waterlogged at times of increased melt meaning water transfer is directed away from preferential flow paths as a result of water pressures, resulting in a reduction in the discharge of cells to supraglacial water channels; and finally, the particles can themselves impede transport by becoming clogged in the interstitial pores (Mader et al., 2006) and flow paths thus reducing the numbers, geometries and so types of cells liberated from the weathering crust and discharged into supraglacial channel meltwaters (Irvine-Fynn et al., 2012). In this instance, an element of selective mobilisation could be proposed here due to the weathering crusts' filtering properties in which only certain particles may be mobilised and transported to supraglacial channels, such as the very small microbes of viruses which are more likely to be able to fit through such interstitial pore spaces. However, larger cells of the size >15 μm have been found to be present in supraglacial stream meltwater (see Stevens, 2019), and under the assumption that the weathering crust is ultimately a source of liberated cells to nearby supraglacial channels, then it can also be proposed that the weathering crust matrix does not act as a filter as previously suggested but instead must have pores large enough to allow for larger cells to be mobilised and transported through the ice matrix too. Additionally, a previous study has comparatively observed that the microbial abundance entrained in the glacier near-surface does in fact equal that of the microbial abundance enumerated in supraglacial streams (Stevens et al., 2020), thus further evidencing the complex nature of supraglacial hydrology and role of the weathering crust, and so the significance of such hydrological transport networks and dynamics in the potential influence on meltwater and microbe fluxes to downstream environments.

The presence of a hydraulic water pressure gradient within the near-surface porous ice matrix is also of important ecological, and hydrological, significance in the supraglacial system. Here, water moves upwards towards the ice surface due to a water pressure gradient (Lliboutry, 1996); water moves from a high to low pressure by capillary action. It could therefore be suggested that the weathering crust presents an eco-hydrological role in promoting the upward migration of cells in meltwater to the near-surface, driven by the water pressure gradient. As previously stated, microorganisms migrate upward to the surface of glaciers as a result of their habitats on the ice surface moving downward due to glacial flow (Takeuchi, 2011), and so the hydrological influence of the water pressure gradient may further enable the emergence of glacier microbes to the ice surface. Additionally, the melting of the surface

itself allows ice to emerge at the surface into the photic zone, and so too microbial cells present within such ice.

Particle storage and liberation within and from the weathering crust will have interannual variability, and it is suggested that particles such as cells and nutrients are delivered, modulated or flushed within and from the weathering crust as a result of sources of seasonal snowmelt and summer season precipitation (Irvine-Fynn et al., 2012). However, instances where microbes experience increased residence time in the porous near-surface due to retention properties here, allows the microbiota, particulates, dissolved nutrients, and viruses found within this near-surface ecosystem to interact and carry out various biogeochemical processes (Rassner et al., 2016). Crucially, viruses can present a strong control on bacterial productivity especially in this retained state (Rassner et al., 2016). When virus particles are eventually liberated in melt and enter supraglacial waters, they are very stable in such an environment and so are also likely to be viable when transported downstream (Rassner et al., 2016). This poses implications for downstream ecosystems however as the viruses may infect downstream resident bacteria, thus further evidencing the ecological significance of the supraglacial system. Additionally, it is apparent that glacier-fed river basins are likely to experience increased heterotrophic activity as a result of biogeochemical changes of Arctic and Alpine streams fuelled by increased glacier recession and associated increases in stream temperature (Milner et al., 2009). It has also been observed that viable bacterial cells can colonize and pioneer the soil development of newly deglaciated exposed soils in Alpine environments (Rime et al., 2016), and so discharged supraglacial microbes could hold the potential to influence the existing ecology of proglacial environments, the biogeochemical reactions, and the food webs already in a state of equilibrium there. However, the exact influences and contributions of supraglacial microbes to the ecology of proglacial environments is less well understood in the current literature.

2.5.3 Flow Cytometry Application to Supraglacial Ecology

Analytical techniques previously used in studies for the enumeration of microbial cells in glacial ice samples include epifluorescence microscopy (EFM), quantitative polymerase chain reaction (qPCR) and flow cytometry (FCM) (e.g. Stibal et al., 2015). However, limited studies have used FCM for quantifying microbes in supraglacial samples thus far (e.g. Irvine-Fynn et al., 2012), and it has previously been stated how FCM analyses present a snapshot of the quantity of microbial communities found within a particular glacial environment, but not a true reflection of the complex habitat and community dynamics that characterize such a cryospheric system (Irvine-Fynn and Edwards, 2014). However, FCM does provide a rapid, robust analytical choice for the enumeration and processing of microbes in glacial environmental samples (Irvine-Fynn and Edwards, 2014).

The key components of a flow cytometer to allow for the effective analysis of cell counts, their size, and internal complexities, are the fluidics system which facilitates the movement of the liquid sample into the flow cytometer, lasers and respective optics which gather scattered light, detectors to sense the light, and a computer system which presents the output data of such FCM analyses as different density plots and histograms. Once a sample has been placed under the flow cytometer SIP pin, the sample is sucked up into the machine where it is then mixed with the sheath fluid to encourage the cells within a sample through a core channel and into a resulting single file movement. Here, the individual cells are then passed through a laser beam and each cell analysed. The laser beam hitting each cell is detected by the flow cytometer as forward scatter (FSC) but also as side scatter (SSC) which is detected perpendicularly to the laser beam, with the FSC proportional to a cell's size and the SSC proportional to the internal complexities of a cell. The more forward scatter there is, the bigger the cell; similarly, the more side scatter there is, the more internal complexities a cell has. Cells may be autofluorescent and so the fluorescence (scattered light) they emit when hit by the laser beam is detected by the flow cytometer. Alternatively, cells may be stained with fluorophore dye(s) which become more excited by the correct wavelength of laser light once passed through the laser beam, thus emitting fluorescence as a result which is then detected by the flow cytometer. SYBR Gold is a common nucleic acid stain used in flow cytometry which binds to the DNA of biological particles, and has been used in various aquatic samples for the enumeration of bacteria and viruses (e.g. Shibata et al., 2006). Once attached to a cell's DNA, or RNA, the SYBR Gold is excited by a blue wavelength of laser light within a flow cytometer at 497 nm thus emitting a green fluorescence at 520 nm, and captured by the optics and detectors of the flow cytometer. Cells stained with SYBR Gold will fluoresce green and shift rightwards in fluorescence on an SSC against FITC (Fluorescein isothiocyanate) density plot, compared to unstained non-biological particles, such as debris.

2.6 Research Gaps and Study Direction

Glaciers are highly responsive to global climatic warming (Battin et al., 2004), with the supraglacial system being a portion of the glacial biome which is ready to expand in extent with such increases in temperature and resulting duration of ablation seasons (Christner et al., 2018). The supraglacial ecosystem presents many microbially active habitats, such as supraglacial channels, cryoconite holes and even in the surface ice itself known as the weathering crust. Here, it is known that cells can be stored within this ice matrix or discharged into nearby supraglacial streams. However, what is less well understood are the processes by which cells are actually liberated from the ice surface before being subsequently carried by surface melt into nearby supraglacial streams. As well as this, the relative contribution of microbes to receiving downstream proglacial environments needs further investigation. Furthermore, it is not known whether such microbes are alive or dead when discharged downstream, or indeed whether they are alive or dead in the first instance before even being liberated from the ice surface. Therefore, there is a need to better characterise microbe fluxes with the rapid decline of valley

and Arctic glaciers, and begin to explore methods to determine the viability of such supraglacial microbes due to their potential to impact downstream aquatic environments. As a result, the highlighted research gaps are as follows:

1) Fluxes of meltwater and microbes, with associated cellular carbon content, to and in supraglacial streams have not been well characterised.
2) Environmental controls have an uncertain role in dictating microbial liberation from the glacier ice surface and resulting subsequent microbe fluxes in supraglacial streams.
3) The viability status of microbes exported from glacier surfaces via supraglacial streams to downstream environments with the potential to contribute to such proglacial ecosystems, is poorly defined.

3 FLOW CYTOMETRIC STANDARD OPERATING PROCEDURE FOR SUPRAGLACIAL SAMPLES

3.1 Introduction

This thesis constrained microbial abundance across several high-Arctic glacier locations using FCM approaches in order to constrain the abundance of cells and associated size fractions found in ice types from Storglaciären, Sweden (Chapter 4); supraglacial streams from Fountain Glacier, Canadian Arctic, as well as from Midtre Lovénbreen and Foxfonna, Svalbard (Chapter 5). Finally, viability analyses of the non-fixed Midtre Lovénbreen and Foxfonna samples has also been determined through the use of the rapid analytical technique of FCM (Chapter 6). However, when conducting such a rapid analytical technique (see Section 2.5.3 for a description of how FCM works), it is important to understand that this approach requires a refinement of its SOP and subsequent experimental choices for any given sample set, in order for the instrument to detect cells efficiently and achieve accurate microbial abundances. This methodology chapter outlines the steps taken to refine such an FCM SOP and the subsequent staining protocols applied in the following analytical results chapters. Again, it is important to reiterate here that the sources of such previously archived samples have been mentioned in the Acknowledgements at the beginning of this thesis.

3.2 Materials and Methodology

3.2.1 Flow Cytometric Refinement

In order to ensure an optimum SOP for the analyses of previously archived supraglacial samples drawn from the above mentioned Arctic valley glacier environments, a series of refinement measures were carried out on the flow cytometer used in this investigation, and on the selected staining protocols. Refinements for the staining protocols used in this investigation were determined using individual 'sacrificial' samples for each sample set location as detailed later within this chapter. This allowed for an insight as to what adjustments- if any, were needed for the staining protocols in the first instance before thawing the rest of the sample set and commencing full staining analyses. Sacrificial samples enabled initial abundance gates to be estimated and constructed on density plots in the BD Accuri C6 Plus software (version 1.0.23.1). As the glacial environmental samples were of a dilute nature compared to clinical or cultured cell samples, no buffers were added in this study to any samples. Before each sample run using the BD Accuri C6 Plus flow cytometer (BD Biosciences, San Diego, CA, USA), a quality control procedure was also performed on the instrument using BD CS&T RUO beads (BD Biosciences, San Diego, CA, USA) in order to monitor and check the flow cytometer's performance.

3.2.1.1 Instrument Threshold

Setting the threshold on any flow cytometer is necessary in order to eliminate the instrumental electronic noise, a result of excess light scatter and low-level signals within the electronic system being detected,

as well as the background noise which may be present due to foreign, sub-micron particles from the external environment having entered the sample in question. The BD Accuri C6 Plus flow cytometer and software used in this investigation defaults a primary threshold of 80,000 based on forward scattered light in the instrument (FSC-H) whereby any signals detected above this threshold are recorded as an 'event'. A trigger channel is the important parameter which determines whether an event is recorded or not, however in a BD Accuri C6 Plus setting a primary threshold also identifies the trigger channel (BD Biosciences, 2012). It is important to select the lowest FSC-H trigger channel and primary threshold signal intensity so that it can be exceeded in order for an event to be enumerated, but also discount electronic/background noise. Too high a threshold however, could partially discount true events from enumeration during sample analyses due to such events being small and so emitting a lower scattered light intensity signal and not being recorded as a result.

A refinement test was carried out on the BD Accuri C6 Plus to detect the 'noise floor' (the boundary between the instrumental electronic noise and the background noise) using clean conditions. The FSC channel threshold was tested using 1 µm sized calibration beads (Molecular Probes, USA) suspended in 0.22-µm filtered Milli-Q water to act as the 'events' being enumerated, whilst also eliminating the instrumental electronic and background noise populations. Five FSC-H trigger channel and primary thresholds were assessed on the BD Accuri C6 Plus (10,000, 20,000, 30,000, 35,000 and 40,000) with the resulting side scatter against forward scatter plots (or SSC-H against FSC-H, respectively) shown in Figure 3.1. The 1 µm bead population was carefully identified and represented using a rectangular gate (R1), a gate constructed based on the horizontal gating of the 1 µm bead population in the equivalent histogram plot shown in Figure 3.1a. The threshold of 10,000 was selected as the lowest threshold to test, that of which effectively eliminated most of the instrumental electronic noise population (Figure 3.1b). However, it was clear that further instrumental and additional background noise was present above this threshold before the presence of the 1 µm bead population gate. The instrumental electronic noise is found at low SSC against FSC responses compared to the additional background noise. The additional background noise in this test could have been as a result of the age of the 1 µm bead population, whereby the beads were not plotting as tightly as they would if they were new. Additionally, the background noise could also have been due to the 0.22-µm filtered Milli-Q water having foreign, sub-micron particles in it from the surrounding environment since analyses were completed in a sediments laboratory, albeit regular cleaning of the area and flow cytometer was carried out. However, it is also important to eliminate such background noise further without removing any part of the 1 µm bead population in the R1 gate. The thresholds of 20,000, 30,000 and 35,000 (Figures 3.1c, d and e, respectively) were tested and resulted in further elimination of the instrumental electronic and background noise. The final FSC-H trigger channel and primary threshold tested of 40,000 was selected as optimum for this investigation's FCM SOP (Figure 3.1f). This was as a result of the additional instrumental and background noise having been eliminated by the 40,000 FSC-H threshold without

encroaching too closely to the 1 µm bead population. A 40,000 FSC-H threshold is optimal and a clearer elimination of the 'noise floor', but also allows for a margin in which cells smaller than the 1 µm size fraction are still able to present a scattered light signal intensity large enough to be detected and enumerated as an ‘event’ during sample analyses.

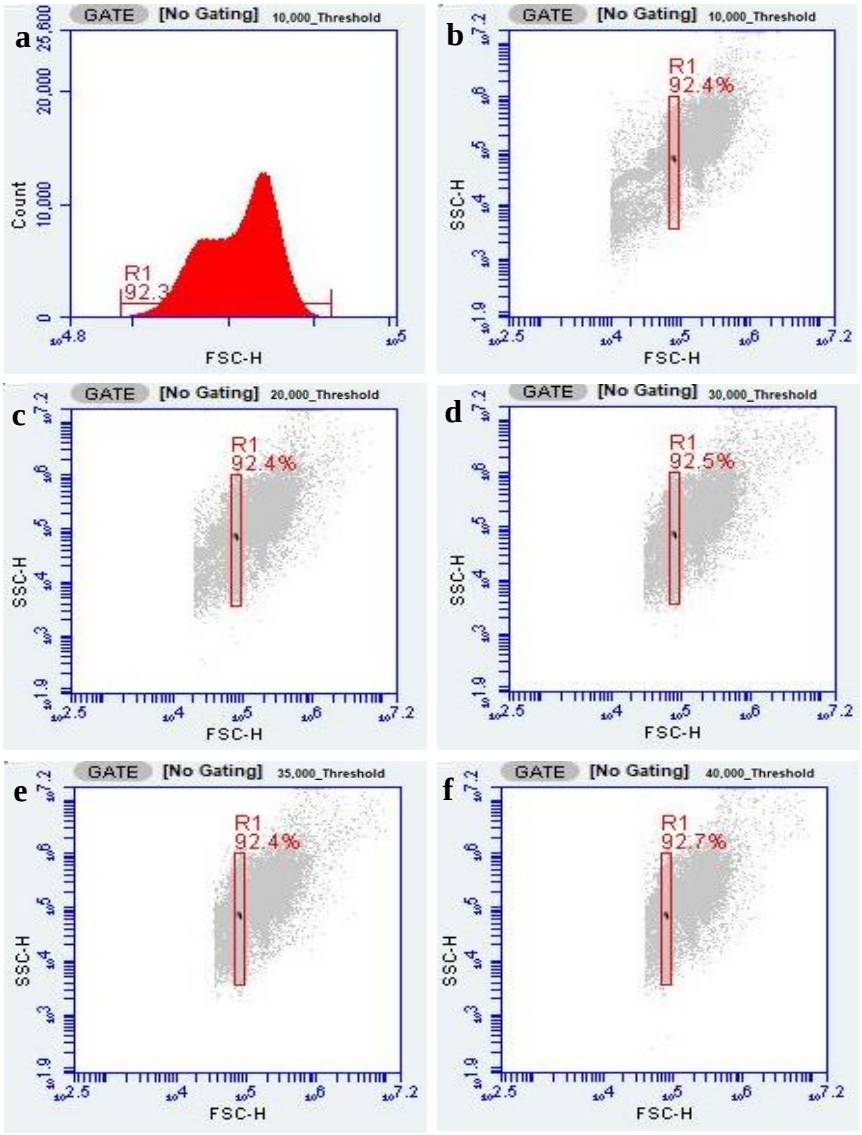

Figure 3.1. Methodological procedure to show the effect differing FSC-H thresholds have when analysing a 1 µm bead population in 0.22-µm filtered Milli-Q water: **(a)** Histogram plot of the 1 µm bead population with an R1 horizontal gate used to identify the 1 µm beads within the density plots; **(b)** FSC-H threshold of 10,000; **(c)** FSC-H threshold of 20,000; **(d)** FSC-H threshold of 30,000; **(e)** FSC-H threshold of 35,000, and **(f)** FSC-H threshold of 40,000. Rectangular marker gate R1 encompasses the 1 µm bead population region identified using the respective R1 horizontal gate.

3.2.1.2 Instrument Fluidic Settings

The BD Accuri C6 Plus system can accommodate up to 10,000 events per second but should never exceed this, instead a flow rate of 2,500 events per second or less when acquiring samples is

recommended for the best resolution in data (BD Biosciences, 2016). Fluidic settings are important for the detection of cells ('events'), but the density of a sample also plays a role in choosing an appropriate flow rate. Dense cell samples typically need a low flow rate to allow for a single-file movement of cells through the laser detection system, compared to lower density cell samples which can therefore have higher flow rates (Santibanez et al., 2016). However, too high a flow rate could result in coincident particle counts causing an under-enumeration of particles in a sample. Example optimisation tests for fluidic settings have been carried out on West Antarctic Ice Sheet Divide ice core samples where it was found that differing flow rates of 14, 32 and 50 µL min^{-1} did not influence cell enumerations of such samples (Santibanez et al., 2016). Therefore, for the supraglacial meltwater analyses in this investigation, an optimum flow rate of 50 µL min^{-1} was selected, with a run limit set to 300 µL and a core size of 20 µm.

3.2.1.3 Establishing 'carry over' in FCM

Potential for 'carry over' between samples during FCM analyses is an important variable to consider in an FCM SOP. Here, 'carry over' simply refers to the transfer of a previous sample into the next sample as a result of residue remaining on the SIP pin of the flow cytometer. The result is less representative cell enumerations for individual samples due to potential carry over of cells from a previous sample. Therefore, a refinement test was carried out to assess the effectiveness of running duplicate 'blanks' between practice environmental samples. The blank consisted of the same 3 mL of 0.22-µm filtered Milli-Q water, in the same Falcon tube, and covered with tin foil between each practice environmental sample run to prevent contamination with external impurities. The blank was ran in the following sequence: blank, blank, first unstained practice environmental sample, SYBR stained replicate environmental sample (see Section 3.2.2 on how to apply this stain), blank, blank, second unstained environmental sample, SYBR stained replicate environmental sample, blank, blank, and so on. Backflushes were also carried out after every six runs of samples on the Accuri C6 Plus to ensure the machine was clean before the next six runs, and to again limit carry over of previous sample particles into the next sample. From this test, running 0.22-µm filtered Milli-Q water in duplicate was effective as both the blanks and backflushes reduced the likelihood of carry over between samples. Therefore, the FCM protocols used in this investigation for actual sample analyses include the use of duplicate blanks of 0.22-µm filtered Milli-Q water to act as controls; and ran at the start, middle, and end of each sample batch run, with backflushes carried out after every sixth aliquot has been analysed.

3.2.2 SYBR Gold Staining, Cell Size, Carbon Content and Uncertainties

The experimental sensitivity and appropriate concentration of SYBR Gold needed to be selected for this investigation, thus a test using various SYBR Gold (Thermo Fisher Scientific, UK) concentrations was carried out. This test included final concentrations of SYBR Gold at ~0.25 ×, 0.5 ×, 1 ×, 1.5 ×, 2 ×, 2.5 ×, and finally 3 ×. A working solution was made by diluting the 10,000 × stock concentrate of SYBR

Gold into a 100 × concentration using TE (Tris-EDTA) Buffer. SYBR Gold is somewhat pH sensitive and so the original 10,000 × SYBR Gold stock was not diluted for this reason using filtered DI (deionised) water which would be unstable. A 100 × working solution of SYBR Gold then enabled the required SYBR Gold concentration tests to be carried out on a handful of archived, fixed environmental supraglacial samples in order to ascertain which SYBR Gold staining concentration produced the most distinctive shifts in FITC fluorescence, and so discriminate the population of cells from the non-biological particles, such as debris. From this test it was concluded that all seven concentrations produced distinctive shifts in fluorescence but no one concentration in particular resulted in a distinctive shift of an order of magnitude greater than the rest. Therefore, the final stain concentration of 1 × was confidently selected for the purpose of this research investigation in order to allow for appropriate enumeration gates to be constructed and so identify the cells from the non-biological particles within the samples. However, as previously mentioned in Section 3.2.1, 'sacrificial' samples were tested with the above SYBR Gold concentrations also, prior to commencing full sample analyses in that particular set. This allowed for an additional confirmation as to whether the 1 × final concentration of SYBR Gold was also appropriate for the differing glacier location sample sets before thawing the rest of the samples and staining them too. All four glacier sample locations' sacrificial samples showed that a 1 × final concentration of SYBR Gold was optimum.

For the SYBR Gold staining protocol, each sample batch to be analysed for each glacier location was thawed for 24 hours in a 4 °C fridge, and kept in the dark. A 100 × working solution of SYBR Gold was then prepared by mixing 1 µL of the original 10,000 × stock concentrate of SYBR Gold with 99 µL of TE, but kept covered with tin foil and refrigerated until use to prevent degradation of the stain from light exposure. The working solution is stable for 24 hours if such storage conditions are maintained. The sample vials were agitated by vortexing for 15 seconds and 495 µL of the cell sample added to a 1.5 mL Eppendorf tube (aliquot). Three technical replicates (triplicates) were included in this protocol for every 1 in 10 sample- triplicates for the first and last sample in the set, and then every multiple of 10 sample in between; allowing for a reliable estimate of the true number of cells in a particular sample and to assess the relative stability and so precision of the analytical FCM instrument in enumerating samples in a given run. The SYBR Gold 100 × working solution was then agitated and used to stain the resulting sample aliquots using 5 µL of the SYBR Gold working solution to give a final concentration of 1 × SYBR Gold in a total 500 µL of stained sample. Sample aliquots were agitated for 15 seconds to uniformly mix the sample and stain together, and left for 30 minutes in the dark, at ambient temperature. Such an incubation time was selected as optimum based on pilot experimental SYBR Gold sample runs, and is a time that has previously varied in other studies from 15 minutes (Christner et al., 2018) to 240 minutes (Irvine-Fynn et al., 2021), in the dark. Before FCM analyses, the sample aliquots were vortexed for 15 seconds to remobilise any cells within the sample. Additional 500 µL control replicate aliquots for each sample were also analysed but unstained in conjunction with its respective stained aliquot pair.

Such aliquots enabled a determination in the fluorescent shift thus discriminating between biological cells which have shifted rightward in FITC fluorescence, and the non-biological particles (Figure 3.2).

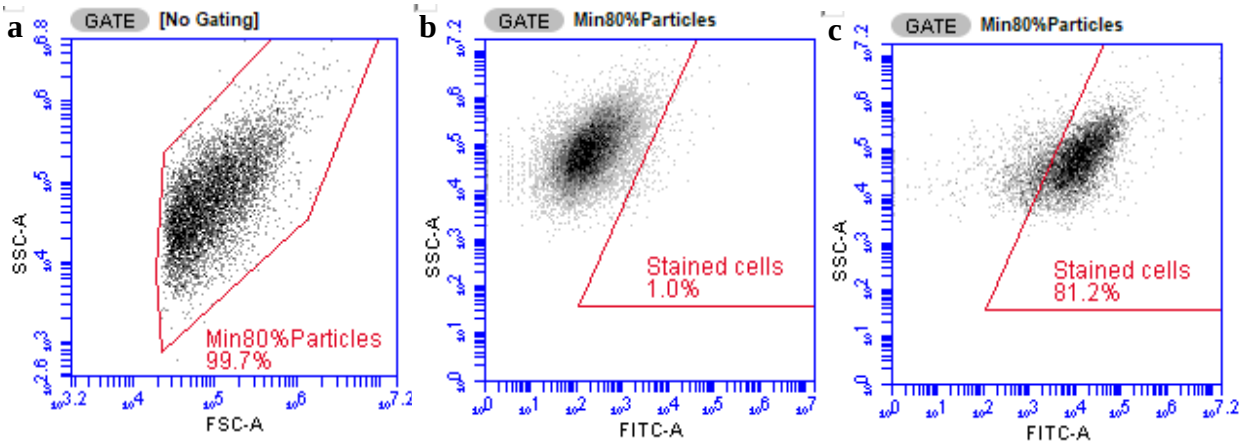

Figure 3.2. Example methodological gating procedure for SYBR Gold stained samples containing cells which are represented by an increase and migration rightwards in the FITC signal due to staining, and debris sediment which remain: **(a)** A morphological gate constructed on an SSC against FSC density plot to represent more than 80 % of the particles of interest within each sample; **(b)** An unstained replicate aliquot of a sample, gated based on the morphological gate, and **(c)** The stained aliquot replicate pair of the unstained aliquot, and gated based on the morphological gate, but clearly showing the stained particles which have migrated rightwards and so classed as cells.

Reporting the relative percentage abundance of cells in particular size fractions allows for a determination of the variation in size of the supraglacial cells. Cell size is determined by the FSC light produced by the laser beam of a flow cytometer, in which the intensity of such FSC is proportional to the size of particles. Size fraction gates for microbe enumerations in FCM were defined using a Flow Cytometry Size Calibration Kit (Molecular Probes, USA) containing separate suspensions of non-fluorescent polystyrene microspheres of known diameters (1, 2, 4, 6, 10 and 15 µm). Such diameters allowed for the following size fraction categories to be defined: ≤ 1 µm, 1-2 µm, 2-4 µm, 4-6 µm, 6-10 µm, 10-15 µm, and > 15 µm. All beads had the same refractive index of 1.591 at 590 nm meaning that the FSC signal produced only represented the size fraction differences of the microspheres alone; as FSC signals have been known to relate to the refractive index of particles (Carter and Ormerod, 2000; Molecular Probes, 2003). However, knowing this detail means that the refractive index of cells in this investigation's supraglacial samples may differ compared to that of the beads, meaning that the size categories established using the calibration beads may not completely represent the actual cell sizes of the supraglacial cells themselves (Molecular Probes, 2003). Furthermore, the refractive index and so the associated size in which a cell may appear, may also be affected by their physiological state, such that dead cells have lower refractive indexes thus giving lower FSC signals, and classing the cells as smaller compared to healthy living cells (Molecular Probes, 2003). Despite the diameter of the microspheres

being consistent and spherical, the morphologies of cells from environmental samples will not be consistent in form but instead could be rod-like in shape. Therefore, the cell sizes recorded in FCM depend on the axes and so orientation in which cells from an environmental sample are hit by the laser beam, it may be either the long-A or short-B axis of each cell, thus not reflecting the true size of the environmental cells in question. However, despite such considerations, the Flow Cytometry Size Calibration Kit is an appropriate proxy for cell size determination in environmental microbial enumerations.

Calculations for estimates of cellular carbon content within microbial abundances are presented in the following analytical results chapters. To do this, the published 20 fg C $cell^{-1}$ was applied- a value which has previously been used to estimate the cellular carbon in aquatic prokaryotes (Whitman et al., 1998), irrespective of shape and size. With this value, the meltwater equivalent (w.e.) mean cellular carbon content could be calculated, representing the mean cellular carbon content that would be assumed to be delivered in meltwater from the bulk ice density to supraglacial channels. For Chapter 4 in particular whereby ice types are explored, the mean carbon content of cells in the bulk density of ice has also been calculated by multiplying the respective meltwater equivalent carbon content values by the density of ice- a value of 0.917 g cm^{-3}.

The estimated uncertainties in microbial abundance have been determined within the analytical results chapters based on the quality control triplicates included in the SYBR Gold analytical runs. As a result, the mean percentage relative standard deviations (% RSD) were calculated for each separate glacier location- Storglaciären, Sweden; Fountain Glacier, Canada, and Midtre Lovénbreen and Foxfonna, Svalbard. For Storglaciären sample analyses, the average % RSD was derived from five sets of triplicate samples enumerated over the entire sample batch analytical run, resulting in five % RSD values based on the events per mL enumerations, thus producing an overall mean average % RSD of ± 20.5 %. For Fountain Glacier, the average % RSD was derived from nine sets of triplicate samples included over four sample batch analytical runs in total, resulting in four mean % RSD values calculated for each batch run (based on the events/mL values), and produced an overall mean % RSD of ± 25.1 %. For Foxfonna Glacier microbe enumerations, the average % RSD was derived from seven sets of triplicate samples included over four sample batch analytical runs in total, resulting in four mean % RSD values calculated for each batch run and based on the events/mL values, thus producing an overall mean % RSD of ± 32.6 %. For the Midtre Lovénbreen, the average % RSD was derived from three sets of triplicate samples included over three sample batch analytical runs in total, resulting in three % RSD values for each batch ran and based on the events/mL values, and produced an overall mean % RSD of ± 45.5 %. For ease in the results chapters, triplicate cell abundances were averaged and the means used in the cell enumeration results and correlations.

3.2.3 BD Cell Viability Dual-Staining and Uncertainties

Viability determination of microbes using the BD Cell Viability Kit (BD Biosciences, San Diego, CA, USA) involves the uptake of TO (thiazole orange) in all cells but then the exclusion of PI (propidium iodide) from intact cells or the uptake of such a dye in damaged/dead cells. This dual-staining approach for viability determination was applied on the non-fixed supraglacial samples of Midtre Lovénbreen and Foxfonna, Svalbard, in which the Midtre Lovénbreen samples presented an opportunity to act as pilot samples to allow for preliminary practice in the use and applicability of the dual-staining protocol with the LIVE/DEAD staining kit. PI permeates all cells that have damaged membranes (non-viable) or injured, thus resulting in a red fluorescent signal when excited in FCM by the laser beam, compared to TO which stains all biological particles (cells) in the sample population to produce a green fluorescent signal, similar to that of SYBR Gold. Such a combination of stains allowed for a determination as to the percentage of live, dead, or injured cells within a sample. During this investigation's analyses of Midtre Lovénbreen and Foxfonna samples, the SYBR Gold staining protocol was ran in parallel to the viability staining protocol by using replicates of each sample, thus allowing for a reference as to the total microbial abundance for each sample. The selected viability determination protocol for this investigation followed the manufacturer's guidance, however one adaptation was to the incubation time for PI and TO staining of aliquots, whereby a time period of 10 minutes was instead selected rather than 5 minutes as stated in the manufacturer guidelines. Such an adaption was the result of surveying further published information by the manufacturer who stated that TO staining is sufficient for analysis at 2 to 5 minutes, but at least 15 minutes allows for a maximum intensity to be achieved as TO enters cells slower when compared to the quick staining of PI (Alsharif and Godfrey, 2002). Therefore, 10 minutes was suitably selected as a time period between the 5 minutes of that stated in the manufacturer guidelines, and the 15 minutes stated in their further publications. Furthermore, in previously published preliminary method development experiments, it was found that PI uptake occurred rapidly in fixed cells within 2 minutes of addition of the stain but that there was no difference in the amount of PI staining shown in cells incubated for 1 hour (Davey and Hexley, 2011). This finding further supports the appropriate selection of a 10 minute incubation period for the dual-staining combination of PI and TO. Sacrificial sample testing revealed that both the Midtre Lovénbreen and Foxfonna glacier samples produced distinct FCM results based on the stated manufacturers dual-staining volumes when incubated for 10 minutes in the dark, at ambient temperature.

The above dual-staining protocol applied in Chapter 6 involved the thawing of the non-fixed sample batches 24 hours before analyses in a 4 ℃ fridge, and in the dark. Again, a 100 × working solution of SYBR Gold was prepared and the same SYBR Gold staining protocol carried out as in Section 3.2.2. Additional 500 µL aliquot replicates of the same sample were decanted ready for the viability staining protocol. In this experiment, there were again triplicates included for the first and last sample in the set, and then every multiple of 10 sample in between. The BD Cell Viability Kit dyes were agitated and then

used to stain the additional 500 µL aliquot with 5 µL of impermeant PI and then 5 µL of permeant TO. Such aliquots were then agitated by vortex for 15 seconds to uniformly mix the sample and two stains together. However, where the SYBR Gold stained aliquot replicates were left for a 30 minute incubation period, the TO and PI dual-stained aliquots were left for 10 minutes in the dark, at ambient temperature, as well as additional 500 µL unstained control aliquots. However, two additional 'killed' replicate aliquots were also included in the analytical runs- one 'killed' by heat, 60 ℃ for 1.5 hours, based on results of such heat treatment shown by Davey and Hexley (2011), and the other aliquot 'killed' with filtered 2 % w/v final concentration of glutaraldehyde, with a fixation time of 30 minutes. Such a fixation time was selected as optimum based on surveyed literature which also stated similar fixation times for glutaraldehyde of 15 to 30 minutes (Brussaard, 2004). Both 'killed' controls were stained with PI and TO after their treatments thus allowing for an assessment as to whether the PI does in fact stain cells in such 'killed' aliquots which would be expected to be dead as a result of the heat and fixative treatments, or establish whether the cells were actually able to remain hardily intact and not be killed/injured. Before analysing in FCM, all sample aliquots were vortexed for 15 seconds after their incubation periods. For a small batch sample run (i.e. 10 samples), the two types of 'killed' control replicate aliquots were only included for samples 1, 6 and 10 in this instance, and so at the beginning, middle, and end of the small batch run. Therefore, this staining protocol saw the inclusion of five aliquot replicates in total for one sample depending on the size of the sample batch run: an unstained control aliquot; an aliquot replicate stained with SYBR Gold; an aliquot replicate stained with PI and TO, and finally, two 'killed' treated replicate aliquots both then stained with PI and TO before FCM analyses.

For the live, dead, and injured density plot gates for viability determination of the Midtre Lovénbreen and Foxfonna samples, a laboratory sub-culture of *Janthinobacterium* sp. (JG1) glacial isolate (acquired from Dr Jarishma Gokul and Dr Arwyn Edwards) was examined with the PI and TO staining protocol. The sub-cultured bacteria supplied in R2B Broth (Lab M Limited, Lancashire, UK) was incubated at +15 ℃, and once the cultures had reached the stationary phase, one would expect 1×10^7 cells mL^{-1} or more to be present. Therefore, the sub-culture of *Janthinobacterium* sp. was diluted 100 × following a dilution series approach in 0.22-µm filtered Milli-Q water to provide 500 µL working stock aliquots used in triplicate form. From here, the working stock aliquots were stained with PI and TO to firstly, help inform the position of the live gate on the FL3 (PI fluorescence) against FL1 (TO fluorescence) density plot on the Accuri software. An additional 2 % w/v final concentration glutaraldehyde-fixed replicate aliquot of *Janthinobacterium* sp. was dual-stained with PI and TO, and then analysed to help provide an indication as to where the dead gates would also be positioned. Note here that for the Accuri software, FL3-A is represented as PerCP-A, and FL1-A represented as FITC-A on the density plot axes for this investigation (see Figure 3.3). Although a vertical shift in PerCP (PI) fluorescence would be expected of live cells having been fixed by glutaraldehyde and so subsequently dead, thus allowing the intake of PI like that shown in technical bulletins with other cultured bacteria populations, that was not

the case in this protocol but instead a horizontal shift in FITC (TO) fluorescence was observed (Figure 3.3a and b). For the purpose of this research investigation, since the only change observed in the fixed 'dead' population of *Janthinobacterium* sp. from dual-staining was that of a rightward shift in FITC (TO) fluorescence rather than vertically in PI fluorescence, this was taken as the basis for which the proportion of 'dead' and 'live' cells found within the supraglacial study samples were estimated. It is important to take into account that the sub-cultured glacial isolate of *Janthinobacterium* sp. will present different viability results to that of the Midtre Lovénbreen and Foxfonna non-fixed environmental samples, and so the live, injured, and dead gates which have been constructed (Figure 3.3). However, such gates represent the most likely outcome for viability staining of glacial bacteria, especially since *Janthinobacterium* sp. is a common bacteria found in both Midtre Lovénbreen and Foxfonna glacier environments.

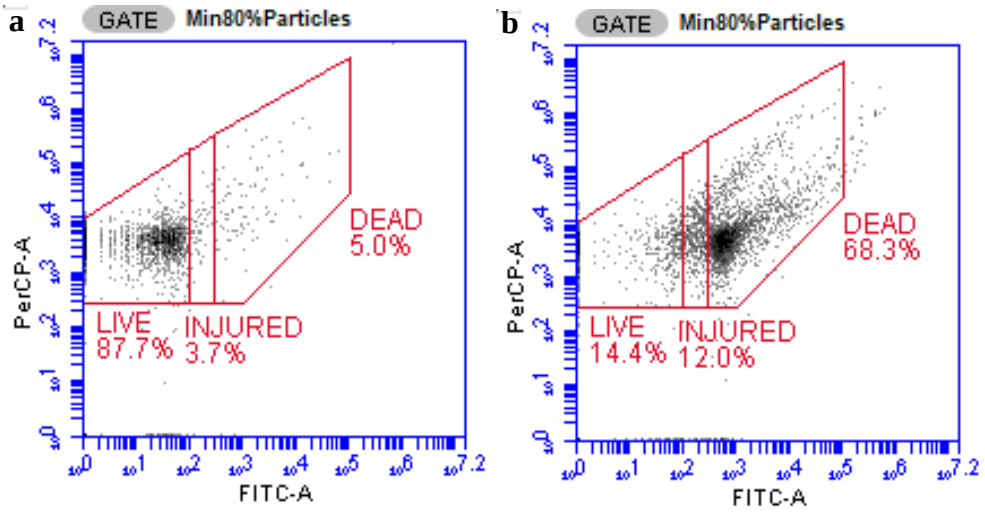

Figure 3.3. Methodological viability gates constructed using live *Janthinobacterium* sp. dual-stained with PI and TO, as well as replicate aliquots of live *Janthinobacterium* sp. fixed with glutaraldehyde and then dual-stained, for viability determination: **(a)** The non-fixed but PI and TO stained sample aliquot, and **(b)** The glutaraldehyde fixed replicate aliquot which has then been stained with PI and TO to determine the dead cell population. Both density plots have been gated with a morphological gate like that used in Figure 3.2a.

The estimated uncertainties in microbial abundances found within each viability category of live, dead or injured, were also calculated in the form of mean % RSD for the non-fixed Midtre Lovénbreen and Foxfonna samples. For Midtre Lovénbreen, the average % RSD was derived from three sets of viability triplicate samples included over the same three analytical runs in which the SYBR Gold analyses were carried out, and resulted in three % RSD values calculated for each batch run (based on the events/mL values). Overall, the mean % RSD values for the live, dead and injured microbe enumerations were found as ± 16.7 %, ± 14.4 %, and ± 0 %, respectively. For Foxfonna Glacier, the average % RSD was derived from seven sets of viability triplicate samples included over the same four analytical runs in

which the SYBR Gold analyses were carried out, and resulted in four mean % RSD values calculated for each batch run (based on the events/mL values). Here, the mean % RSD values for the live, dead and injured microbe enumerations were found as ± 20.3 %, ± 5.4 %, and ± 10.7 %, respectively. Again, triplicate microbe relative percentage abundances for viability (live, dead and injured) were averaged for ease and means presented and used in the viability status enumeration results in Chapter 6.

3.2.4 Uncertainty in Storage Impact on Microbe Abundances

Four storage durations and conditions were tested in order to see what impact storage might have had on the degradation of cell numbers in the archived samples. Here, the first storage experiment tested included leaving sample aliquots in the light on a work bench and at room temperature; the second experiment involved leaving aliquots in the dark on a work bench covered with tin foil and at room temperature; the third experiment involved leaving aliquots in the dark covered with tin foil but in the fridge at 4 ℃, and the fourth storage experiment involved sample aliquots being left in the dark covered with tin foil but in a freezer at -20 ℃. Each storage experiment involved 495 µL replicate sample aliquots (the aliquots to be stained with 5 µL SYBR Gold after storage), and additional 500 µL replicate aliquots (the aliquots representing the paired control to be analysed unstained after storage), being left for a duration of 1,4, 11, and 14 days before being stained with SYBR Gold following the SOP outlined in Section 3.2.2. The storage time periods were selected based on surveyed supraglacial ecology literature which stated similar time periods seen for bacterial biomass doubling times (e.g. Rassner et al., 2016; Anesio et al., 2010; Williamson et al., 2018; Christner et al., 2018). Replicates were taken from both Fountain and Foxfonna Glacier samples, and such samples selected for the storage experiments if they had previously produced the highest, middle and lowest cell abundances within their sample batch run from the SYBR Gold staining as described in Section 3.2.2. This meant that where the initial (0 hour) SYBR Gold analyses were ran over four days and so four batches for Fountain and Foxfonna Glacier, then there were also four sets of highest, middle and lowest cell abundance samples that were subsequently selected and replicates taken for storage experimental analyses. The first batch of selected highest, middle and lowest cell abundance samples for a glacier location were assigned to storage experiment 1, and then the same principal was followed for the proceeding selected samples from the other three batches. It was important to ensure that enough replicates from selected samples (for stained and unstained aliquots) were taken to endure a storage time of 1, 4, 11, and 14 days. Triplicates were also included within the storage experiments for each storage duration time period, with such triplicate cell abundances averaged.

Significant trends observed for the fixed Fountain Glacier and non-fixed Foxfonna Glacier selected sample replicates as a result of changing storage length and condition are shown in Figures 3.4d and 3.5a, respectively. The fourth experimental condition of freezer storage in the dark, presented significant increases in cellular abundances with length of storage for the low ($r^2 = 0.888$, $p = 0.017$), medium (r^2

= 0.849, p = 0.026), and high abundances (r^2 = 0.929, p = 0.008) (see Figure 3.4d for regression trendlines). Comparatively, for the non-fixed Foxfonna Glacier sample replicates selected, a significant decrease in the microbial abundances over the length of storage from the 0 hour analyses was observed for storage experiment 1, albeit only for the high abundance sample replicates (r^2 = 0.822, p = 0.034) (see Figure 3.5a for regression trendline). Such trends could be used to exemplify how sample cell abundances have the potential to be effected by storage condition and duration of such storage. However, since such experimental analyses were carried out on previously archived samples that would have already experienced freeze-thaw, such regression trends are less reliable in this assessment. For example, the Fountain Glacier samples were fixed and stored refrigerated for a couple of weeks before being frozen at -80 °C, and so this long period of 'cool' storage would have resulted in expected degradation following Kamiya et al. (2007)'s observations of microbes in storage. In comparison, Foxfonna Glacier samples were non-fixed and stored 'cool' for up to 5 days only, and then frozen at -80 °C. Therefore, variations between these sample set abundances are likely due to the difference in 'cool' storage experienced prior to freezing of the samples. It would instead be more informative if this same experiment was carried out on freshly collected supraglacial samples; which one would expect to see clearer declining trends in microbe abundance with storage length.

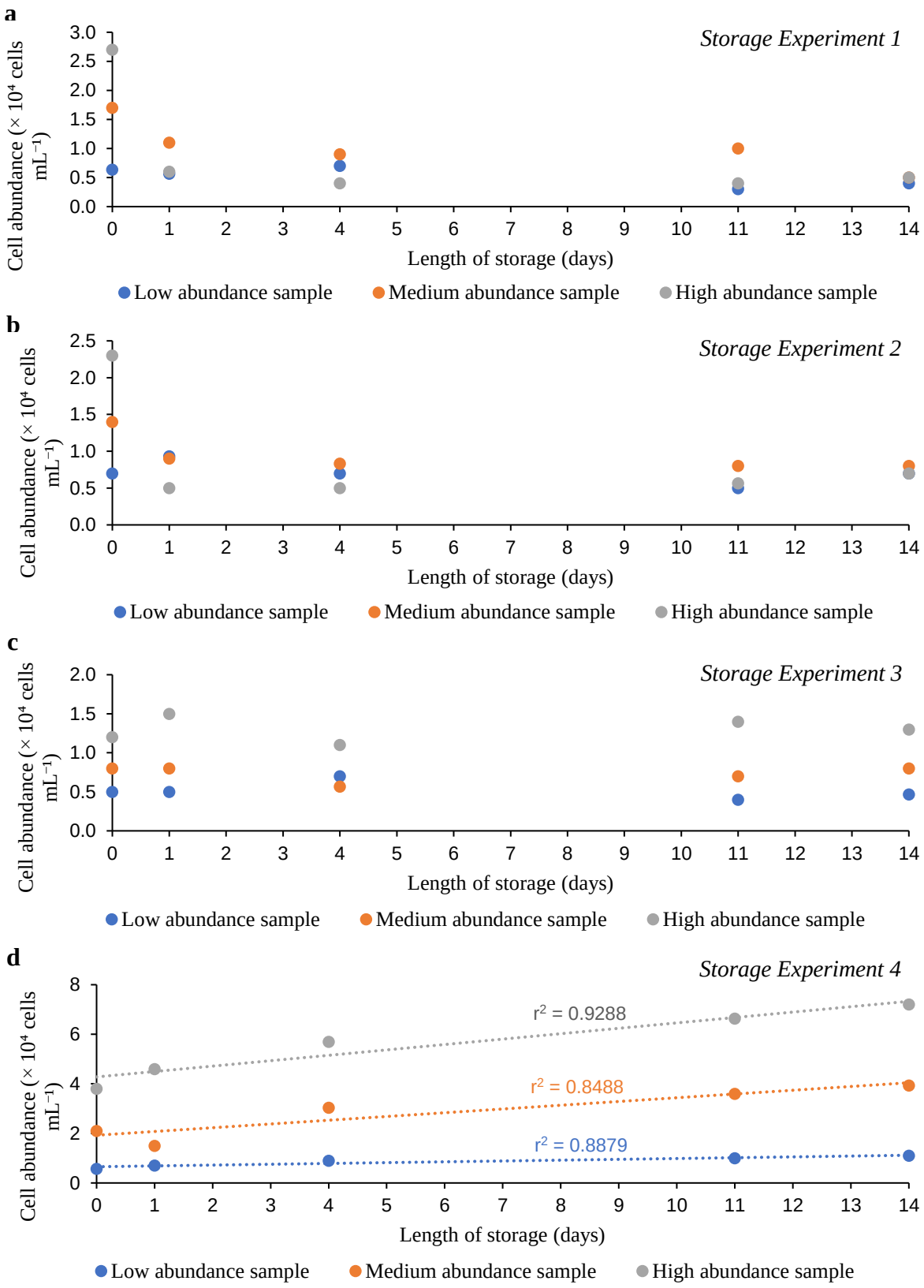

Figure 3.4. Scatter plots showing the cellular abundances of the fixed Fountain Glacier sample replicates with differing storage conditions and times: **(a)** storage experiment 1- light, room temperature; **(b)** storage experiment 2- dark, room temperature; **(c)** storage experiment 3- dark, fridge storage, and **(d)** storage experiment 4- dark, freezer storage; with trendlines showing significant regression analyses.

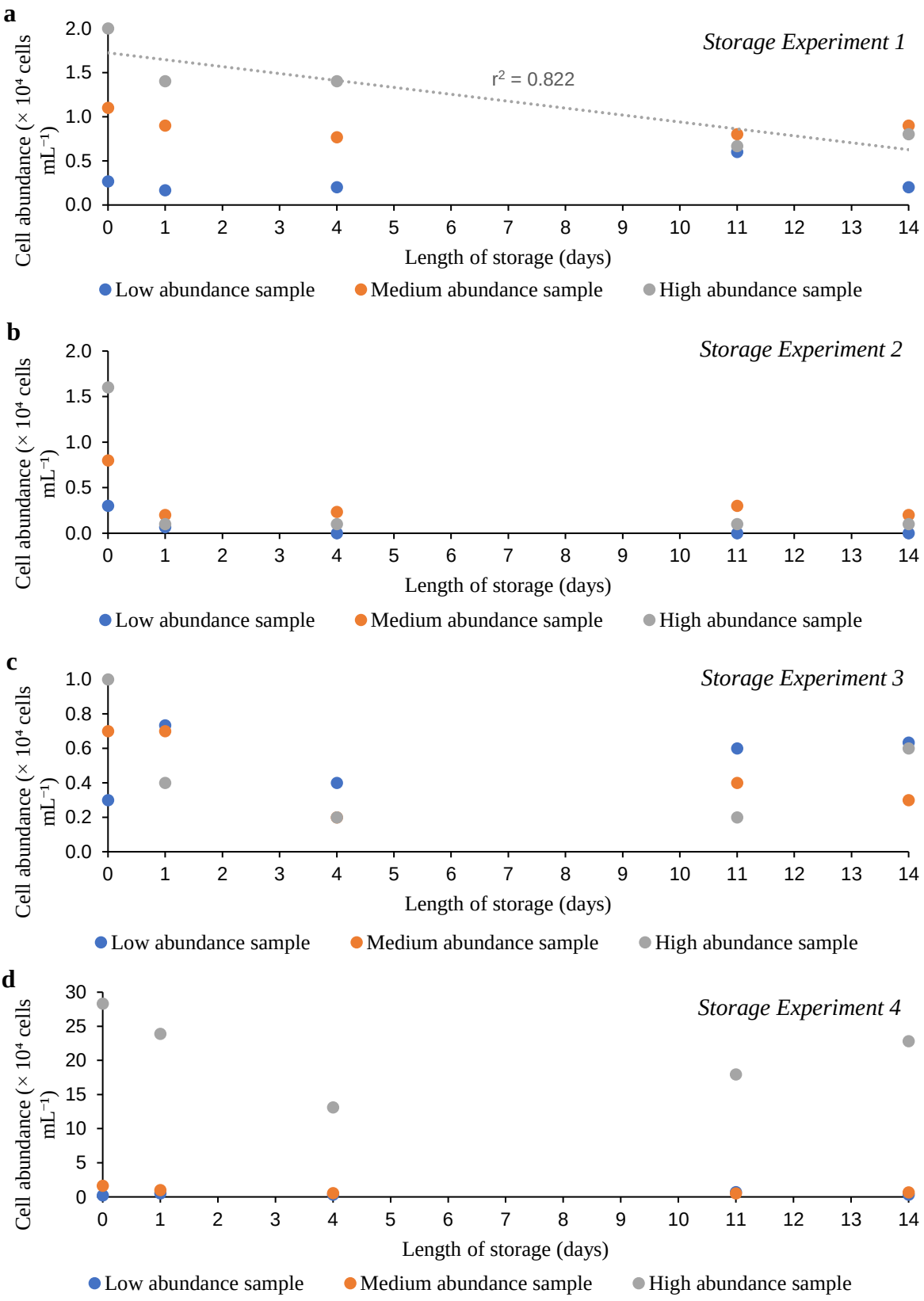

Figure 3.5. Scatter plots showing the cellular abundances of the non-fixed Foxfonna Glacier sample replicates with differing storage conditions and times: **(a)** storage experiment 1- light, room temperature; trendline showing significant regression analysis; **(b)** storage experiment 2- dark, room temperature; **(c)** storage experiment 3- dark, fridge storage, and **(d)** storage experiment 4- dark, freezer storage.

3.3 Summary

This chapter presents a standard operating procedure suitable for the reliable enumeration of supraglacial cells from four Arctic valley glacier settings. FCM is a rapid analytical technique which can be used to further contribute to existing knowledge surrounding the abundance, size, and viability of microbes within supraglacial environments. An enumerating protocol has been identified with the use of 1 × final concentration of SYBR Gold, incubated for 30 minutes in the dark at ambient temperature, and ran with a flow rate of 50 µL min^{-1}; a run limit set to 300 µL; a core size of 20 µm, and an FSC-H trigger channel and primary threshold of 40,000. The refined SOP detailed in this chapter will be applied for the microbial enumeration of varying supraglacial ice type samples (Chapter 4), and the abundance and cell sizes of supraglacial microbes in varying stream, cryoconite, and weathering crust environments (Chapter 5). A viability determination protocol using PI and TO dual-staining was also identified in this chapter in order to assign cells as live, dead or injured. However, this viability protocol's applicability and unexpected preliminary results in the fluorescent shift of FITC (TO) fluorescence rather than PerCP (PI) fluorescence for cells 'killed' with glutaraldehyde, will be discussed further in the exploratory Chapter 6 of this research thesis.

4 MICROBE ABUNDANCE ON THE ICE SURFACE OF STORGLACIÄREN

4.1 Introduction

The surface of glaciers harbour ecological habitats and niches in which active microbial cells can reside and carry out their important biogeochemical interactions. As previously established, the surface of glaciers can be referred to as carbon sinks and sources due to the active microorganisms present there that can sequester inorganic carbon dioxide from the atmosphere, but then also produce such a compound in metabolic respiration (Stibal et al., 2012). Therefore, enumerating the microbial abundance found within the ice surface of glaciers, particularly within varying ice types, is important in order to contribute to the eco-hydrological understanding of the supraglacial ecosystem. Wherever water is present, even within small interstitial spaces found within and between ice crystals, a perfect habitat is available for microbes to survive, thrive and carry out their important metabolic processes. The shape and structure of microbial communities is primarily dependent on the spatial distribution of such microbes on the glacier surface, but ice type also presents an important secondary factor (Varliero et al., 2021). Ice types reflect seasonal climatological variations which subsequently impact on the formation of initial snowpack (Wadham and Nuttall, 2002). Therefore, identification of the ice types found on the surface of glaciers could be used to not only characterise seasonal climatological variations affecting snowpack formation like shown in other literature, but to also characterise the microbial abundance and sizes that may be residing within such ice types on the surface of glaciers- microbes that have the ability to act as carbon sources and sinks. Therefore, the aim of this chapter is to quantify the number of cells, and their size fractions, found within five differing ice types on the surface of Storglaciären, Sweden. Such ice types include: glacier coarse clear ice (CC), coarse bubbly ice (CB), fine ice (FI), as well as superimposed ice (SI) and an additional ice type comprised of refrozen rill meltwater- rill ice (RI); with the differing ice types explained further in Section 4.2.2. Note, the archived samples analysed here were originally collected by Tristram Irvine-Fynn, Stephen Jennings, Arwyn Edwards and Ottavia Cavelli, supported by EU FP7 InterAct grant awarded to Tristram and Arwyn.

The statements hypothesised below will be investigated within this analytical chapter and such findings used to either support or reject the below statements in the context of this chapter's aim:

1) The optimised FCM SOP outlined in Chapter 3 will allow for reliable microbial enumerations, and associated size fractions, to be determined within varying ice types samples from an northern hemisphere glacier.
2) Statistical analyses will determine whether the microbe abundances found within each ice type across the nine sample sites on Storglaciären significantly differ from one another.
3) Statistical analyses will determine whether the microbe abundance in each size fraction, across the nine sample sites of Storglaciären significantly differ between ice types.

4) Statistically significant relationships are expected to be found between microbe abundance against ice crystal hexagonal cross-section, and specific perimeter of the crystals, whereby more cells would be expected to be found in ice types with larger specific perimeters and so crystal boundaries, and ultimately a smaller cross-section.

4.2 Storglaciären, Sweden

4.2.1 Background

Storglaciären is a small valley glacier found in the Tarfala Valley, northern Sweden (67.90° N, 18.56° E) (Figure 4.1). This Swedish Arctic glacier occupies a length of 3.2 km, a total surface area of 3.1 km², and extends in an east to west direction (Monz et al., 2021). Previous reconstruction of the mass balance of Storglaciären has suggested that the glacier was in an equilibrium-like state between the dates of 1880 and 1910s, but soon experienced drastic melting until the 1970s which made up 76 % of the glacier ice mass lost between 1910 and 2015 (Holmlund and Holmlund, 2019). However, favourable conditions until the late 1990s did present a stabilisation in the mass balance of Storglaciären, but as previously stated, soon saw the glacier losing ice mass again hereafter (Holmlund and Holmund, 2019). Storglaciären can also be described as a polythermal glacier (Glasser et al., 2003) which has a cold surface ice layer that remains cold, but is also dependent on the net ablation at the ice surface as well as the position of the CTS within the ice mass (Pettersson et al., 2003), and so influences the thermal regime of Storglaciären (see Chapter 2, Figure 2.1 for illustration exemplifying CTS spatial distribution within polythermal ice masses). It is explained that on Storglaciären when a strong negative temperature gradient is present in the cold surface layer (i.e. the top layer of ice is lower in temperature than the temperate ice below it), a higher rate of heat transfer occurs towards the surface as temperate ice freezes below and so removes latent heat to this layer, and so the CTS migrates downwards thus reducing the cold surface layer from thinning (Pettersson et al., 2003). However, between the years of 1989 and 2009, this cold surface layer experienced a reduction by one third, following an average thinning rate of 0.80 ± 0.24 m a^{-1}, a result of climatic warming since the 1980s, and so the subsequent increase in englacial temperature, which is still ongoing (Gusmeroli et al., 2012).

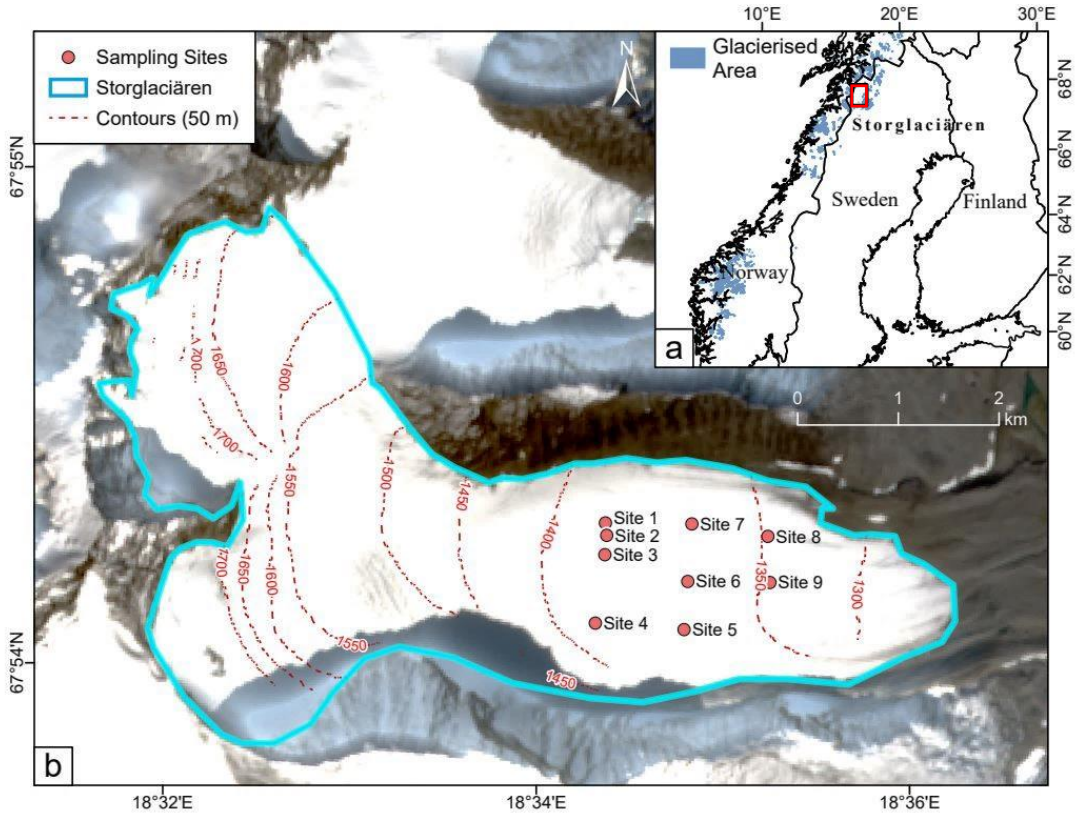

Figure 4.1. (a) Location of Storglaciären in Sweden; **(b)** approximate glacier extent of Storglaciären shown using a background Sentinel-2 image sourced from QGIS with an acquisition date of 27 August 2021. Elevation data acquired from Tarfala Research Station; glacier contours are at 50 m intervals.

4.2.2 Review of Ice Crystal Structure on the Surface of Glaciers

The glacier itself, its thermal regime, and flow, all combine to yield ice structure and so varied sizes and types of ice crystals in the emergent ice surface that is the weathering crust. A weathered ice surface in the ablation zone presents an appropriate opportunity for crystallographic analysis, especially if the ice crystals have sufficiently etched out of the surface (Hubbard and Glasser, 2005). Varying ice types at the glacier surface include: coarse clear ice which is indicative of meltwater that has refrozen as a layer below the winter snowpack; coarse bubbly ice which is typical of temperate glacier surfaces, whereby thick layers of this ice type represent the partial melting and refreezing of winter snow accumulation; fine ice which is recrystallised glacier ice formed following shear deformation; and finally, superimposed ice which is the result of a refrozen saturated snowpack, which can be found in a dense form, but with retained air bubbles, for some or most of the accumulation (Jennings and Hambrey, 2021). Examples of such ice types being found can be seen in temperate valley glaciers whereby the analyses of the microstructure of ice crystals taken from Charles Rabots Bre, Norway, have shown large sized crystals of coarse bubbly ice reaching tens of centimetres (Jennings and Hambrey, 2021). In zones of foliation, it is often clear to see the differentiation in particular ice facies as fine and coarse bubbly ice which appear light in colour, compared to coarse clear ice which appears darker (Jennings and Hambrey,

2021). On Storglaciären, previous observations of such ice types present on the surface of the glacier, have been interpreted with respect to the dynamic flow of the glacier. For example, the presence of coarse clear ice as well as other fracture planes within the surface of Storglaciären, and running parallel to the ice flow, suggest the main body of the glacier experiences shear deformation (see Glasser et al., 2003). In addition to this, other studies on Storglaciären describe the presence of clear ice bands at the glacier surface whereby englacial meltwater channels or fractures have slowly frozen and excluded air bubbles giving it a clear appearance, and are then uplifted by glacial movement to the surface ablation zone (Varliero et al., 2021).

The effect of temperature and meltwater on ice crystal structures has been explored. For example, in temperate regions where ice is subject to strong thawing by short-wave incident radiation and so sensible heat energy, thus resulting in glacier ice at the pressure melting point, the boundaries of small ice crystals tend to melt and this meltwater percolates in thin films through interstitial spaces, but when the temperature falls, such meltwater refreezes onto the larger crystals and increases their growth (Seligman, 1949). However, the refreezing of such meltwater films also releases latent heat which can indeed induce further melting, thus making the surrounding ice warmer or more likely to melt with the passage of such meltwater, and so reducing crystal size in this way. Furthermore, in cold-based glaciers where the penetration of a cold wave is present, the speed of ice crystal growth is reduced (Seligman, 1949). Therefore, it is clear that ice crystal size and varying crystal type can present a story about the dynamic structure and flow of a glacier, as well as the seasonal/climatological effects on the glacier in question. However, interrogating such surface ice types for their microbial abundance presents a further carbon source and sink ecological story, as well as the potential processing of such microbes to be liberated in surface melt, or refreezing, of such ice crystals and transported to downstream ecosystems.

4.2.3 Ice Type Sample Collection and Interrogation

A total of nine sites (see Figure 4.1) were chosen across the ablation zone on Storglaciären for sample collection which took place from 25 to 26 July 2014 (Day of Year (DOY) 206-207). At each site, five different ice types were identified and collected (glacier CC, CB, FI, as well as SI, and RI which produced long, narrow crystals, typically less than 0.5 cm in thickness). For the collection of each ice type sample, surface ice was disaggregated with gentle leverage using an ice axe which had been thrice rinsed with supraglacial stream water. Samples of each ice type were handled using nitrile gloves and transferred into sterile Whirl-Pak sample bags. Ice type samples were transferred to the laboratory, thawed, and agitated, resulting in meltwater which was then subsampled into 15 mL sample vials and fixed with 2 % w/v final concentration of glutaraldehyde for FCM analyses.

To determine each ice type and individual crystal cross-sections however, a selection of individual crystals (or a bulk sub-sample) were first placed on a black square with a carpenter's rule as a scale in

both the X and Y directions, and images of the crystal sub-samples were captured using a Pentax Optio-WG1 camera. ImageJ was then used to process such images by importing and rescaling them using the visible carpenter's rule to define the resolution in both the X and Y directions. Image contrast was enhanced to be able to clearly define the individual ice crystals against the black background, and subsequent measurements manually made of individual crystals in the image. In addition to this, to provide a quantitative proxy for the amount of interstitial space found within the ice crystals sampled, a portion of each ice type was extracted and each individual crystal separated, and measured for the mean A-long and B-width axes for between 12 and 50 crystals, with resulting combined uncertainties in A- and B-axes measurement probabilistically estimated to be ± 4.95 %. Such axes measurements provided an estimate of the cross-sectional scale of the hexagonal crystals as it is assumed that all the ice crystals followed a typical elongated hexagonal form exposed at the ice surface. The elongated hexagonal cross-sectional area and perimeter were calculated for each ice crystal sample, with an additional 'specific perimeter' (SP) in units of m m^{-2} being calculated to show how many hexagonal ice crystal boundaries there are per unit area, and so a proxy for the crystal boundaries where microbes would be expected to be present. For example, the smaller the ice crystal hexagons, the more boundaries there were that occupied the unit area and so a higher specific perimeter, compared to larger crystals with less boundaries in the unit area. It is important to note that the five different ice types obtained for this chapter will be analysed with the following in mind, whereby coarse bubbly, coarse clear and fine ice types represent that of the glacier ice, compared to superimposed ice and the additional refrozen rill meltwater ice types.

4.3 Storglaciären Ice Microbe Enumeration Results

As described in Section 3.2.1.1, an appropriate FSC-H threshold was tested and selected in order to eliminate the instrumental electronic and background noise populations for this research's FCM analyses. However, for the first half of the Storglaciären sample analyses, an initial FCM protocol was carried out whereby an FSC-H threshold of 64,000 was used. It was indeed this action which identified the need to refine the threshold cytometric settings of the BD Accuri C6 Plus, thus resulting in the subsequent refinement threshold tests detailed in Section 3.2.1.1. As a result, an optimised protocol using an FSC-H threshold of 40,000 was selected and used for the remaining half of the Storglaciären samples, but the initial protocol was also carried out. This approach allowed for a comparison between the initial threshold protocol data and the optimised threshold protocol data for the remaining half of the Storglaciären samples. Here, it was important to appropriately estimate the new optimised microbe abundance, and relative percentage abundance results of the size fractions, for the first half of the Storglaciären samples which used the initial threshold protocol. To produce such estimates and ensure confidence in these results, an empirical correction was carried out whereby a relationship between the initial protocol results, in events per mL of SYBR Gold stained cells , and the optimised protocol results for the second half of the Storglaciären samples were examined. The two sets of results were plotted

against one another and a linear transformation equation was revealed (see Appendix 1). This linear equation could then be applied to the first half of the Storglaciären sample's results obtained using the initial threshold protocol, and so calculate more optimally estimated results that would have been likely if ran under the optimised FSC-H 40,000 threshold protocol. Here, the linear equation $y = mx + c$ was applied whereby y is the optimised protocol result (events per mL) from an FSC-H 40,000 threshold; m is a constant derived using the scatter plot shown in Appendix 1; x is the initial protocol result (events per mL) from an FSC-H 64,000 threshold, and c is another constant derived using the scatter plot (see Appendix 1). This same approach was then applied in order to find estimates for the relative percentage abundance of microbes found within the various size fractions, for the first half of the Storglaciären analyses instead of the initial threshold protocol results. All samples were analysed using FCM following the SOP outlined in Section 3.2.2.

The statistical analyses for Storglaciären, and for the subsequent chapters hereafter, were carried out using PAST 4.04 software, and include the data for microbe abundances found within the differing ice types, as well as the accompanying cell size fraction data. Additionally, the hexagonal cross-sections data for the ice type samples have been used in the results of this chapter to represent a proxy for ice crystal 'size' as there is no C-axis data to truly know the crystal size or 3D interstitial space. Furthermore, the specific perimeter has also been used in the results to represent a proxy estimation for the ice crystal boundaries/interstitial spaces, that of which is where one would expect microbes to be found. The normality distribution of such data sets had to be established and this was determined using the Anderson Darling normality test with the knowledge that data with a significance level of more than 0.05 are classed as normally distributed. As a result of the normality testing, the appropriate statistical tests were applied such as the non-parametric test of Spearman's Rank Correlation Coefficient (r_s) if one or both data sets to be correlated were non-normally distributed, or the parametric test of Pearson's Correlation Coefficient (r) if both data sets to be correlated were normally distributed. Pairwise Mann-Whitney U-testing was also used to determine whether the microbe abundance found within each ice type significantly differed from one another, and to ascertain whether the microbe abundance in each size fraction significantly differed between ice types. This particular statistical test was applied on the basis that some of the data sets were non-normally distributed, but also as a result of the small number of observations recorded in the ice types, and so a conservative approach of using this non-parametric test was necessary for statistical analyses. Furthermore, for ease microbe abundance triplicates have been averaged to allow for paired values for correlation testing between microbe abundance of each ice type against hexagonal cross-section, and specific perimeter for the respective ice crystals. Furthermore, it is important to note that two anomalies were identified within the Storglaciären results as such anomalies presented microbial abundance results that were an order of magnitude higher when compared to other microbe abundances enumerated for the same ice types, thus the resulting abundances for the coarse clear ice sample from Site 5 and the coarse bubbly ice sample from Site 3 were excluded from all data

figures and statistical tests presented within this chapter, including the accompanying ice crystal hexagonal cross-section and specific perimeter data for these particular samples.

Table 4.1 shows mean microbial cell abundance for the five ice types by combining all of the nine sampling site abundances for that particular ice type, thus revealing SI to exhibit the highest cell abundance, followed by glacier FI, CC, CB ice, and then the additional RI type with the lowest. Furthermore, due to the interest in the carbon sink and source role that the microbes found within the five different ice types present, the mean cell abundances for each ice type, across the nine sample sites combined, have been used to estimate the mean carbon content of such cells in the bulk density of each ice type. Estimates for mean cellular carbon are shown in Table 4.1 with meltwater equivalent (w.e.) mean cellular carbon content also presented for each ice type to represent the mean cellular carbon content that would be assumed to be delivered in meltwater from the bulk ice density to supraglacial channels (Table 4.1).

Table 4.1. Estimated mean microbe abundance, and cellular carbon content in the bulk density of each ice type and the water equivalent (w.e.) based on the mean cell abundances for each ice type across the nine sample sites combined. Standard deviation included in brackets as ± 1 SD.

Ice Type	Mean microbe abundance ($\times 10^4$ cells mL^{-1})	Estimated mean cellular carbon (kg C m^{-3} of ice)	Estimated mean cellular carbon (kg C m^{-3} w.e.)
CC	3.30 (± 3.33)	6.05×10^{-7}	6.59×10^{-7}
CB	1.83 (± 1.43)	3.36×10^{-7}	3.67×10^{-7}
FI	6.13 (± 2.02)	1.13×10^{-6}	1.23×10^{-6}
SI	10.78 (± 10.64)	1.98×10^{-6}	2.16×10^{-6}
RI	1.47 (± 0.11)	2.70×10^{-7}	2.95×10^{-7}

Furthermore, Pairwise Mann-Whitney U-test statistical analyses were applied here to determine whether the medians of the microbe abundance data, across the nine sample sites, and found within each ice type statistically significantly differ from one another. Using the events per mL found within each ice type across the nine sample sites, it has been deduced that glacier CC and FI are statistically significantly different from one another ($U = 10$, $p = 0.014$), as well as RI and glacier FI ($U = 0$, $p = 0.045$), and glacier CB and FI ($U = 2$, $p = 0.004$) (Table 4.2).

Table 4.2. Pairwise Mann-Whitney U-test results testing whether the medians of the microbe abundances (using the events per mL) found within each ice type across the nine sites, statistically significantly differ from one another. Mann-Whitney U values are shown in the lower portion of the matrix table, and the p-values shown in the upper portion of the matrix table. Statistically significant relationships are bold and italicised for clarity.

	CC	**FI**	**RI**	**CB**	**SI**
CC		***p = 0.014***	p = 0.085	p = 0.400	p = 0.268
FI	***10***		***p = 0.045***	***p = 0.004***	p = 0.724
RI	1	***0***		p = 0.867	p = 0.126
CB	17	***2***	6		p = 0.077
SI	24	36	2	11.5	

The cell size distributions of microbes found within the five different ice type crystals, across all nine sample sites combined, can be seen in Figure 4.2. Here, overall the size fraction 2-4 µm exhibits the highest average relative percentage abundance of microbes found in the five different ice types, across the combined nine sample sites' data, with the size fraction of ≤ 1 µm being the second most dominant. However, the 10-15 and > 15 µm cell size fractions present the smallest average relative percentage abundance of microbes within the ice types, across the nine sites. As CC, CB and FI represent glacier ice here, it is apparent that for the 2-4 µm size fraction glacier CC ice harbours the highest average relative percentage abundance of microbes (55.47 %) compared to glacier FI (47.03 %) and CB ice (33.39 %). However, when compared to SI, the average relative percentage abundance of cells in the 2-4 µm size fraction for glacier CC and FI is higher than that of SI (35.28 %), albeit with CB glacier ice slightly lower than SI. However, comparing these results to the additional RI average relative percentage abundance of cells in the 2-4 µm size fraction, RI exhibits the highest abundance of cells (57.76 %). Additionally, when looking at the second highest size fraction of ≤ 1 µm for average relative percentage abundance of cells, the glacier ice types of CC (18.25 %) and FI (16.85 %) present the lowest in abundance, and CB as the highest (36.89 %). The SI average relative percentage abundance of cells for this size fraction is the overall second highest however (35.17 %), with the additional RI type at 23.27 %, and so RI here isn't the ice type with the highest average relative percentage abundance of cells for the ≤ 1 µm size fraction, but is for the 2-4 µm size fraction as previously stated. Pairwise Mann-Whitney U-test analyses were also applied here to allow for a determination as to whether the relative percentage abundance of microbes in each size fraction significantly differed for ice types in the overall nine sample sites. Using the relative percentage abundance of microbes found in each cell size fraction, statistically significant differences between ice types were observed with a significance level of less than 0.05, but

other ice type pairings not mentioned are classed as similar in abundance. For the cell size fraction of ≤ 1 µm, CC and CB ice, CC and SI ice, FI and CB ice, and finally FI and SI, are statistically significantly different, as well as for cell size fraction of 1-2 µm- CC and CB, CC and SI, FI and CB, and FI and SI. For 2-4 µm size fraction, all ice types had relative percentage abundances of microbes statistically significantly different from each other at $p < 0.05$, excluding CC and RI, RI and CB, and CB and SI. The 4-6 µm size fraction saw significant differences in microbe relative percentage abundance between CC and CB, CC and SI, and FI and CB, at $p < 0.05$. The 6-10 µm size fraction however, saw no statistically significant differences between the ice types for their relative percentage abundances of microbes. The 10-15 µm size fraction did present significant differences between CC and FI, CC and CB, CC and SI, FI and RI, and RI and SI, at $p < 0.05$ for their relative percentage microbial abundance. Finally, the > 15 µm presented significant differences in the relative percentage abundances of microbes at $p < 0.05$ level for ice types CC and SI, FI and RI, and RI and SI, overall for the nine sample sites. SI and RI types are expected to be different from the glacier ice types of CC, CB, and FI.

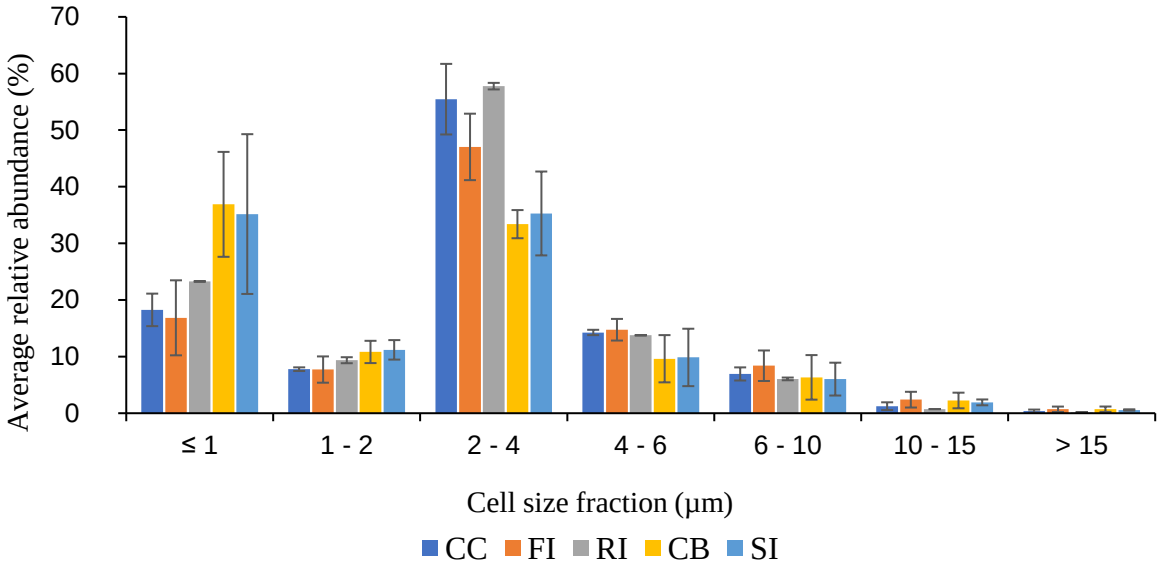

Figure 4.2. Bar chart showing the average relative percentage abundance of microbes found within each size fraction for each ice type, across all nine sample sites combined. Standard deviation shown as error bars at ± 1 SD.

The final objective of this research chapter stated how statistically significant relationships would be expected between microbe abundance against ice crystal hexagonal cross-section, and specific perimeter of the crystals, whereby more cells would be expected to be found in ice types with larger specific perimeters and so crystal boundaries and so ultimately a smaller cross-section. For this, the microbial cell abundances in events per mL found within each ice type sample across the nine sample sites were plotted against the ice crystal hexagonal cross-sections, and against the specific perimeter of such ice crystals. When looking at the association between the microbe abundances found in the glacier CC ice type samples across the nine sample sites against the ice crystal hexagonal cross-sections, Spearman's

Rank Correlation Coefficient was calculated since one of the data sets to be correlated was non-normally distributed, however no statistically significant relationship was observed (r_s = -0.3133, p = 0.4439) (Figure 4.3a). For the ice types of glacier FI, CB, and then SI, the Pearson's Correlation Coefficient has been reported as both the microbial cell abundance data in events per mL for these ice types, and the ice crystal hexagonal cross-sections, are normally distributed. However, again no statistically significant relationships were observed for glacier FI (r = -0.3934, p = 0.2949), CB (r = 0.2676, p = 0.6081), and SI (r = 0.3662, p = 0.3324) (Figure 4.3b, d and e, respectively). It is important to note here that no statistical analysis was able to be calculated for the RI microbial cell abundances against ice crystal hexagonal cross-sections due to only two data points being provided (Figure 4.3c). Similarly, associations between microbe abundance for the different ice types across the nine sample sites against the specific perimeters of such ice crystal samples, equally presented no statistically significant associations (see Appendix 2).

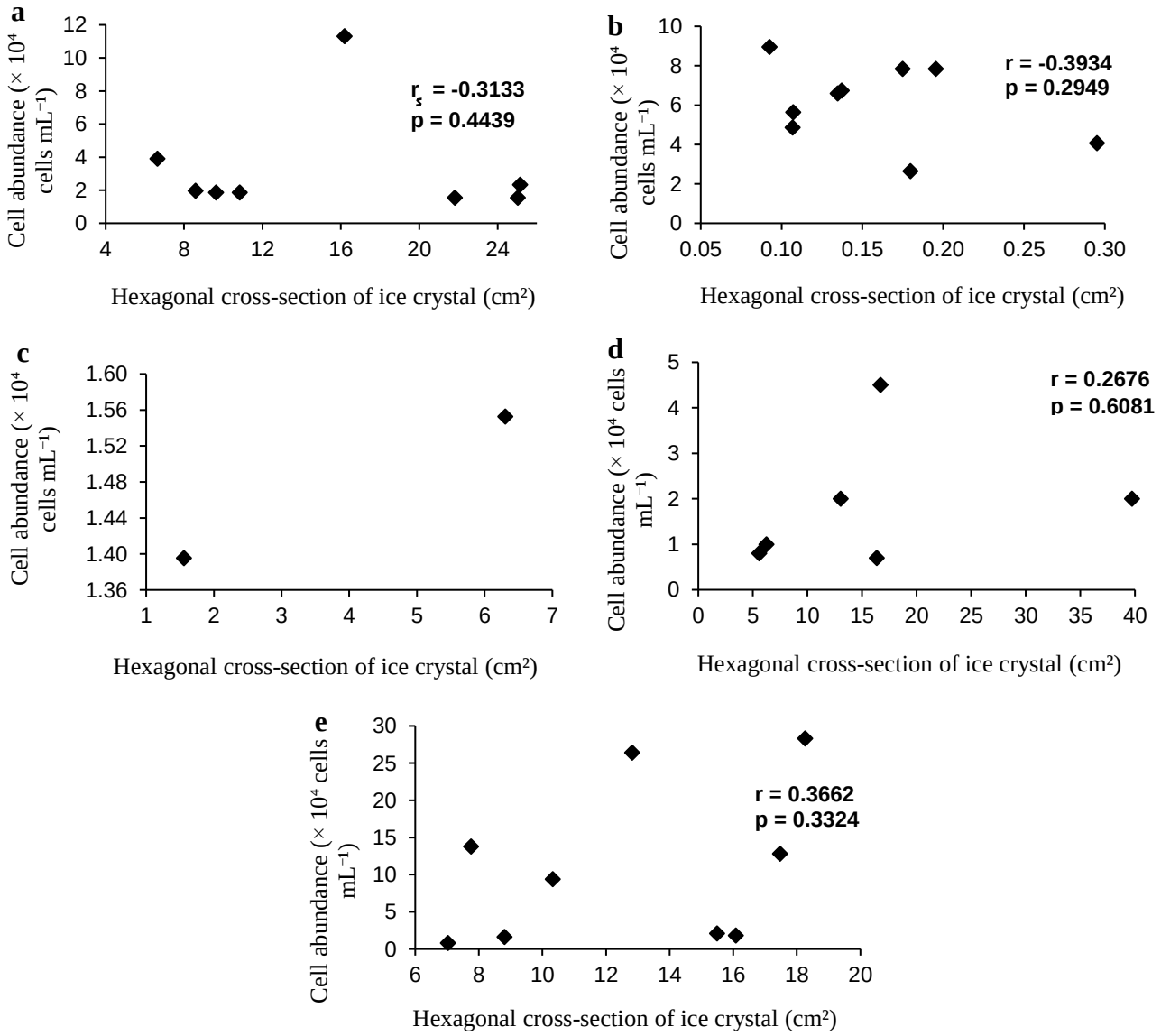

Figure 4.3. Scatter plot associations showing the microbial cell abundance against ice crystal hexagonal cross-section for: **(a)** CC; **(b)** FI; **(c)** RI; **(d)** CB, and **(e)** SI. No association was able to be calculated for RI due to only two data points, and so there is an absence of accompanying correlation statistics.

4.4 Interpretation and Discussion

The glacier ice surface can harbour microbes which have been transported to the surface in precipitated snow, through aeolian deposition (Franzetti et al., 2017), or even by re-emergence to the ice surface from within the body of glacier ice (Miner et al., 2021). However, microbial abundance can vary within differing ice types. Across the five different surface ice types in this study, a range of 1.47 to 10.78 × 10^4 cells mL^{-1} has been observed for mean microbial abundances, across the nine sample sites combined. This range compares well to Varliero et al. (2021) who sampled Storglaciären uplifted englacial clear ice band cores that ranged in prokaryote abundance from 2 × 10^3 to 3 × 10^4 cells mL^{-1}, and in some instances even up to as high as 1 × 10^5 cells mL^{-1} in high algal content samples. When looking more specifically at the individual ice types, SI followed by the glacier ice type of FI were found to have the highest mean abundance of microbes, across the nine sample sites combined, with 10.78 × 10^4 cells mL^{-1} and 6.13 × 10^4 cells mL^{-1}, respectively. Comparatively, in other studies clear surface ice, or CC in this case, produced the highest cell count compared to other ice types sampled (see Varliero et al., 2021), but glacier CC ice was only the third highest for mean microbial abundance in this thesis investigation, followed by glacier CB ice, and then finally the additional RI type. It is important here to acknowledge the mechanical structure of the ice types in order to suggest why high mean microbial abundances in the SI and glacier FI types have been observed. Firstly, SI and glacier FI are likely to have high microbial abundance owing to their small crystal sizes, which present lots of interfaces/boundaries per crystal area for the microbes to attach to and reside within. SI is refrozen saturated snow and so made up of many small crystals. Likewise, glacier FI also produces many small crystals as a result of extreme shear deformation within a glacier and causing zones of foliation in the ice. In comparison, glacier CC and CB ice have larger crystals and so present fewer interfaces per crystal area for cells to exist. Lastly, the RI is the same as meltwater that is found in supraglacial streams which has refrozen and so more cells might be excluded from this ice type due to the fluvial action discharging such microbes through the rills, and so few are entrapped in the refrozen rill meltwater; hence the mean microbial abundance observed for this ice type was the lowest.

A seasonal variability in ice type microbial abundance could be suggested, whereby higher abundances may have been observed in the ice types as a result of such ice forming in the presence of more meltwater from summer season snowmelt. For example, SI forms during summer snow accumulation, melt and then refreezing, compared to glacier CC and CB ice types which form due to meltwater refreezing below the winter snowpack, and then also due to the partial melt and refreezing of winter snowpack accumulation, respectively (Jennings and Hambrey, 2021). Therefore, since the highest abundance in microbes was observed in the SI compared to the glacier CC and CB ice, then it could be suggested that less microbes were present and so entrapped within the glacier ice types of CC and CB during the winter season, compared to the higher abundance of microbes entrapped in the summer season during the refreezing of SI melt. Meltwater content at ice crystal boundaries is vital for microbes to live, and is

where many nutrients are present and biogeochemical reactions occur (Hodson et al., 2008). Therefore, such a high abundance of microbes found at these boundaries can become entrapped when the meltwater refreezes. Comparatively, in the formation of FI there is potential for frictional melt due to extreme shear deformation in the glacier ice, which results in recrystallisation and so the production of fine ice. Subsequently, microbial growth may be promoted here in the ice as a result of such frictional melt and so presenting a potential explanation for the higher microbial abundance revealed in the FI type in this investigation.

Since SI is refrozen snowmelt, it is appropriate to compare the mean microbial abundance found in this chapter for this ice type (10.78×10^4 cells mL^{-1}) with that of snow microbial abundances on other previously studied glacier ice masses. For example, the average cell abundances observed in the snowpack on Kongsvegen Glacier, Svalbard, ranged from 2.0×10^4 cells mL^{-1} to 2.0×10^5 cells mL^{-1} (Amato et al., 2007), and so comparing well with the SI mean microbial abundance observed, which would be expected since superimposed ice is refrozen snowmelt. In addition to this, the high mean abundance in microbes in the SI ice type could also be explained by the fact that microbes, and particles, precipitated to the glacier surface in snow, may have simply become entrapped when the snowmelt refroze to form such superimposed ice. However, meltwater drainage and refreezing in snowpack has the potential to increase particle and ion concentrations at the supraglacial surface, and so could suggest a reason for a high mean microbial abundance in SI on the surface of Storglaciären. Snowmelt percolating down within the snowpack on glacier ice, and so too subsequent particles and ions drained here, reach impermeable ice which subsequently prevents further percolation, but results in the accumulation of the particles at this boundary (Goto-Azuma et al., 1994). However, in instances where this snowmelt then refreezes from the bottom and so near the impermeable glacier ice, particles are rejected by this refreezing layer and become more concentrated in the snow meltwater above, which then also eventually refreezes and so results in a high concentration of particles and ions emerging at this snow/ice surface (Goto-Azuma et al., 1994). Therefore, the formation mechanisms described for such refrozen snowmelt (superimposed ice) and the resulting particle and ion concentrations in the surface ice, could also be used to explain the high mean microbial abundance observed in the SI ice type on Storglaciären.

The size fraction of 2-4 µm presented the overall highest average relative percentage abundances of microbes in this size category for the different ice types, across the combined nine sample sites; followed by the ≤ 1 µm size fraction. Limited studies have examined the size fractions of enumerated cells from the supraglacial ecosystem, such as Irvine-Fynn et al. (2012) which observed the highest average relative percentage abundances of microbes found in the ≤ 0.5 µm cell size fraction for snow, ice core and stream samples on Midtre Lovénbreen, Svalbard. In addition to this, Stevens (2019) observed a modal cell size class of 1-2 µm for stream and weathering crust samples, with the ≤ 1 µm size fraction being the second

most common, like that presented in this research chapter but then followed by the 2-4 µm cell size fraction instead. It has previously been explained how larger cells can stay trapped within ice crystals compared to cells smaller than 2 µm, and ultra-small cells, which are more likely to be found in the liquid veins/interstitial spaces between ice crystals (Miteva, 2008). Additionally, previous studies of ice core microbial abundances from Greenland observed that the majority of cells present were ≤ 1 µm in size (Sheridan et al., 2003). This finding could further exemplify the emergence of microbes from within the glacier ice mass to the ice surface, since the results of this chapter have also observed ≤ 1 µm sized cells in the surface ice types, thus linking back to the melting and refreezing mechanisms of which can result in the concentration of microbes at the ice surface from originally being deeper within the ice surface (see Goto-Azuma et al., 1994).

No statistically significant associations were observed in this investigation for ice type microbial abundance against crystal hexagonal cross-section, and specific perimeter of such ice crystals. However, it is likely that larger crystals of glacier ice, such as the CB ice with crystal hexagonal cross-sections going up to 40 cm^2 in this study, present fewer interstitial veins, and so specific perimeter, for microbes to reside in, compared to glacier FI with up to 0.3 cm^2 in cross-section as shown in this chapter, and so more meltwater boundaries surrounding the crystal unit area for microbes to be present and metabolise in. For example, it has previously been explained how cells are expelled from an ice crystal during freezing and instead become incorporated in the liquid veins at the crystal boundary, as long as the cells are small enough (Mader et al., 2006). Therefore, less microbes are found within the ice crystal hexagonal cross-sections themselves and more likely to be found in the interstitial meltwater veins surrounding such crystals, thus suggesting a reason for the lack of associations between microbial abundances and ice type cross-sections. Subsequently, it would then be expected that there should have indeed been associations between microbial abundances and the specific perimeters of such ice types, but this was not the case either. Instead, this result could simply be explained by the fact that the sampling approach may not necessarily have collected ice type samples that contained water-saturated crystals and so more interstitial meltwater veins. Instead, the ice type samples collected likely reflect microbial communities that remain attached to ice crystals in unsaturated ice, with only a small water film around the crystal rather than saturated interstitial meltwater veins, and so less microbes have been found here as a result of the small water film 'specific perimeters'.

Ultimately, the range in mean microbial abundances for the ice types on Storglaciären ranging from 1.47 to 10.78 × 10^4 cells mL^{-1}, represent the abundance of cells trapped within ice crystals at the ice surface, compared to Stevens (2019) Storglaciären ice surface bail-recharge holes' mean abundance of 1.4 ± 3.1 × 10^4 cells mL^{-1} which represents the abundance of cells liberated from ice melt in the glacier near-surface weathering crust. Additionally, when then looking at the mean microbe abundances found within supraglacial stream channels, such as an average of 3.5 ± 0.9 × 10^3 cells mL^{-1} on Storglaciären, and 2.6

± 3.2 × 10^4 cells mL^{-1} on Protektorbreen, Svalbard (Stevens, 2019), which represent the abundance of cells discharged from weathering crust surface melt into the stream channels, an interrelation between such supraglacial environments for microbial liberation can be further implied. For example, the mean abundance observed within the weathering crust meltwater on Storglaciären by Stevens (2019) compares well to the mean 1.47 × 10^4 cells mL^{-1} observed for the RI type in this study, and since RI here represents meltwater that is found in supraglacial streams which has just been refrozen, a hydrological link between the meltwater in the weathering crust which is then assumed to be discharged into nearby supraglacial channels is further evidenced. Also, as it has previously been observed, the microbial abundance entrained in the weathering crust surface has been seen to equal that observed in supraglacial streams (Stevens et al., 2020).

4.5 Summary

This chapter has shown how an optimised FCM SOP was used to reliably enumerate microbial cells, and associated size fractions, found within varying ice types on the surface of an northern hemisphere glacier thus supporting the first objective of this chapter. Statistically significant differences in ice type microbe abundances were found between glacier CC and FI, RI and glacier FI, and finally the ice types of glacier CB and FI. However, no statistically significant relationships were present between microbe abundance against ice crystal hexagonal cross-section, and specific perimeter of the crystals, and so the final objective of this analytical chapter is rejected. Although more cells would be expected to be found in ice types with larger specific perimeters and so crystal boundaries, and ultimately a smaller cross-section, it is speculated that this result may be due to the ice type samples that were collected having little water-saturated crystals and so less prevalence of interstitial meltwater veins in which microbes could reside. However, potential for microbe emergence and liberation to the glacier ice surface has been identified through melt and refreezing mechanisms of ice, particularly in superimposed ice which presented the highest mean abundance of cells on Storglaciären in this study. Such liberated microbes likely expelled from ice crystals during refreezing, have the potential to be mobilised in ice melt at the glacier surface, discharged into nearby supraglacial channels, and transported downstream. However, the variability in the abundance of such microbes discharged during ice melt, and the hydrometeorological factors which influence such fluxes, needs further investigation.

5 MICROBE FLUXES IN SUPRAGLACIAL STREAMS

5.1 Introduction

Currently, there have been only limited attempts reported in the literature to enumerate and evaluate microbe fluxes within supraglacial streams (e.g. Irvine-Fynn et al., 2012; Foreman et al., 2013), and so further investigation into the eco-hydrology of supraglacial streams is important. Ultimately, microbe fluxes in supraglacial streams are discharged from glacier surfaces to downstream ecosystems, and with declining mountain and Arctic glaciers, knowledge of such fluxes, or variations thereof, are key to quantify in order to improve understanding of how connected ecosystems may respond to the decline of glaciers in climatic global warming. Therefore, the aim of this chapter is to quantify the number of cells, and associated size fractions, discharged through supraglacial streams from Fountain Glacier, Canada and Foxfonna Glacier, Svalbard, with an opportunity to explore potential for meltwater cell sample degradation with storage length using Midtre Lovénbreen, Svalbard, meltwater samples. Note, the archived samples analysed in this chapter, and the accompanying hydrometeorological data, were originally collected by Tristram Irvine-Fynn and Brian Moorman, supported by the NERC project award to Tristram and NSERC, and PCSP funding to Brian for the Fountain Glacier samples; Tristram and Arwyn Edwards, supported by Andy Hodson and UNIS for the Foxfonna Glacier samples; and finally, Tristram, Jon Telling and Jon Hawkins, supported by NERC project award to Andy Hodson and Alex Anesio for the Midtre Lovénbreen samples.

The statements hypothesised below will be investigated within this analytical chapter and such findings used to either support or reject the below statements in the context of this chapter's aim:

1) The optimised FCM SOP outlined in Chapter 3 will allow for reliable microbial enumerations, and associated size fractions, to be determined within Arctic supraglacial meltwater samples.
2) Statistically significant associations are expected between streamflow hydrological data and meteorological data for Fountain Glacier and Foxfonna Glacier.
3) Statistically significant associations are expected between the hydrometeorological data and stream microbe enumerations for Fountain Glacier and Foxfonna Glacier.
4) Cell sample degradation due to increased length of storage is expected to result in decreased microbial abundance through the analyses of the same supraglacial meltwater samples from Midtre Lovénbreen which were also enumerated over 10 years ago for the previously published study by Irvine-Fynn et al. (2012).

5.2 Fountain Glacier, Canadian Arctic

5.2.1 Background

Fountain Glacier is located on the southern portion of Bylot Island in the Canadian Arctic (72.97° N, 78.51° W) (Figure 5.1). This valley glacier occupies a length of approximately 16 km and a width of 1.5 km at the terminus (St Germain and Moorman, 2019). The centre of Bylot Island is covered by a 4500 km^2 icefield, and is where many of the Island's valley glaciers have their accumulation zones, including Fountain Glacier (Wainstein et al., 2010). The direction of flow for the glacier occurs in a north to south direction for the top portion of the glacier, but then changes orientation to a west to east direction for the bottom portion of the glacier. Between 1982 and 2007, the terminus of Fountain Glacier experienced thinning by approximately 25 m, and this part of the glacier now terminates at a vertical cliff face, reaching up to 35 m in some places (Wainstein et al., 2008; Whitehead et al., 2013). Fountain Glacier can also be described as a polythermal glacier due to having a temperate core but with a cold surface ice layer. For this research investigation on Fountain Glacier, a single stream draining a supraglacial catchment was chosen for meltwater sample collection which was carried out at the same site each time, as well as the assessment of hydrological stream parameters (see Figure 5.2a and b). Shallow ice cores were also taken in a transect up the catchment using an ice screw thrice cleaned with meltwater; additional opportunistic samples were also collected.

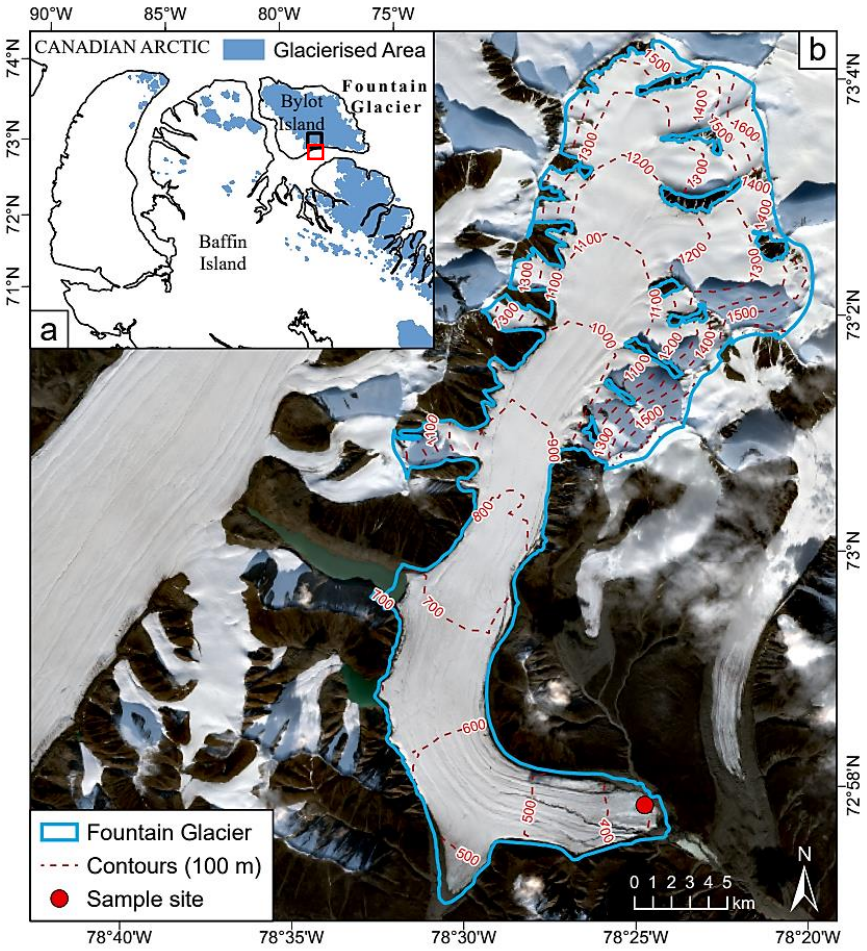

Figure 5.1. (a) Location of Fountain Glacier in the Canadian Arctic on Bylot Island; **(b)** approximate glacier extent of Fountain Glacier shown using a background Sentinel-2 image sourced from QGIS with an acquisition date of 31 August 2021. Glacier outline data is from the Randolph Glacier Inventory 6.0. Elevation data acquired from Esri ArcticDEM Explorer; glacier contours are at 100 m intervals.

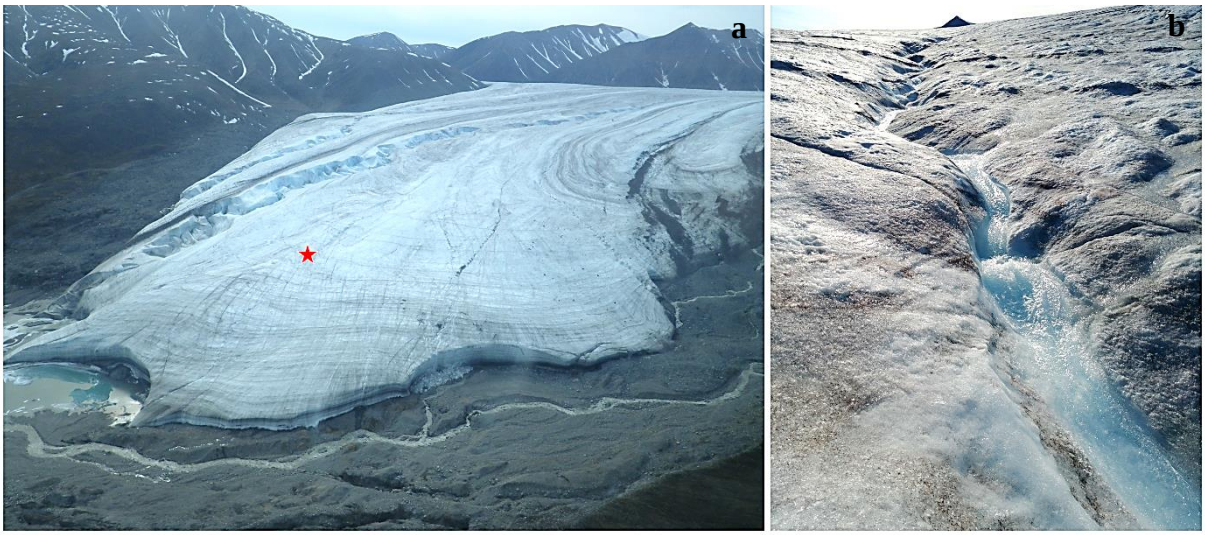

Figure 5.2. (a) View of the Fountain Glacier field site; **(b)** the chosen supraglacial study stream. The red star indicates the location of the study stream on the glacier. Photographs provided by T. Irvine-Fynn.

5.2.2 Hydrometeorological Data Collection and Processing

5.2.2.1 Meteorological Data

An automatic weather station (AWS) on Fountain Glacier at approximately 375 m above sea level (a.s.l) yielded hourly meteorological data for the study period 11 to 17 July 2019 (DOY 192-198). The AWS recorded short-wave incident radiation, wind speed, air temperature, and relative humidity. In order to estimate melt over the study period as a context for the supraglacial discharge on the surface of Fountain Glacier, a point-based surface energy balance model was employed (Brock and Arnold, 2000). Here, the model was applied at the location of the AWS at 375 m a.s.l, using an average albedo of 0.403, a Canadian Arctic ice aerodynamic roughness length of 0.0067 m after Brock et al. (2006), and the inclusion of the absolute vapour pressure (AVP) which was calculated using standard relationships between relative humidity and air temperature (after Irvine-Fynn et al., 2014).

During the study period of DOY 192-198, the AWS recorded a mean short-wave incident radiation of 203 W m^{-2}, with a range in values from 33 to 675 W m^{-2}. A mean wind speed of 1.57 m s^{-1} was also observed, and ranged from 0.65 to 4.98 m s^{-1}. The mean air temperature was observed as 8.9 °C, ranging from 5.6 to 12.1 °C. Finally, a mean relative humidity of 75.2 % was recorded, and ranged from 62.4 to 90.8 %. The mean estimated melt ascertained from a point-based surface energy balance model was found to be 1.2 mm h^{-1}. Clearly between DOY 192-198, there are as expected, peaks and troughs in short-wave incident radiation whereby at midnight there is minimal short-wave incident radiation due to it being dark, compared with the daylight hours where short-wave incident radiation is at its highest (Figure 5.3a). The highest short-wave incident radiation occurred on DOY 196, closely followed by DOY 192, and the lowest instances of short-wave incident radiation seen on DOY 193 and 195 (Figure 5.3a). The wind speed observed over the study period shows sharp instances of high and then low wind speeds, with DOY 194 experiencing the highest wind speed (Figure 5.3b). The air temperature appears to show a slight decrease in trend from DOY 192-198; again with peaks in air temperature more prominent during daylight hours (Figure 5.3c). Relative humidity can be seen to present a slight upward trend over the study period, but still with evident peaks and troughs (Figure 5.3d). Finally, the estimated modelled melt for Fountain Glacier over the study period likewise experiences peaks during the day and troughs at night (Figure 5.3e), thus following a similar trend to that of the short-wave incident radiation with equally low melt occurring on DOY 193 and 195, with DOY 196 appearing to have the highest instance of melt over the 192-198 study period.

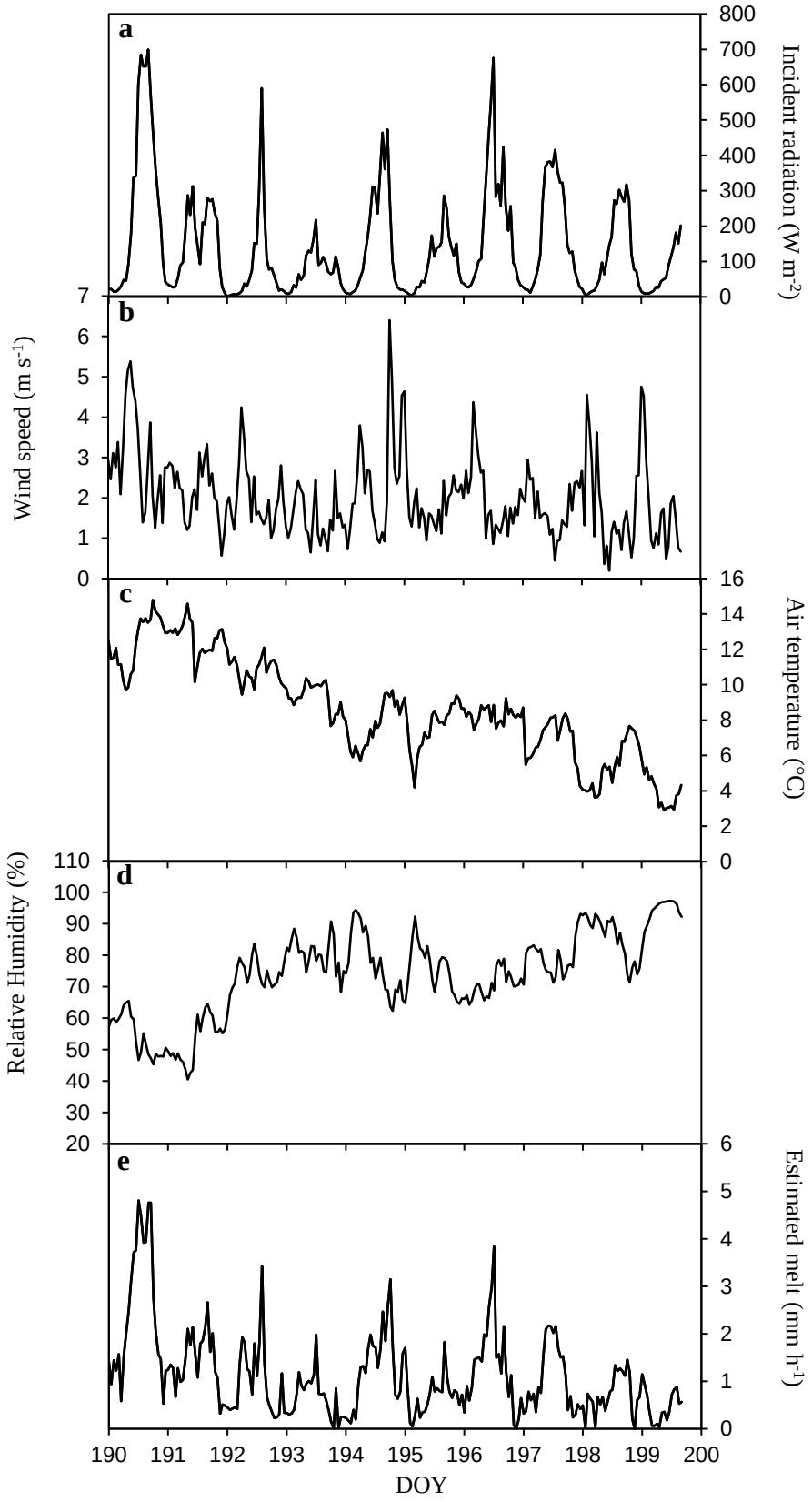

Figure 5.3. Time-series showing meteorological data collected at the AWS on Fountain Glacier: **(a)** short-wave incident radiation; **(b)** wind speed; **(c)** air temperature; **(d)** relative humidity, and **(e)** estimated melt.

5.2.2.2 Hydrological Stream Data

The hydrological data for the Fountain Glacier supraglacial stream in this investigation includes estimated discharge, electrical conductivity (EC), pH, and stream temperature. The salt dilution gauging method was used to estimate the discharge of the study stream, whereby 50 mL of supraglacial water and 10 g of salt were used to make up a dissolved salt tracer solution which was then injected 20-25 m upstream of the sample site. The EC and stream temperature were logged using a Reed Instruments SD-4307 conductivity meter with a stated accuracy of ± 2 %. A Hanna Instruments HI-98129 compact water quality probe with a relative instrumental accuracy of ± 0.05 was used to record pH. Stream temperature and pH were recorded before carrying out the salt dilution gauging method. All probes were calibrated before data collection in the field. However, with knowledge that pH measurements can 'drift' over time, a laboratory simulation was applied here to estimate a maximum pH drift uncertainty of ± 0.35 for the six day study period from DOY 192-198. Stream discharge was determined with a probabilistic uncertainty of ± 10 %.

For this investigation, the mean estimated discharge from the observations over the study period of DOY 192-198 was found to be 0.012 $m^3 s^{-1}$, ranging from 0.003 to 0.032 $m^3 s^{-1}$. The mean EC was recorded at 1.8 µS cm^{-1}, with a range of 1.3 to 4.3 µS cm^{-1}. Additionally, the mean recorded pH was found to be a nearly neutral 6.0, but ranging from a more acidic 4.6 to a more alkaline 8.3. Finally, the mean temperature of the Fountain Glacier supraglacial study stream was recorded at 0.4 °C, and ranged between the temperatures of 0.2 to 0.9 °C. Estimated discharge presented (Figure 5.4a), appears to show larger ranges in discharge for the DOY 192 and 193 compared to the other days of the study period, with discharge reaching its maximum peak on DOY 192, but its lowest record on DOY 195. Furthermore, the stream discharge appropriately appears to experience peaks during midday compared to at night when the discharge drops coinciding with similar peaks and troughs as seen for short-wave incident radiation and estimated melt (Figure 5.3a and e, respectively). The measurements for EC over the entire study period are consistent except for DOY 193 which experiences the highest peak EC reading (Figure 5.4b). The recorded pH values for the supraglacial study stream appear to remain fairly consistent fluctuating between 5.0 and 7.0, but there are instances where the pH peaked towards a more alkaline nature on DOY 192 (Figure 5.4c). Additionally, the pH dropped and became more acidic in nature on DOY 196. Lastly, the stream temperature appears to exhibit similar fluctuations to that of pH, with fluctuations between 0.2 and 0.5 °C remaining broadly stable, but with the highest peak stream temperature reached on DOY 192.

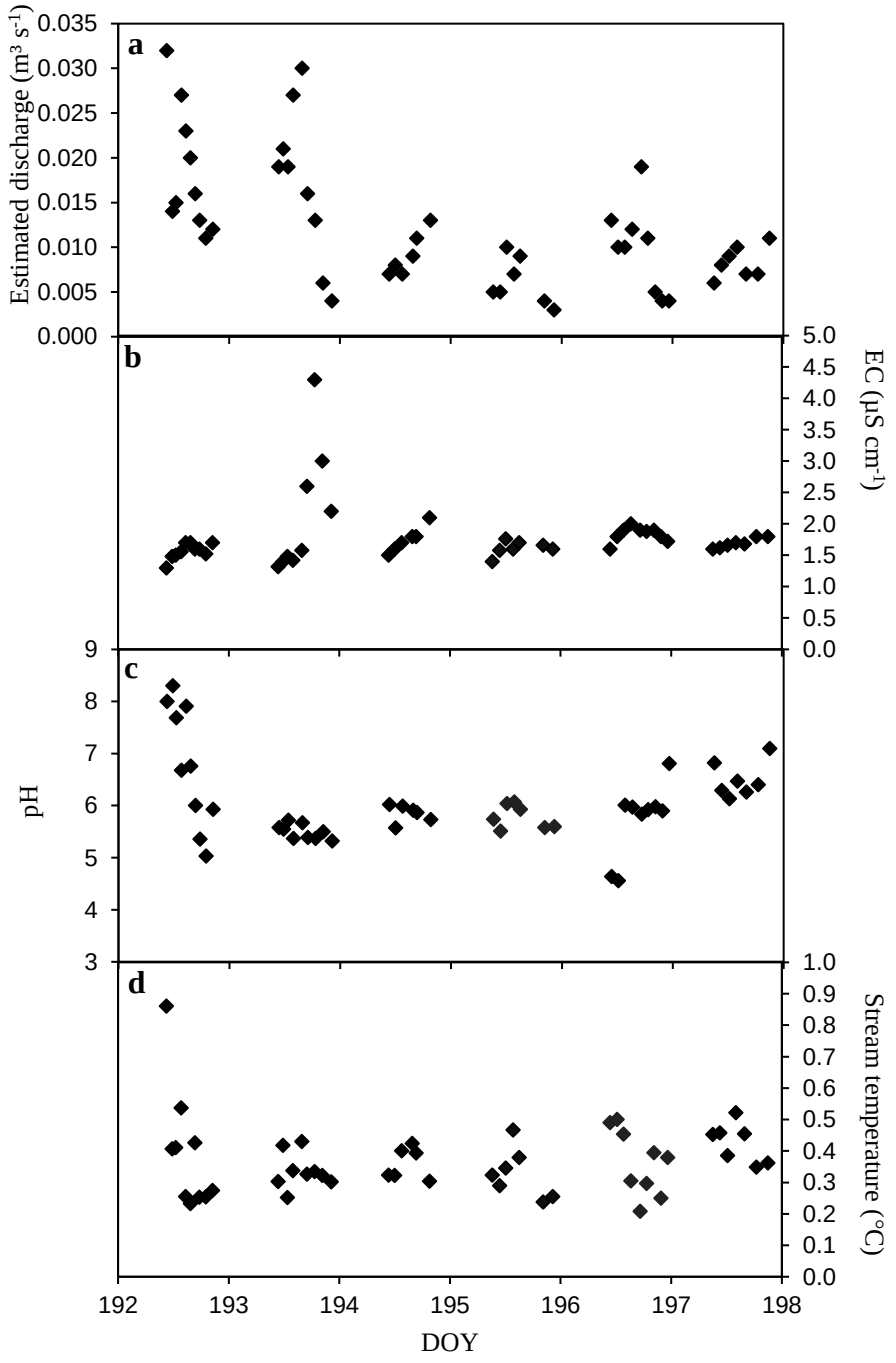

Figure 5.4. Time-series showing hydrological streamflow data collected on Fountain Glacier: **(a)** estimated discharge; **(b)** EC; **(c)** pH, and **(d)** stream temperature.

5.2.2.3 Hydrometeorological Data Associations

In order to determine whether there are significant relationships between streamflow hydrological data and meteorological data, it was first important to establish whether the data followed a normal distribution. This assessment was carried out using the Anderson Darling normality test with the knowledge that data with a significance level of more than 0.05 are classed as normally distributed. As a result of the normality testing, the appropriate non-parametric statistical test of Spearman's Rank Correlation Coefficient (r_s) was selected as there were instances were one or both data sets to be

correlated were non-normally distributed. It is important to note that the meteorological data was recorded every hour compared to the hydrological stream data which had measurement times that varied. Therefore, in order to correlate consistently between the meteorological and respective hydrological data, the meteorological data was paired with the appropriate hydrological data variables, and cell data (see Section 5.2.4), using the preceding hour. For example, a 10:30 hydrological data measurement was paired with a 10:00 meteorological data variable thus establishing consistency within correlation analyses and treatment of data.

Statistical analyses of the key hydrometeorological data, and shown in Table 5.1, presents a positive correlation between short-wave incident radiation and estimated melt at a significant $p < 0.001$ value; an expected result being that short-wave incident radiation is the primary driver of melt on the surface of glaciers. Interestingly, other statistically significant correlations were identified, such as short-wave incident radiation and stream temperature showing a positive correlation at a statistical significance of $p = 0.013$. Another correlation can also be seen between air temperature and estimated discharge with a positive correlation at a statistical significance of $p < 0.001$. Additionally, air temperature also negatively correlates with EC at a p-value of 0.041, as well as estimated discharge negatively correlating with EC at $p = 0.023$. Lastly, melt can be seen to positively correlate with stream temperature at a statistical significance of $p = 0.017$, and stream temperature correlate with pH ($p = 0.033$).

Table 5.1. Summary table of associations found between key Fountain Glacier hydrological and meteorological data variables, whereby Spearman's Rank Correlation Coefficient (r_s) values are shown for the correlations in the lower portion of the matrix table, and the p-values shown in the upper portion of the matrix table. Statistically significant relationships are bold and italicised for clarity.

	Short-wave incident radiation	**Air temp.**	**Estimated melt**	**Estimated discharge**	**EC**	**Stream temp.**	**pH**
Short-wave incident radiation		p = 0.206	***p < 0.001***	p = 0.533	p = 0.916	***p = 0.013***	p = 0.166
Air temp.	-0.178		p = 0.766	***p < 0.001***	***p = 0.041***	p = 0.233	p = 0.417
Estimated melt	***0.892***	-0.042		p = 0.225	p = 0.279	***p = 0.017***	p = 0.181
Estimated discharge	0.088	***0.670***	0.171		***p = 0.023***	p = 0.309	p = 0.999
EC	-0.015	***-0.285***	-0.153	***-0.316***		p = 0.207	p = 0.974
Stream temp.	***0.343***	-0.168	***0.330***	0.144	-0.178		***p = 0.033***
pH	0.195	-0.115	0.188	-0.0002	-0.005	***0.297***	

5.2.3 Microbe Enumeration and Size Distribution Results

Meltwater samples from the supraglacial study stream were also collected on DOY 192-198 before the salt dilution gauging and other hydrological data measurements were taken. Once the 10 mL meltwater samples were collected and kept dark and cold in a cool-bag on the ice but in the shade, they were fixed with 2 % w/v final concentration of glutaraldehyde within 12 hours, stored cold, and then frozen at -80 °C on return to the UK. The Fountain Glacier meltwater samples from the supraglacial study stream, weathering crust, shallow (15 cm) ice cores, and additional opportunistic samples, have been enumerated using the FCM SOP outlined in Section 3.2.2.

A mean microbial abundance of 1.16×10^4 cells mL^{-1} was found in the study stream, and ranged between 0.50 and 2.70×10^4 cells mL^{-1} from the observations over the study period of DOY 192-198. Higher microbial abundance can be seen around midday in the stream, but the abundance of microbes across the study period remained broadly consistent (Figure 5.5). In comparison, weathering crust surface ice samples presented the highest mean abundance of 1.77×10^4 cells mL^{-1}, ranging between 0.60 and 3.80×10^4 cells mL^{-1} (Table 5.2). Cryoconite holes and shallow ice core meltwater presented very similar mean microbe abundances at 0.91×10^4 cells mL^{-1} (ranging between 0.57 and 1.90×10^4 cells mL^{-1}) and 0.92×10^4 cells mL^{-1} (ranging between 0.50 and 2.10×10^4 cells mL^{-1}), respectively (Table 5.2). Here, Pairwise Mann-Whitney U-tests were applied to assess whether any significant differences existed between the microbe abundances of these supraglacial habitats, especially since most of the microbial abundance data sets to be tested were non-normally distributed. It was found, using the events per mL, that only the weathering crust surface ice and shallow ice cores presented microbial abundances that were significantly different from one another ($U = 22$, $p = 0.033$), with the microbial abundances for the other supraglacial habitats therefore deemed as similar. Furthermore, the mean microbial abundances were also used to estimate meltwater equivalent mean cellular carbon content (Table 5.2). Additionally, when looking more closely at the average relative percentage abundance of microbes within each size fraction for the different supraglacial habitats, it is clear that the highest relative abundance of cells is of the size ≤ 1 µm for the stream (37.00 %), cryoconite hole (45.29 %), and shallow ice core meltwaters (43.10 %); with the second highest abundance of cells found within the 2-4 µm size fraction for these habitats (Table 5.2). However, the opposite is true for the weathering crust surface ice whereby the highest relative abundance of cells are of the size 2-4 µm (38.18 %), with the second highest abundance of cells found within the ≤ 1 µm size fraction (Table 5.2). Finally, using the method described by Irvine-Fynn et al. (2012) (following Tranter et al., 2002), a linear regression model between estimated discharge and cell flux was constructed (see Appendix 3). Such a model allowed for a robust estimate of mean cell flux due to a resulting linear equation. Here, the mean discharge of 0.012 $m^3 s^{-1}$ was simply entered into the equation of the best fit line and revealed an estimated mean microbial flux of 5.46×10^{11} cells h^{-1} for the Fountain Glacier study stream.

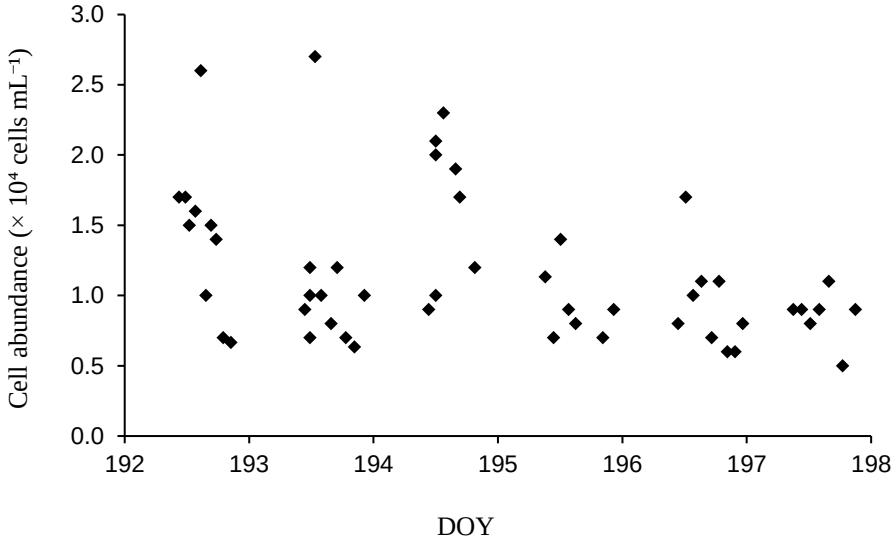

Figure 5.5. Time-series showing the FCM microbe enumerations of the study stream meltwater samples from Fountain Glacier.

Table 5.2. Mean microbe abundance for Fountain Glacier meltwater samples taken from the active supraglacial study stream and additional opportunistic samples; with estimated meltwater equivalent (w.e.) mean cellular carbon content based on the mean cell abundances for each supraglacial source. Accompanying average relative percentage abundance distributions in each size fraction are also presented. Standard deviation included in brackets as ± 1 SD.

Source	**Stream**	**Surface weathering crust ice**	**Cryoconite hole supernatant**	**Shallow ice cores**
Samples (*n*)	52	7	6	15
Mean microbe abundance ($\times 10^4$ cells mL^{-1})	1.16 (± 0.52)	1.77 (± 1.11)	0.91 (± 0.49)	0.92 (± 0.46)
Estimated mean cellular carbon (kg C m^{-3} w.e.)	2.32×10^{-7}	3.53×10^{-7}	1.82×10^{-7}	1.84×10^{-7}
Average relative abundance (%)				
≤ 1 µm	37.00	35.44	45.29	43.10
1-2 µm	11.82	11.09	11.57	11.91
2-4 µm	36.82	38.18	31.09	33.73
4-6 µm	8.62	9.93	6.65	6.59
6-10 µm	4.12	4.11	3.75	3.17
10-15 µm	1.15	0.86	1.09	0.97
> 15 µm	0.48	0.39	0.56	0.52

5.2.4 Compiled Hydrometeorological and Microbe Data Associations

The non-parametric statistical test of Spearman's Rank Correlation Coefficient was again used to determine whether there were statistically significant associations between the hydrometeorological data and stream microbe enumerations, since most of the data sets to be correlated were non-normally distributed. Such statistical analyses found that there were significant positive correlations between short-wave incident radiation and microbe abundance ($r_s = 0.343$, $p = 0.013$) (Figure 5.6a); melt and microbe abundance ($r_s = 0.471$, $p = 0.0004$) (Figure 5.6b); and finally, discharge and microbe abundance ($r_s = 0.321$, $p = 0.020$) (Figure 5.6c). Interpretation and discussion of such results and correlations in this section will be presented in Section 5.5.1.

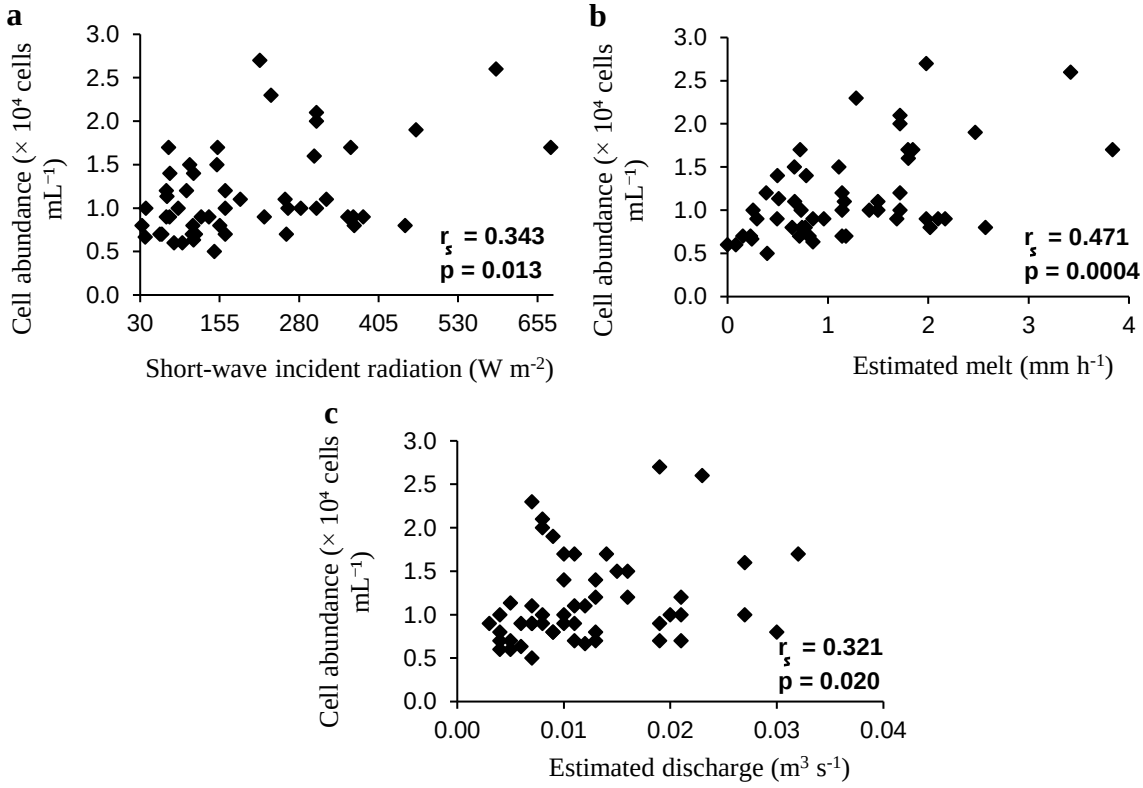

Figure 5.6. Scatter plot associations for Fountain Glacier showing the supraglacial stream microbial cell abundances against hydrometeorological variables: **(a)** short-wave incident radiation; **(b)** estimated melt, and **(c)** estimated discharge.

5.3 Foxfonna, Svalbard

5.3.1 Background

Foxfonna is an Arctic valley glacier ice cap located in western Svalbard, Norway (78.14° N, 16.17° E) (Figure 5.7). Foxfonna measures at approximately 5 km^2 and 2.9 km in length (Alexander et al., 2020), with the ice cap dome typically experiencing melt for a short period of approximately 45 days over summer (Gokul et al., 2016). During such summer ablation periods, a network of supraglacial channels

develops on the surface of Foxfonna Glacier (Alexander et al., 2020). During 2007 to 2014, Foxfonna Glacier experienced an average annual negative surface mass balance of -0.25 ± 0.36 m w.e. a^{-1} (Rutter et al., 2011; Gokul et al., 2016), with such variability in mass balance being the result of occasional years experiencing positive mass balances, such as in 2008 and 2012 (Gokul et al., 2016). This Arctic ice cap is cold, but Lower Foxfonna is polythermal, and a transient ice surface that reaches the pressure melting point during the summer ablation season (Koziol et al., 2019). For this investigation on Foxfonna Glacier, a main single-channel stream draining a supraglacial catchment was chosen for meltwater sample collection, as well as additional opportunistic supraglacial stream meltwater samples, whilst also assessing hydrological stream parameters (see Figure 5.8a and b).

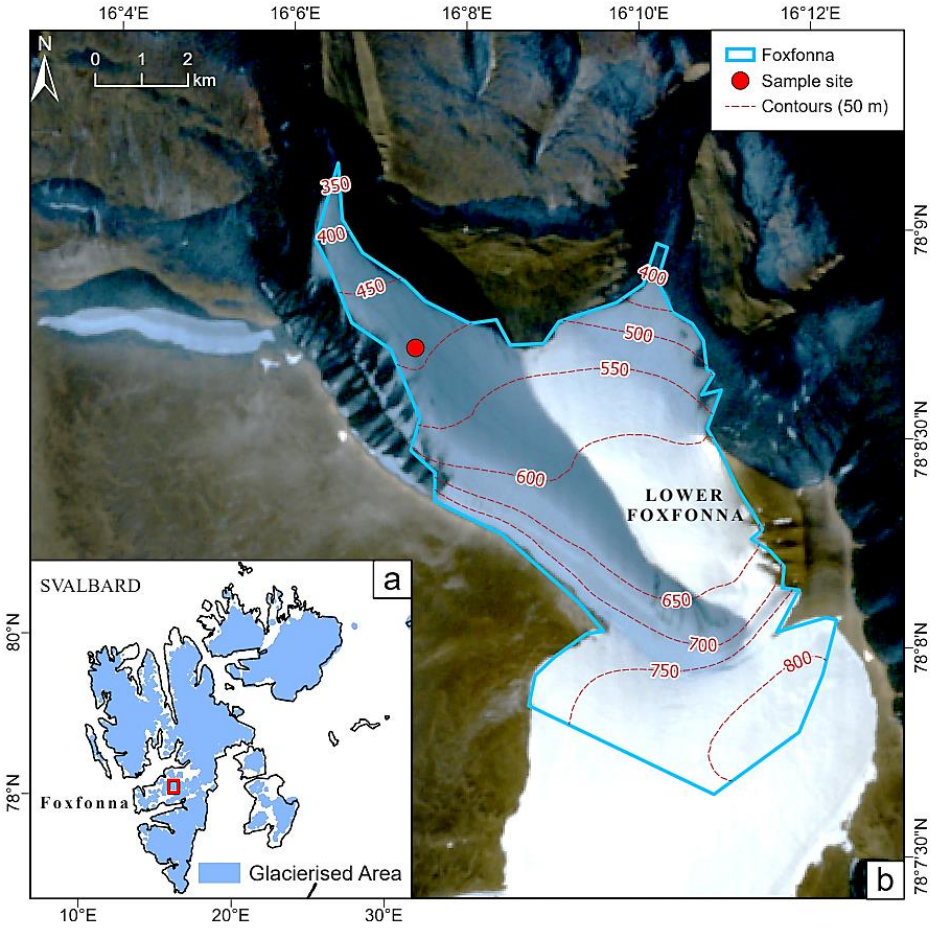

Figure 5.7. (a) Location of Foxfonna in the Norwegian archipelago of Svalbard; **(b)** approximate extent of Lower Foxfonna Glacier shown using a background Sentinel-2 image sourced from QGIS with an acquisition date of 11 September 2021; where the study stream can be found. Elevation data acquired from Norwegian Polar Institute; glacier contours are at 50 m intervals.

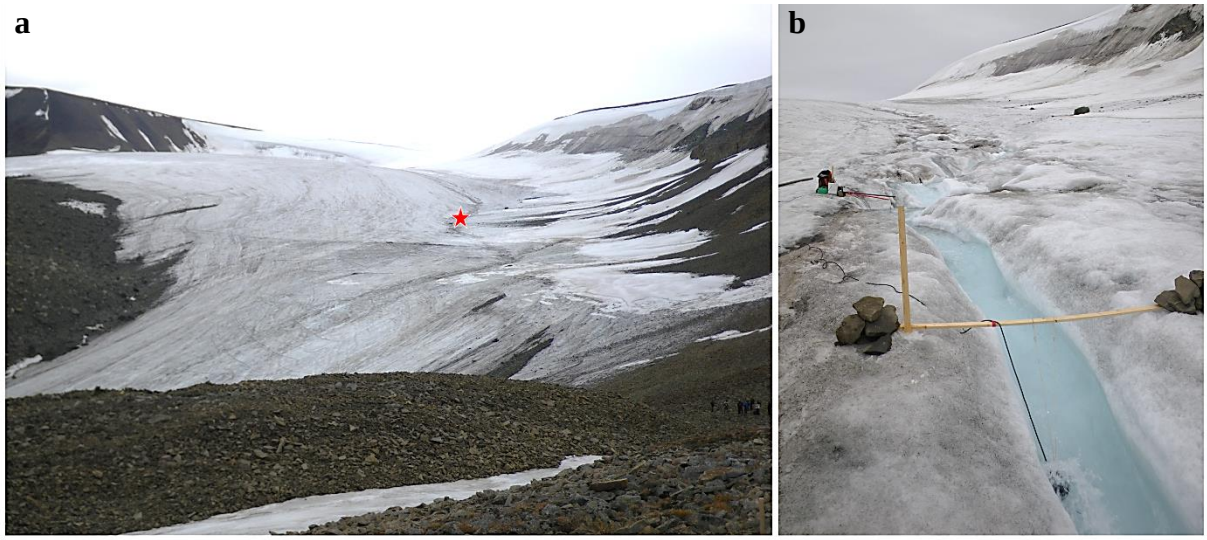

Figure 5.8. (a) View of the Foxfonna Glacier field site; **(b)** the chosen supraglacial study stream. The red star indicates the location of the study stream on the glacier. Photographs provided by T. Irvine-Fynn.

5.3.2 Hydrometeorological Data Collection and Processing

5.3.2.1 Meteorological Data

An AWS on Foxfonna Glacier at approximately 600 m a.s.l yielded hourly meteorological data for the study period 3 July to 27 August 2011 (DOY 184-239). Like in Section 5.2.2.1, a point-based surface energy balance model was again employed (Brock and Arnold, 2000) in order to estimate melt over the study period. The model was applied at the location of the AWS, using a spatio-temporal mean value for albedo of 0.4 after Irvine-Fynn et al. (2022) which reports albedo ranging between 0.25 and 0.8 for Foxfonna; a Polar glacier ice aerodynamic roughness length of 0.00065 m after Brock et al. (2006), and the inclusion of the AVP, calculated using standard relationships between relative humidity and air temperature (after Irvine-Fynn et al., 2014).

During the study period of DOY 184-239, the AWS recorded a mean short-wave incident radiation of 193 W m^{-2}, with a range in values from 0 to 532 W m^{-2}. A mean wind speed of 1.24 m s^{-1} was also recorded, and ranged from 0.09 to 4.87 m s^{-1}. The mean air temperature was recorded as 3.0 °C, ranging from -0.9 to 8.7 °C. Finally, a mean relative humidity of 85.0 % was recorded, and ranged from 64.8 to 96.5 %. The mean estimated melt ascertained from a point-based surface energy balance model was found to be 0.86 mm h^{-1}. It is clear that the peaks and troughs in short-wave incident radiation (Figure 5.9a) and the estimated melt (Figure 5.9e) follow a similar trend across the field study period; an expected observation due to the primary driving properties of short-wave incident radiation on ablation at the surface of glaciers. The wind speed over the study period equally experienced consistent fluctuations with the highest wind speed observed on DOY 230, but with higher wind speeds overall

experienced from DOY 222 onwards (Figure 5.9b). Greater positive air temperatures appeared towards DOY 226 onwards, but instances of negative air temperatures also occurred, particularly between DOY 222 and 226 (Figure 5.9c). Relative humidity consistently fluctuated between 60.0 and 100.0 % across the study period, with the lowest relative humidity occurring on DOY 230 (Figure 5.9d).

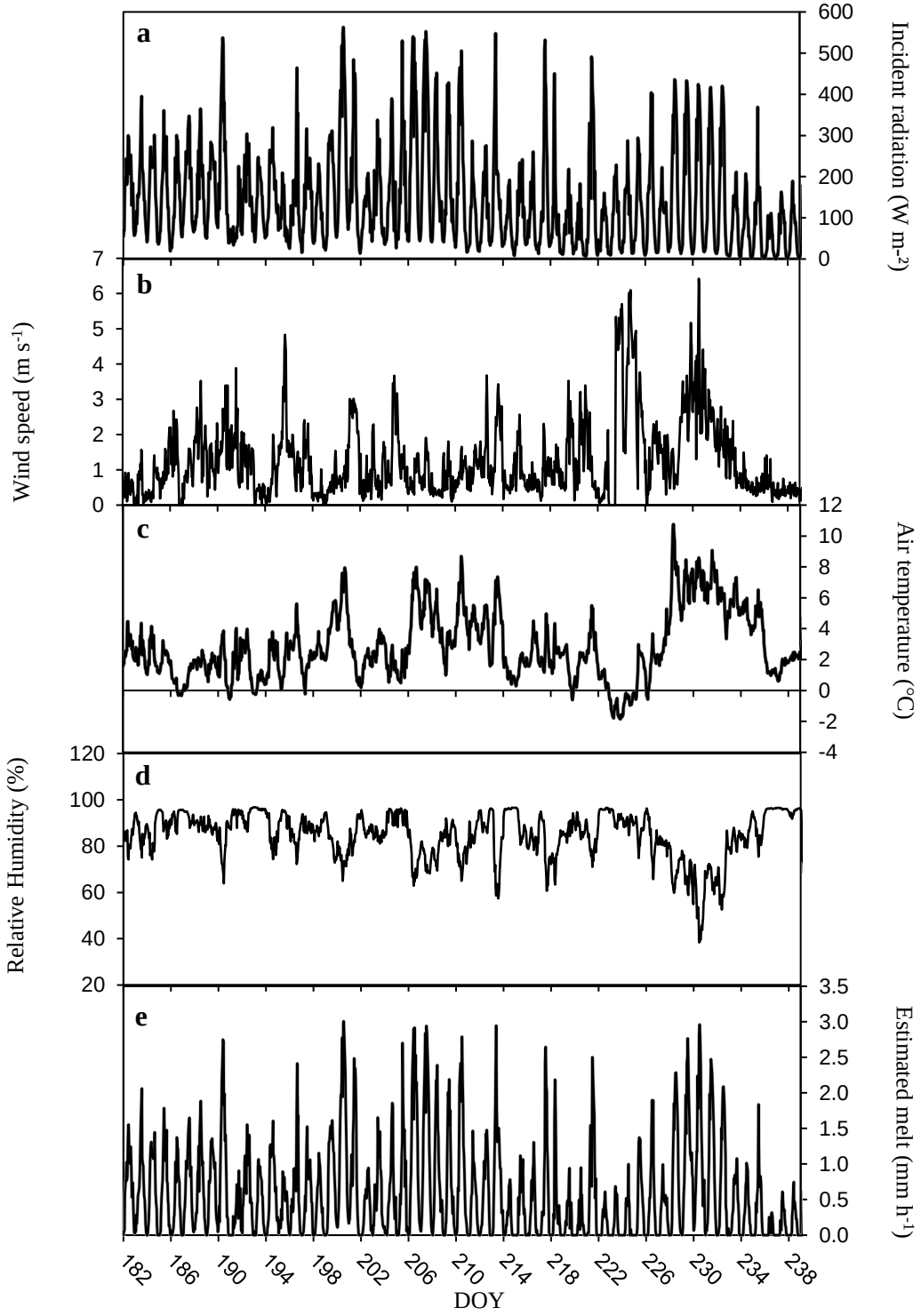

Figure 5.9. Time-series showing meteorological data collected at the AWS on Foxfonna Glacier: **(a)** short-wave incident radiation; **(b)** wind speed; **(c)** air temperature; **(d)** relative humidity, and **(e)** estimated melt.

5.3.2.2 Hydrological Stream Data

The hydrological data collected from the Foxfonna supraglacial study stream in this investigation includes estimated discharge, EC and stream temperature. The salt dilution gauging method was used to estimate the discharge of the study stream, whereby 50 mL of supraglacial water and 10 g of salt were used to make up a dissolved salt tracer solution which was then injected 15-20 m upstream of the sample site. The EC and stream temperature were measured using a CS-547A probe attached to a Campbell Scientific CR1000 data logger, with a stated accuracy in EC and temperature of ± 5 % and ± 0.2 ºC, respectively. Stream temperature was recorded before carrying out the salt dilution gauging method. All probes were calibrated before data collection in the field. Stream discharge was determined with a probabilistic uncertainty of ± 10 %. However, it is important to note that the EC data presented within this section is an incomplete record due to a change in the EC logger during data collection, in which the second EC logger used had a reduced sensitivity thus rendering any EC data with this EC probe hereafter unreliable (anomalous). As a result, a best estimate for discharge data has been displayed in this section as a 'complete' record for discharge, albeit not for all of the stream samples collected due to the limited EC data. Finally, three anomalies were identified within the Foxfonna Glacier estimated discharge data, and then two for stream temperature data due to the probe not having stabilised in the field during data collection. Subsequently, the results presented in this section exclude such anomalous data.

The mean estimated discharge was found to be 0.188 $m^3 s^{-1}$, ranging from 0.034 to 0.385 $m^3 s^{-1}$ from the observations over the study period of DOY 184-239. The mean EC of the data that was able to be collected was recorded as 8 µS cm^{-1}, with a range of 2.3 to 12.1 µS cm^{-1}. Finally, the mean temperature of the Foxfonna Glacier supraglacial study stream was recorded at 0.06 °C, and ranged between the temperatures of -0.08 to 0.6 °C. However, it is important to note again the stream temperature accuracy of ± 0.2 ºC here meaning the sub-zero temperatures are within the stated accuracy. Estimated discharge experiences a wider range in values from DOY 208 towards the end of the study period (Figure 5.10a), but it is important to reiterate that the data for discharge here is not continuous and showing diurnal discharge values, but instead singular discharge measurements for each day, thus making it difficult to see a trend of diurnal discharge over the study period. From the EC data that is available, brief observations could be made that EC appears to decrease from DOY 184 to 198 (Figure 5.10b). Supraglacial stream temperature for the period 184-239, appears to remain consistent between -0.1 and 0.2 °C, but presented peaks in temperature on DOY 184, 201 and 202 (Figure 5.10c).

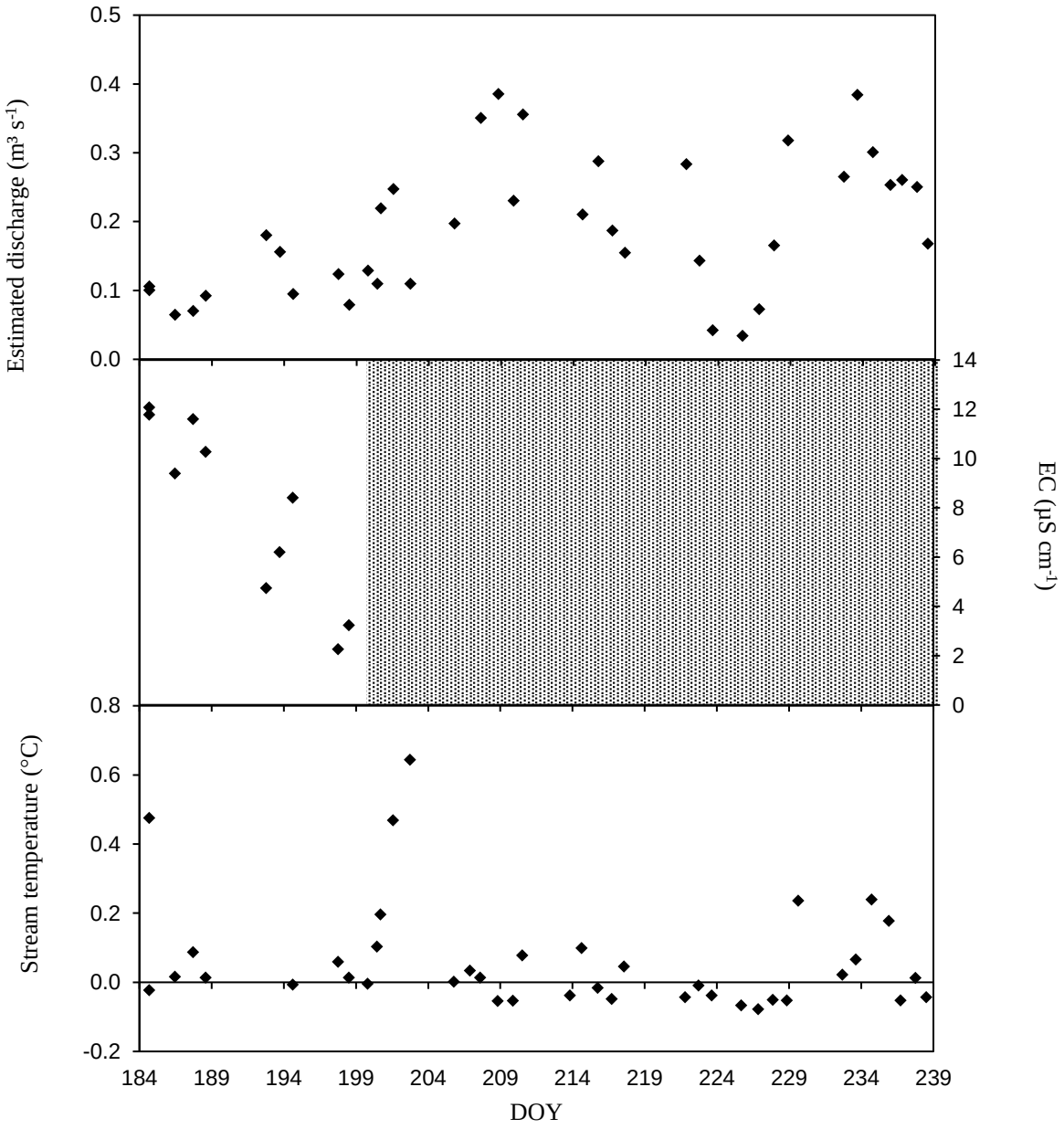

Figure 5.10. Time-series showing hydrological streamflow data collected on Foxfonna Glacier: **(a)** best estimated discharge; **(b)** incomplete EC, and **(c)** stream temperature. Note that the recorded EC data presented is incomplete due to a change in EC loggers, with the second EC logger having a reduced sensitivity and so subsequent anomalous data hereafter.

5.3.2.3 Hydrometeorological Data Associations

To determine the statistically significant associations between streamflow hydrological data and meteorological data for this study site, the data were assessed regarding their normality distribution. The Anderson Darling normality test was again employed with the knowledge that data with a significance level of more than 0.05 are classed as normally distributed. As a result of the normality testing, the appropriate non-parametric statistical test of Spearman's Rank was selected due to instances were one or both data sets to be correlated were non-normally distributed, as well as the parametric test of

Pearson's Correlation Coefficient for correlating EC and discharge which presented normally distributed data. Like stated in Section 5.2.2.3, the meteorological data was recorded every hour compared to the hydrological stream data which had measurement times that varied. Thus, to keep consistency in the treatment of data and correlation analyses, hydrological data have been paired with equivalent meteorological data based on the preceding hour of their data collection times where necessary.

Statistical analyses of the key hydrometeorological data, and shown in Table 5.3, presents a clear positive correlation between short-wave incident radiation and estimated melt at a significant $p < 0.001$ value. Other statistically significant correlations include short-wave incident radiation and air temperature with a positive correlation at a p-value of 0.029, as well as short-wave incident radiation and stream temperature with a positive correlation at a significant p-value < 0.001. Furthermore, air temperature can be seen to positively correlate with estimated melt and discharge with p-values of 0.003 and 0.011, respectively. Finally, melt and stream temperature also present a positive correlation at a statistical significance of $p < 0.001$.

Table 5.3. Summary table of associations found between key Foxfonna Glacier hydrological and meteorological data variables, whereby Spearman's Rank Correlation Coefficient (r_s), and Pearson's Correlation Coefficient (r) value for EC against discharge only, are shown for the correlations in the lower portion of the matrix table, and the p-values shown in the upper portion of the matrix table. Statistically significant relationships are bold and italicised for clarity.

	Short-wave incident radiation	**Air temp.**	**Estimated melt**	**Estimated discharge**	**EC**	**Stream temp.**
Short-wave incident radiation		***p = 0.029***	***p < 0.001***	p = 0.462	p = 0.154	***p < 0.001***
Air temp.	***0.333***		***p = 0.003***	***p = 0.011***	p = 0.713	p = 0.244
Estimated melt	***0.973***	***0.445***		p = 0.655	p = 0.266	***p < 0.001***
Estimated discharge	-0.127	***0.421***	-0.077		p = 0.191	p = 0.828
EC	0.486	-0.134	0.389	-0.451		p = 0.977
Stream temp.	***0.587***	0.197	***0.573***	0.037	-0.024	

5.3.3 Microbe Enumeration and Size Distribution Results

Meltwater samples were collected from the supraglacial study stream, as well as additional opportunistic

supraglacial stream meltwater samples from a transect of the same study stream, before the salt dilution gauging and other hydrological data measurements were taken on DOY 184-239, but such meltwater samples were not fixed and instead stored at -80 °C before FCM analyses; following the FCM SOP outlined in Section 3.2.2.

A mean of 0.72×10^4 cells mL^{-1} for the supraglacial study stream was found, and ranged between 0.27 and 2.0×10^4 cells mL^{-1} from the observations over the study period DOY 184-239, with the opportunistic supraglacial stream meltwater samples yielding a mean of 5.44×10^4 cells mL^{-1}, ranging between 0.2 and 28.30×10^4 cells mL^{-1}. Clearly there was a higher abundance of cells in the opportunistic supraglacial meltwater samples. All microbe abundance values across the study period appear to stay consistent between 0.2 and 1.0×10^4 cells mL^{-1}, with peak cell abundances occurring on DOY 184, 209, and 236 towards the end of the study period (Figure 5.11). Here, the Mann-Whitney U-test was applied to assess whether a significant difference existed between the microbe abundances of the study stream and opportunistic supraglacial meltwater samples, especially since both data sets to be tested were non-normally distributed. It was found, using the events per mL, that the microbial abundances were not significantly different from one another and therefore similar ($U = 206.5$, $p = 0.459$). Again, the mean microbial abundances were also used to estimate meltwater equivalent mean cellular carbon content (Table 5.4). Looking more closely at the average relative percentage abundance of microbes within each size fraction for the supraglacial stream and opportunistic samples, it is clear that the highest relative percentage abundance of cells are of the size 2-4 μm for the study stream (37.91 %) and opportunistic supraglacial meltwater samples (40.51 %). However, this result is closely followed by the ≤ 1 μm size fraction which presents the second highest abundance of cells, with a difference of 0.11 % in average relative percentage abundance between the 2-4 and ≤ 1 μm size fractions for the study stream (Table 5.4). Finally, an estimated mean microbial flux of 4.81×10^{12} cells h^{-1} in the Foxfonna Glacier supraglacial study stream was found by adopting the same method as previously described by Irvine-Fynn et al. (2012) (following Tranter et al., 2002), and so constructing a linear regression model between estimated discharge and cell flux (see Appendix 4), with the mean estimated discharge of 0.188 $m^3 s^{-1}$ used.

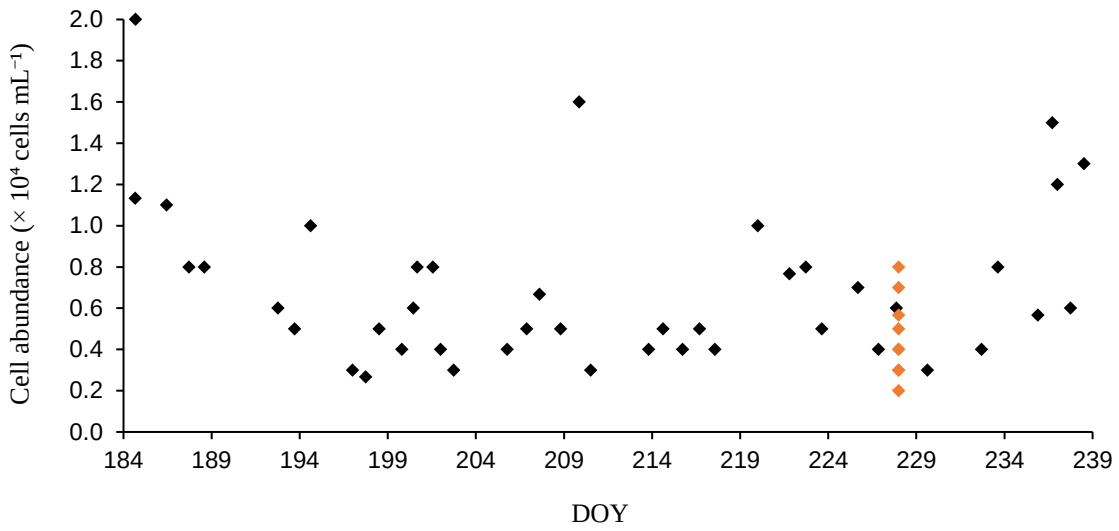

Figure 5.11. Time-series showing the FCM microbe enumerations of the Foxfonna Glacier study stream, with additional red dots representing the opportunistic supraglacial stream meltwater sample enumerations.

Table 5.4. Mean microbe abundance for Foxfonna Glacier meltwater samples taken from the active supraglacial stream and additional opportunistic supraglacial stream meltwater samples; with estimated meltwater equivalent (w.e.) mean cellular carbon content based on the mean cell abundances for each supraglacial source. Accompanying average relative percentage abundance distributions in each size fraction are also presented. Standard deviation included in brackets as ± 1 SD.

Source	**Stream**	**Opportunistic supraglacial stream meltwater samples**
Samples (*n*)	44	11
Mean microbe abundance ($\times 10^4$ cells mL^{-1})	0.72 (± 0.40)	5.44 (± 11.08)
Estimated mean cellular carbon (kg C m^{-3} w.e.)	1.43×10^{-7}	1.09×10^{-6}
Average relative abundance (%)		
≤ 1 µm	37.80	32.52
1-2 µm	13.06	12.68
2-4 µm	37.91	40.51
4-6 µm	6.91	8.78
6-10 µm	3.17	4.07
10-15 µm	0.84	1.02
> 15 µm	0.30	0.42

5.3.4 Compiled Hydrometeorological and Microbe Data Associations

The non-parametric statistical test of Spearman's Rank was again used here to determine whether there are statistically significant associations between the hydrometeorological data and the study stream microbe enumerations, due to instances were one or both data sets to be correlated were non-normally distributed. Despite the incomplete EC record, there was only a positive correlation found between EC and microbe abundance (r_s = 0.878, p = 0.0008). Interpretation and discussion of such results and correlations in this section will be presented in Section 5.5.1.

5.4 Exploring Cell Sample Degradation with Storage Length

All four of the glacier location sample sets, such as the Storglaciären (2014) samples explored back in Chapter 4 and the previously explored samples from Fountain Glacier (2019) and Foxfonna Glacier (2011) as shown in this Chapter 5, and the soon to be explored Midtre Lovénbreen (2010) samples, have all been archived and so subject to long-term storage at -80 ℃ for, in some instances, over 10 years. Such samples have likely experienced cell sample degradation with their storage duration and condition thus affecting microbe enumeration results; compared to otherwise freshly collected environmental glacier samples analysed at a field-site immediately after sample collection, or within a few months of being back at a laboratory. The concern presented here is that over time cells will degrade with storage, such as that observed in previous studies whereby bacterial cell counts obtained with SYBR Gold even decreased within 3 to 7 days by 7.3 to 31 %; despite having been stored at 4 ℃ and fixed with formaldehyde (Shibata et al., 2006). However, the long temporal storage of the four glacier location sample sets presents uncertainties in this investigation's microbial enumeration results. Therefore, additional experiments were devised to explore what impact storage length and the type of storage condition may have on microbe enumerations found within replicate aliquot samples taken from the most recently collected fixed Fountain Glacier samples, as well as the non-fixed Foxfonna Glacier samples (see Section 5.4.3). However, firstly a more readily available assessment of such a storage impact can be made by analysing the 2010 non-fixed Midtre Lovénbreen sample set for microbial abundance since such a sample set is in fact the same as that collected, analysed, and used for Irvine-Fynn et al. (2012). Therefore, a comparison between this investigation's Midtre Lovénbreen microbe data to that of the microbial abundance published in Irvine-Fynn et al. (2012) can be made to see how such long-term storage has impacted the cell samples.

5.4.1 An Example of Midtre Lovénbreen, Svalbard

Midtre Lovénbreen is an Arctic valley glacier located in north west Svalbard, Norway (78.88° N, 12.04° E) (Figure 5.12). This north flowing, land terminating valley glacier occupies a total area of 5 km^2, with an elevation ranging from 50 to 690 m a.s.l, and an average annual negative mass balance of -0.49 m w.e. a^{-1} over the temporal period 2000 to 2019 (Schuler et al., 2020). Midtre Lovénbreen has

experienced accelerated rates of ice mass loss, with thinning rates being four times larger for 2003 to 2005 compared to the average mass loss rate for the first measurement period of 1936 to 1962 (Schuler et al., 2020). The term polythermal can also be used to describe Midtre Lovénbreen due to the presence of a cold surface ice layer overlying a temperate ice zone. For the previous research investigation carried out on Midtre Lovénbreen, a single stream draining a supraglacial sub catchment was chosen for meltwater sample collection (see Figure 5.13a and b), as well as additional downstream opportunistic samples; with the assessment of hydrometeorological parameters also. However, for the purpose of this research section, only the microbial abundance data has been presented here and analysed to allow for a comparison with the microbe enumerations previously presented by Irvine-Fynn et al. (2012) for the same supraglacial stream samples on Midtre Lovénbreen collected in 2010.

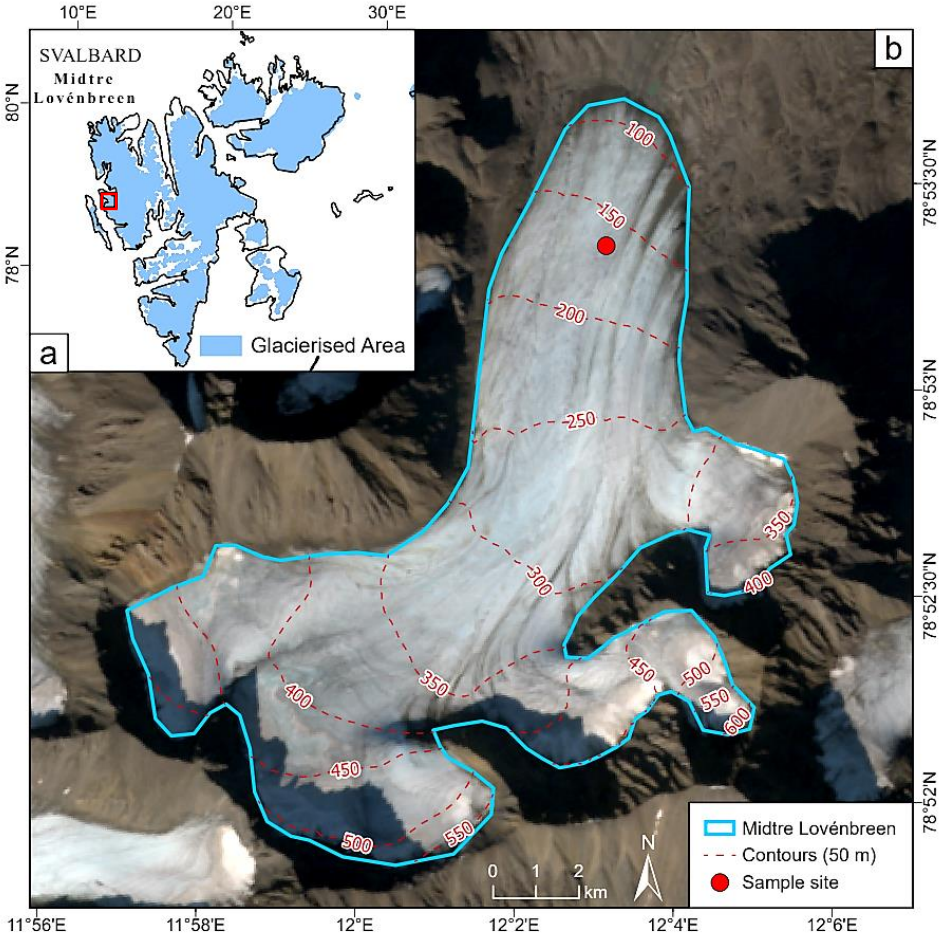

Figure 5.12. (a) Location of Midtre Lovénbreen in the Norwegian archipelago of Svalbard; **(b)** approximate glacier extent of Midtre Lovénbreen shown using a background Sentinel-2 image sourced from QGIS with an acquisition date of 31 July 2020. Elevation data acquired from Norwegian Polar Institute; glacier contours are at 50 m intervals.

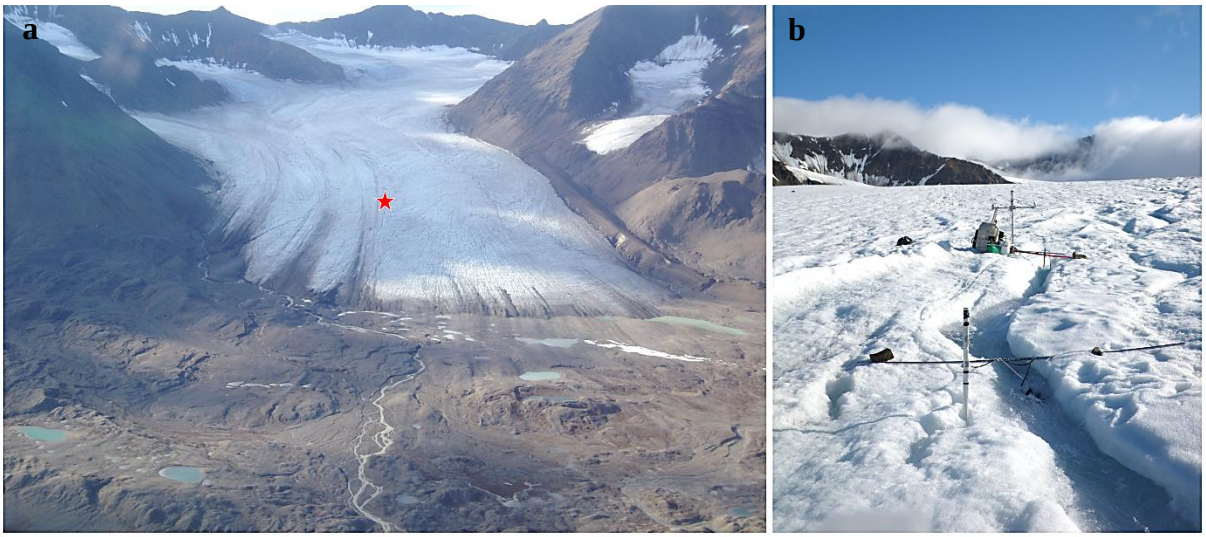

Figure 5.13. (a) View of the Midtre Lovénbreen field site; **(b)** the chosen supraglacial study stream. The red star indicates the location of the study stream on the glacier. Photographs provided by T. Irvine-Fynn.

5.4.2 Microbe Enumeration and Size Distribution Results

Meltwater samples from the supraglacial study stream were collected during the study period 15 July to 15 August 2010 (DOY 196-227), as well as additional samples from a downstream transect of the same stream (starting up-glacier and then down to the main sample collection site). Such samples were not fixed and so stored at -80 °C before FCM analyses. It is important to note that the microbe enumeration data presented in this section are the result of FCM analyses from only a select handful of meltwater samples from the same sample set used by Irvine-Fynn et al. (2012). Therefore, such analyses on the handful of samples following the FCM SOP outlined in Section 3.2.2 have provided a comparison to the microbe data presented in Irvine-Fynn et al. (2012), especially with the samples having been in storage for a long duration.

A mean of 0.20×10^4 cells mL^{-1} for the microbial abundance of the study stream was found, and ranged between 0.10 and 0.40×10^4 cells mL^{-1} from the observations over the study period of DOY 196-227, albeit only from a select handful of stream samples. Similarly, a mean of 0.14×10^4 cells mL^{-1} for the microbial abundance downstream transect of the study stream was found, and ranged between 0.10 and 0.20×10^4 cells mL^{-1} for the investigation period. Some of the highest abundances in microbes occurred on DOY 209, 218 and 227, but the majority in abundance of microbes across the study period remained fairly consistent between 0.15 and 0.25×10^4 cells mL^{-1} (Figure 5.14). Here, the Mann-Whitney U-test was again able to be applied to assess whether a significant difference existed between the microbe abundances of the study stream and opportunistic downstream transect meltwater samples, especially since both data sets to be tested were non-normally distributed. It was found, using the events per mL, that the microbial abundances were not significantly different from one another and therefore similar (U

= 30.5, p = 0.156). Additionally, when looking more closely at the average relative percentage abundance of microbes within each size fraction for the stream and downstream transect supraglacial microbes, it is clear that the highest relative percentage abundance of cells are of the size 2-4 µm for both the stream (38.45 %) and downstream transect (36.12 %) samples; with the second highest relative percentage abundance of cells found within the ≤ 1 µm size fraction for both (Table 5.5). A comparison of such results with that presented in Irvine-Fynn et al. (2012) will be explored in Section 5.5.2.

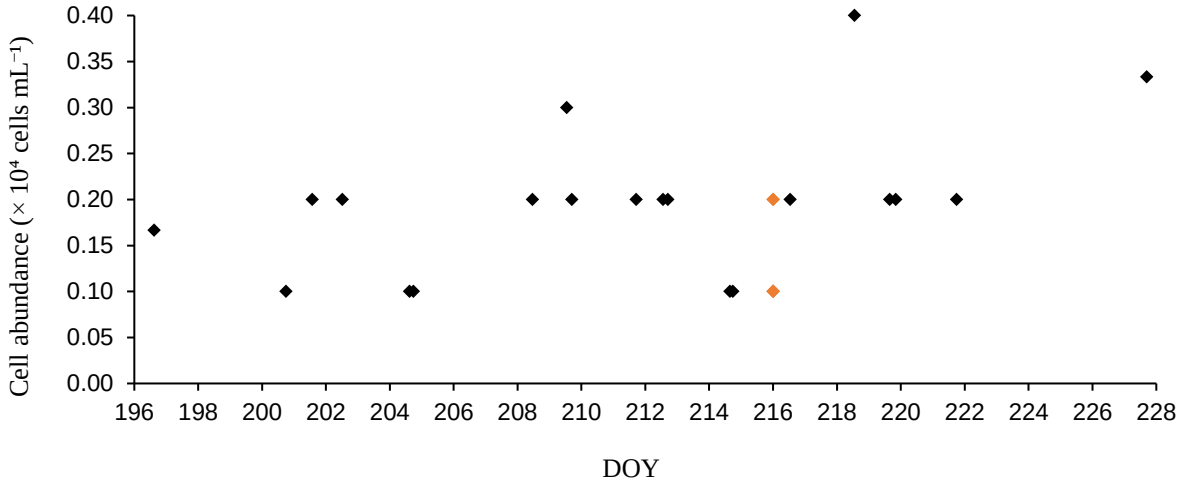

Figure 5.14. Time-series showing the FCM microbe enumerations of the study stream, with additional red dots representing downstream transect meltwater samples for comparison from Midtre Lovénbreen.

Table 5.5. Mean microbe abundance for Midtre Lovénbreen meltwater samples taken from the supraglacial study stream and downstream transect of the same stream for an additional comparison; with accompanying average relative percentage abundance distributions in each size fraction. Standard deviation included in brackets as ± 1 SD.

Source	Stream	Downstream transect
Samples (*n*)	20	5
Mean microbe abundance (× 10^4 cells mL^{-1})	0.20 (± 0.08)	0.14 (± 0.05)
Average relative abundance (%)		
≤ 1 µm	33.45	34.88
1-2 µm	13.03	11.19
2-4 µm	38.45	36.12
4-6 µm	8.33	8.88
6-10 µm	4.76	5.63
10-15 µm	1.40	2.16
> 15 µm	0.57	1.14

5.5 Interpretation and Discussion

5.5.1 High Arctic Hydrometeorological Assessments and Microbe Fluxes

For both high Arctic glacier locations of Fountain and Foxfonna Glacier, key hydrometeorological data were assessed and associations between such hydrometeorological data and microbe enumerations identified. For Fountain, an estimated mean discharge for the supraglacial study stream of 0.012 m^3 s^{-1} was found; similar to that observed in existing studies of supraglacial stream discharge, such as St Germain and Moorman (2016)'s discharge values ranging between 0.01 and 1.0 m^3 s^{-1}. Similarly, the estimated mean discharge of the supraglacial study stream on Lower Foxfonna was found to be 0.188 m^3 s^{-1}; similar to previously observed discharges observed in a proglacial channel in the adjacent Rieperbreen–Foxfonna catchment with discharge values of 0.16 m^3 s^{-1} and 0.22 m^3 s^{-1} (Rutter et al., 2011). Although not measured in the supraglacial study stream on Foxfonna, a mean pH measurement of 6.0, ranging between 4.6 and 8.3, was observed for the study stream on Fountain Glacier. This observation can be compared to an investigation previously carried out on a polythermal glacier in the Canadian Arctic- John Evans, whereby a median pH of 7.5, ranging between 6.4 and 8.1 was found for supraglacial stream meltwater (Bhatia et al., 2006), and so close to the mean pH value of 6.0 and maximum pH value of 8.3 observed in this thesis investigation. However, the minimum acidic pH value of 4.6 in this investigation is not comparable with previous studies. Therefore, questions are raised regarding the acidic character observed in the supraglacial stream on Fountain Glacier, but this could simply be explained by rain entering the supraglacial stream networks which can be slightly acidic (e.g. pH 5.6), thus presenting a consideration for the lower pH results observed in the stream as there was a lot of light rain on Bylot Island during the field data collections. More speculatively, the lower pH values could be explained by the mountain geology surrounding Fountain Glacier which is mainly composed of crystalline Canadian Shield bedrock, with the lower elevations where larger glaciers flow on Bylot Island, comprised of poorly consolidated mudstone and sandstone (Wainstein et al., 2008). Therefore, such migmatite Canadian Shield bedrock, as well as the additionally silica rich nature of the mudstone and sandstones, present potential surfaces for chemical weathering and the release of suspended sediment, resulting in the subsequent dissolution of such minerals from rock materials when discharged into supraglacial streams, thus influencing acidic conditions in the hydrochemistry. It cannot be discounted that atmospheric pollutants may indeed lower the pH if they become incorporated in such supraglacial stream water, either through aeolian deposition, precipitation to the glacier ice surface, or during the exchange of atmospheric CO_2 at the stream water-atmosphere interface, and so increasing stream acidity in this manner also (Metcalf, 1984). However, pH is difficult to measure and so only speculative causes for instances of low pH in the Fountain Glacier study stream are stated here.

Expected hydrometeorological associations were also identified for Fountain and Foxfonna Glacier, including the positive correlation between short-wave incident radiation and melt; an important relationship for the development of the near-surface weathering crust due to the penetration of such

irradiance at the ice surface (Stevens et al., 2018). However, no such relationship was observed between melt and discharge for both glacier locations, but is the likely result of the inefficient hydrological properties of the porous weathering crust aquifer which subsequently delays onset melt from entering supraglacial channels as discharge (Munro, 2011). A positive correlation between short-wave incident radiation and stream temperature, as well as melt and stream temperature were also observed for both glacier locations, which are expected results since high solar radiation and high melt can drive up stream water temperature. Positive correlations were also observed for air temperature and discharge for both glacier locations, an observation also previously seen in another study on Foxfonna whereby an increase in discharge was a result of increased air temperatures (Rutter et al., 2011). For Fountain Glacier only, a negative correlation between EC and discharge was observed which is a common relationship between such hydrological stream variables since solutes are diluted at times of higher meltwater discharge, and so the EC decreases (e.g. Krainer and Mostler, 2002). A negative correlation between EC and air temperature was also observed for Fountain Glacier and is a result previously seen, along with a negative correlation between EC and discharge also, in a study evaluating the EC in meltwater (see Han et al., 2015). Such an observation is the result of a positive correlation between air temperature and discharge, suggesting how variations in meltwater EC reflect glacier ablation with changes in air temperature (Han et al., 2015). The study stream on Fountain Glacier also saw a positive relationship between stream temperature and pH which is unusual considering an increase in stream temperature would expectantly decrease pH due to more H^+ ions present with increasing temperature. However, this could be explained by the summer sunlight radiation heating meltwater and the resulting solubility of atmospheric CO_2 decreasing and so outgassing of CO_2 can occur (Metcalf, 1984), thus increasing the pH level. Lastly, for Foxfonna Glacier, a positive correlation result was also revealed between incident radiation and air temperature, and air temperature and melt, an expected result since warmer air temperatures as a result of increased solar irradiance to the glacier surface, will drive melt. Therefore, the hydrometeorological associations discussed here are typical for glaciers, but the eco-hydrology of such glaciers and so the microbial fluxes are also of interest.

A mean microbe abundance in the Fountain Glacier supraglacial study stream of 1.16×10^4 cells mL^{-1} was observed, equating to an estimated mean microbial stream flux of 5.46×10^{11} cells h^{-1}. A mean abundance of 1.77×10^4 cells mL^{-1} in the weathering crust was also observed. In comparison, the Foxfonna Glacier study stream exhibited a mean microbial abundance of 0.72×10^4 cells mL^{-1}, equating to an estimated mean microbial stream flux of 4.81×10^{12} cells h^{-1}. A mean abundance of 5.44×10^4 cells mL^{-1} was observed in the additional opportunistic supraglacial stream meltwater samples. Such mean cellular abundances observed in this thesis investigation compare well with existing mean microbe enumerations in current literature, such as $3.6 \pm 4.0 \times 10^4$ cells mL^{-1} and $3.3 \pm 4.1 \times 10^4$ cells mL^{-1} for Fountain Glacier stream water and weathering crust, respectively (Stevens, 2019), and $1.30 \pm 0.2 \times 10^4$ cells mL^{-1} for Borup Fjord Pass Glacier, Canada, surface meltwater (Trivedi et al., 2018). Additionally,

a mean microbial abundance of 2.28 ± 1.91 × 10^4 cells mL^{-1} has been shown in the recharged auger holes of a weathering crust environment on the Greenland Ice Sheet (Irvine-Fynn et al., 2021), thus representing the microbial abundance mobilised in meltwater in the near-surface ice matrix, and indeed comparing well with this investigation's mean microbe abundance for the Fountain Glacier weathering crust. Such a mean abundance in the Fountain Glacier weathering crust can also be seen to compare well with the mean microbial abundances presented for Chapter 4's Storglaciären glacier ice types of CC (3.30 ± 3.33 × 10^4 cells mL^{-1}) and CB (1.83 ± 1.43 × 10^4 cells mL^{-1}). However, lower mean abundances for Fountain Glacier's cryoconite hole meltwater at 0.91 × 10^4 cells mL^{-1} and shallow ice core meltwater at 0.92 × 10^4 cells mL^{-1} were also observed for this investigation, but also revealed similar to previous studies, such as 1.3 ± 0.8 × 10^4 cells mL^{-1} for Patriot Hills Glacier, Antarctica, cryoconite hole water (Hodson et al., 2013). However, it is clear that the weathering crust presents a supraglacial habitat on Fountain Glacier which occupies more cells than the other supraglacial habitats analysed, thus presenting a source of microbes with the potential to be liberated in melt into the nearby supraglacial stream channels; a likely process since the microbial abundances from the weathering crust and supraglacial study stream on Fountain Glacier were not found to significantly differ. Furthermore, the higher abundance in cells exhibited in the weathering crust compared to that of the supraglacial stream channel could further suggest the storing properties of the weathering crust matrix and modulation of particles within and from such a habitat (Irvine-Fynn et al., 2012). Furthermore, significant differences found between the microbial abundances of the shallow ice cores and the weathering crust surface ice from Fountain Glacier, could further support the earlier notion of microbes being rejected from ice crystals within glacier ice and to the weathering crust surface during ice formation, such as in superimposed ice like that explained in Chapter 4, and so a process of cell liberation. Therefore, the availability and liberation of microbes at the supraglacial ice surface, and eventually delivered by meltwater from the weathering crust surface and into nearby supraglacial channels, is a complex phenomenon but other processes may also result in the liberation of cells microbes at the ice surface for subsequent discharge in meltwater to nearby stream channels.

Microbes of the cell size ≤ 1 µm were observed to be the highest average relative percentage abundance in the Fountain Glacier supraglacial stream (37.00 %), cryoconite hole (45.29 %) and shallow ice core (43.10 %) samples; with the weathering crust having a higher average relative percentage abundance of cells of the size 2-4 µm (38.18 %). Storglaciären also presented the 2-4 µm size fraction to be of the overall highest average relative percentage abundances of microbes for the different ice types, followed by the ≤ 1 µm size fraction. Likewise, for Foxfonna Glacier both the supraglacial study stream and other stream samples presented the same dominant cell size fraction of 2-4 µm, with their highest average relative percentage abundances of 37.91 % and 40.51 %, respectively, and so larger than the previously observed dominant ≤ 0.5 µm microbes found in the supraglacial habitat samples on Midtre Lovénbreen, Svalbard (see Irvine-Fynn et al., 2012). Miteva (2008) states how cells smaller than 2 µm are usually

found within the liquid veins of ice crystals, with larger cells instead trapped within such crystals, and so it could be inferred that the dominant ≤ 1 µm cells found in the Fountain Glacier supraglacial stream are the result of such small cells being released in melt through the ice crystal interstitial veins and transferred into the nearby supraglacial stream. The larger 2-4 µm sized cells therefore remain entrapped in such ice crystals and are evidenced here by the high average relative percentage abundances of microbes in this size fraction in the Fountain Glacier weathering crust, and overall Storglaciären ice types. It is important to recognise that a vertical gradient in pore/interstitial space in a weathering crust exists whereby more pore space is present in the upper-most crust compared to the saturated crust at the water table interstitial spaces (see Figure 2.6). Therefore, smaller cells released in melt from interstitial veins of ice crystal boundaries may instead be mobilised through the water table into nearby supraglacial streams and not just from surface runoff as the surface may not be as saturated in meltwater to mobilise such cells. Furthermore, similarities in the dominant 2-4 µm sized cells found in the Fountain Glacier weathering crust and Storglaciären ice types, could also suggest the presence of superimposed ice. However, Foxfonna Glacier's stream samples also presented the dominant cell size fraction of 2-4 µm within their supraglacial meltwaters, and so this suggests limited evidence to support the trapping and storage of accumulated cells in this ice matrix (Stevens et al., 2020) as larger cells have been mobilised and discharged into the supraglacial study stream.

Processes that have the potential to dictate the liberation of cells in surface meltwater into supraglacial streams can be determined through the associations between key hydrometeorological data and supraglacial stream microbial abundances. As positive correlations for microbe abundance against short-wave incident radiation, melt, and discharge were found for Fountain Glacier, it is inferred that high melt rates primarily driven by incident-solar radiation at the ice surface, and sufficient discharge of such meltwater, increase the abundance of microbes in supraglacial stream channels. The liberation of microbes from the weathering crust in meltwater to streams is apparent as it is established that these two habitats are not dissimilar in microbial abundance. Although melt and discharge do no correlate in this investigation due to the likely low transfer rate of meltwater in the hydrologically inefficient weathering crust, there is limited evidence here to suggest the substantial storage or accumulation of cells in this ice matrix (Stevens et al., 2020), especially since positive correlations are presented for microbial abundance against melt and discharge in the Fountain Glacier study stream. Such a positive association between discharge and microbial abundance can also be likened to that seen in the context of riverine sediment transport dynamics, whereby the correlation here is universally a positive discharge to suspended sediment concentration relationship (e.g. Li et al., 2020). Also, such associations observed for Fountain Glacier contradict the existing observation of an inverse, non-linear association between meltwater discharge and microbe abundance by Irvine-Fynn et al. (2012), as well as no correlation found between microbial abundance and stream discharge in other studies (Stevens et al., 2020) and indeed for Foxfonna Glacier in this study. A further speculative explanation for the positive association between

microbial abundance against melt, and discharge, in the Fountain Glacier study stream could be the result of a high concentration of nearby unstable cryoconite hole microbes being 'flushed' into the supraglacial stream at times of high surface melt (Hodson et al., 2008), and so more cells present to be discharged down glacier through the supraglacial channel. The presence of superimposed ice, like that on Storglaciären, could also result in more microbes being liberated at the ice surface and available to be transferred by melt into supraglacial streams and discharged through such channels. The presence of such an ice type could be suggested with the positive correlation between microbial abundance and EC for the Foxfonna Glacier study stream. Increased solute ions, and so EC, in the catchment of Rieperbreen–Foxfonna have previously been observed due to an increase in the presence of Cl^- after being released in summer ablation snowpack elution (Rutter et al., 2011). Typically, Cl^- is the last to elute from the snowpack thus resulting in such high concentrations residing in the snow and so when Cl^- is released, it would increase EC in the Foxfonna study stream in this instance, and the microbial abundance along with it, thus revealing the potential presence of superimposed ice at the Foxfonna Glacier surface. As shown in Chapter 4 following the work published by Goto-Azuma et al. (1994), during the refreezing of snowmelt and so the formation mechanism of superimposed ice, ions, particles and so cells, are rejected by this refreezing layer to the snow/ice surface meaning high concentrations of ions emerge at the surface thus further increasing EC, and high numbers in cells along with it like that seen for the superimposed ice type on Storglaciären, which can then be liberated in superimposed ice melt due to the primary driver of short-wave incident radiation, and ultimately delivered to nearby supraglacial stream channels in surface runoff. Additionally, previous studies on glaciers have also seen a positive correlation between Cl^- ions and bacterial abundance (Liu et al., 2009), and so at times of Cl^- elution and release into supraglacial channels, the ion concentration will increase along with the EC, and so microbes present in such meltwater may utilise these ions for their metabolic processing, thus suggesting why a reason for the positive correlation between EC and microbe abundance here. Additionally, the net retention of OC on the surface of Foxfonna Glacier (Koziol et al., 2019), means that ample DOC can become incorporated in supraglacial stream channel discharge in periods of high melt, increase the EC as a result, and be used by heterotrophic microbes in their biogeochemical reactions also.

5.5.2 Cell Sample Degradation with Storage Length

By re-examining a handful of supraglacial stream samples from Midtre Lovénbreen, differences between microbe enumerations, and respective cell size fraction abundances, were observed with that outlined in Irvine-Fynn et al. (2012). Such results presented an opportunity to assess whether long storage periods of such archived samples had impacted on the microbe abundances compared to when the same samples were last analysed in the study by Irvine-Fynn et al. (2012) after collection in the field. However, it is important to note that a different FCM platform and SOP were used for the microbe

enumerations in this research investigation compared to that of Irvine-Fynn et al. (2012), and so results should not be taken as a direct comparison but as an estimate.

For this thesis investigation, a mean microbe abundance of 0.20×10^4 cells mL^{-1}, ranging between 0.10 and 0.40×10^4 cells mL^{-1} was found for the Midtre Lovénbreen study stream, with further downstream transect microbe enumeration analyses presenting a mean abundance of 0.14×10^4 cells mL^{-1}, ranging between 0.10 and 0.20×10^4 cells mL^{-1}. Compare this to the mean abundance of cells in the supraglacial stream water presented by Irvine-Fynn et al. (2012), and it is apparent that this investigation's enumeration values are lower for both the stream and downstream transect environments than that presented in the published study at $\sim 2.0 \times 10^4$ cells mL^{-1}. This investigation also presents mean microbe enumerations that are lower than that in other published studies also, such as 1.4 to 4.9×10^4 cells mL^{-1} for supraglacial meltwater on Midtre Lovénbreen (Mindl et al., 2007). The highest relative percentage abundance of cells were found to be of the size 2-4 μm for both the supraglacial stream (38.45 %) and downstream (36.12 %) sources in this thesis investigation, with the second highest relative percentage abundance of cells found within the ≤ 1 μm size fraction for both environments. However, the ≤ 0.5 μm size fraction presented the highest relative percentage abundance of cells in the Irvine-Fynn et al. (2012) study at 53.80 %, and then the ≤ 3.0 μm as the second highest size fraction with 26.70 % of cells of this size. Again, a direct comparison cannot be achieved here as the size fraction groups are different. Only a select handful of Midtre Lovénbreen samples were analysed for this investigation unlike the Irvine-Fynn et al. (2012) study which presents results for the entire sample set collected. However, a likely explanation for the lower mean enumeration results observed in this thesis investigation for Midtre Lovénbreen compared to that previously examined in the published study, is that of such samples having been stored in a -80 °C freezer for over 10 years, experiencing cell sample degradation and freeze-thaw stress, especially with the samples having been non-fixed. Previously, it has been suggested that bacterial loss, and so low microbe enumerations, but in preserved samples, can occur due to the lysis of cells (Kamiya et al., 2007) thus releasing DNA. In the context of the handful of non-fixed Midtre Lovénbreen samples analysed, if could be suggested that microbial attachment to the inner wall of the sample vials occurred during storage (see Turley and Hughes, 1992) thus resulting in lower microbe enumerations observed during FCM analyses. Albeit, every effort was made to ensure the meltwater cell samples were fully vortexed and cells mobilised before decanting into aliquots for staining by SYBR Gold and FCM analyses. However, when looking at bacteria numbers in preserved seawater samples, sonification does not entirely ensure the full recovery of cell numbers and so an accurate estimate of the original cell abundance prior to storage in that particular sample (Turley and Hughes, 1992). Although the seawater samples presented by Turley and Hughes (1992) were fixed and the Midtre Lovénbreen samples were not, storage alone has been shown to result in a rapid decrease in bacterial counts in the first three days of storage at 4 °C followed by a slower decrease in marine bacteria in previous studies (see Kamiya et al., 2007).

Ultimately, the results of the non-fixed Midtre Lovénbreen sample analyses compared to that of Irvine-Fynn et al. (2012) emphasises the importance of adopting appropriate and consistent storage conditions and length for environmental samples before FCM analyses. Previously, a model for marine bacterial counts determined that such microbe numbers would drop from the initial abundance after 3, 10, and 90 days, to 78 %, 65 %, and 45 %, respectively, albeit such declines may be influenced by the fixatives used and particular conditions of storage (Kamiya et al., 2007). It was further stated how storage of 1 and 3 days at 4 °C after fixation of the environmental water samples would allow for accurate estimates of total microbe numbers (Kamiya et al., 2007). Ideally, samples should be analysed as soon as possible after field sample collection, with refrigeration again being shown to present a better option for short-term storage (~3-5 days) for the analyses of environmental DNA concentration for example, and so could be applied to environmental cells (Hinlo et al., 2017). Where sample analyses cannot be completed soon after collection however, then freezing of samples is appropriate but it is important to recognise the impact of freeze-thaw cycles (Hinlo et al., 2017), and how such a stress on cells thawing from previously frozen samples may result in reduced microbial abundance.

5.6 Summary

This chapter has presented the reliable enumeration of microbes found within high-Arctic supraglacial stream environments. Statistically significant associations were found as expected between streamflow hydrological data and meteorological data for Fountain Glacier and Foxfonna Glacier, such as short-wave incident radiation being the primary driver of melt on the surface of glaciers. Additionally, statistically significant associations were expected between hydrometeorological factors and microbial abundance as stated in the hypothesised objectives at the beginning of this chapter, but it was found that only short-wave incident radiation, melt, discharge and EC were environmental factors shown to potentially dictate microbial abundance on a glacier surface. Again, mechanisms promoting ice formation, such as for superimposed ice, could be proposed here as a further process influencing the liberation of microbes at the glacier surface which are then dictated by the key hydrometeorological factors mentioned previously. It is clear that microbes are discharged into nearby supraglacial channels from the surrounding glacier weathering crust surface, and that such microbial fluxes will subsequently feed downstream freshwater ecosystems. However, the downstream impact of such microbes is still unknown but knowing whether such cells are alive (viable) or dead would aid in such an assessment as to the potential impact of supraglacial microbes in proglacial environments, and indeed if such viability of microbes changes with season or melt conditions, thus such questions will be explored in Chapter 6.

6 VIABILITY DETERMINATION OF SUPRAGLACIAL MICROBES

6.1 Introduction

It was identified in Chapter 4 that between 1.47 to 10.78 × 10^4 cells mL^{-1} were found for mean microbial abundance within different ice types on the surface of Storglaciären, with estimated mean cellular carbon content in the bulk ice density ranging from 2.70 × 10^{-7} kg C m^{-3} of ice to 1.98 × 10^{-6} kg C m^{-3} of ice (2.95 × 10^{-7} to 2.16 × 10^{-6} kg C m^{-3} meltwater equivalent (w.e.), respectively, which would be assumed to be transferred in melt into supraglacial streams from the ice surface, see Table 4.1). Additionally, it was observed that there was a mean microbe abundance in the Fountain Glacier supraglacial study stream of 1.16 × 10^4 cells mL^{-1} with an estimated mean cellular carbon content of 2.32 × 10^{-7} kg C m^{-3} w.e. (see Table 5.2), and a mean microbial flux of 5.46 × 10^{11} cells h^{-1} through the study stream. Also, a mean abundance of 0.72 × 10^4 cells mL^{-1} with an estimated mean cellular carbon content of 1.43 × 10^{-7} kg C m^{-3} w.e. (see Table 5.4), and a mean microbial flux of 4.81 × 10^{12} cells h^{-1} in the Foxfonna Glacier supraglacial study stream was observed. Therefore, it is clear that microbes, and their respective cellular carbon content, are entrained in meltwaters from the glacier ice surface and exported to downstream aquatic ecosystems, but the viability of such microbes is unknown. The viability of microbes is a difficult physiological state to define and equally difficult to measure (Davey and Guyot, 2020). Currently, there have been no attempts reported in the literature to determine the viability of microbial cells found within supraglacial stream environments. Therefore, further investigation to explore if there is a viability story for such supraglacial microbes is important and can be assessed through the use of a viability determination dual-staining protocol, albeit there are different staining methods and so will be discussed in Section 6.2.2. Such an assessment of the viability statuses of supraglacial stream microbes will allow for an estimate as to what proportion of cells delivered to the downstream proglacial ecosystems are alive, or indeed dead. Such an assessment will provide an insight as to the proportion of cells that have the potential to be biogeochemically active in such downstream systems, and so enable a further understanding as to how connected ecosystems may respond to the decline of glaciers in climatic global warming, with the microbial flux of potentially viable cells to such ecosystems. Therefore, the aim of this exploratory chapter is to quantify the proportion of cells that are alive, injured or dead using non-fixed supraglacial samples from Midtre Lovénbreen and Foxfonna Glacier, Svalbard, as the "assessment and quantification of viable cells from the supraglacial ecosystem remains undetermined" (Irvine-Fynn et al., 2012, p.3003).

The statements hypothesised below will be investigated within this analytical chapter and such findings used to either support or reject the below statements in the context of this chapter's aim:

1) Cell viability assessment of non-fixed supraglacial microbes using the LIVE/DEAD BD Cell Viability dual-staining kit in FCM will allow for reliable proportions of live and dead supraglacial cells to be determined.

2) Statistically significant associations are expected between viability and hydrometeorological factors, such as the viability of microbes changing with melt conditions, especially since hydrometeorological factors were found to correlate with microbial abundance as discovered in Chapter 5.

6.2 Review of the Viability of Microbes

6.2.1 Defining Viability

The process of defining viability in microbial cells is more complex than simply stating whether a cell is alive or dead. Instead, a microbial cell's trajectory from life to death encompasses many stages. Davey (2011) describes the various stages in between life and death whereby a cell is alive and actively metabolising thus showing the microbial cell as viable; a cell is still alive but may have reduced metabolic activity; a cell may be fully intact but have reduced RNA content; a cell may again be intact but have no detectable metabolic activity; then the cell may exhibit extensive membrane damage which results in a cell with degraded DNA; and finally, the resulting stage is when only cell fragments remain and so the microbial cell is deemed as dead. As well as these different stages from the life to death of a microbial cell, other studies have shown how some cells may experience a recovery period and are able to resuscitate themselves (see Davey and Hexley, 2011). Therefore, it is clear that there is more to viability determination than just assigning a 'live' or 'dead' status to microbial cells; there are more stages between life and death involved that need careful consideration, especially when designing an experimental protocol for determining the viability of a microbial load found in an environmental sample. In addition to this, Davey and Guyout (2020) have also described the different physiological states of microbial cells which reflects their viability, these states include: healthy cells capable of division; viable and culturable cells but damaged; cells with limited culturability and associated limited divisions thus producing micro or invisible colonies; dormant cells which are capable of division but only once resuscitated; leaky cells in which their membranes are damaged but can also be repaired; cells which exhibit activity but their ability to culture is unsuccessful; cells which have a moribund physiological state and so are not metabolically active and incapable of division but appear intact when observed microscopically; and finally, the cells which occupy a dead physiological state whereby all integrity of the cell has been lost. Davey and Guyout (2020) have clearly identified here the many physiological states that cells can manifest thus emphasising the need for a robust approach in determining the viability of cells clearly.

Traditionally, culturability was the key factor used to determine the viability of microbial cells. As stated by Postgate (1969, p.611), "An organism is viable if it is capable of multiplying to form two or more progeny in conditions that are 'optimal' for the species and strain of microbe concerned". It is clear how culturability and viability have previously been used synonymously, and so the approach of culturing microbes on an agar surface was deemed the 'gold standard' method for determining the viability of

microbial cells. This plate count method is thoroughly well-known and widespread, and involves the individual organisms being observed microscopically and scored as viable by an operator. However, as shown previously, viability is more complex than just solely basing viability on culturability. This approach ultimately states that cells are alive and so viable if cellular division is present, and are dead and so not viable if there is no cellular division present. However, a cell may be viable and not culturable, but the plate count method would not be able to score this viability status to such a cell and so would score it as dead. Furthermore, the scoring of cells using the plate count method also presents a high likelihood for operator fatigue. Therefore, a faster alternative approach is more appropriate here such as the cytochemical staining of microbial cells; a method which provides a clearer insight into the physiology of individual cells, thus allowing for various viability statuses to be determined (Davey and Guyout, 2020).

6.2.2 Staining Techniques

Alternative approaches to the 'gold standard' microbial culturability assessment have been developed in order to determine the viability of cells. Miteva (2008) states how very few microbial cells collected from natural, environmental samples can actually be cultivated, and so various methods for assessing the integrity and activity of cells have been developed, such as the use of cytochemical assays in staining procedures. Cytochemical assay analyses have previously been coupled with the analytical technique of flow cytometry whereby each stain has its own excitation and emission spectra and is detected by a flow cytometer, thus resulting in each stain exhibiting a specific coloured fluorescence. Examples of common cytochemical assays include the nucleic acid stains of SYBR Gold, as discussed in Chapter 3, and SYBR Green I which bind to the single- and double-stranded DNA and RNA of biological cells; in turn emitting a green fluorescence and so showing the detection of cells by shifting rightward in fluorescence on an FCM histogram away from the less/non-fluorescent non-biological particles in that particular sample. Both SYBR Gold and SYBR Green I have been compared in their reliability for bacterial and virus counts in epifluorescence microscopy of natural marine samples, whereby no significant difference was shown between the two stains (Shibata et al., 2006).

Commercially available bacterial viability kits can also be readily obtained for viability determination, such as the LIVE/DEAD BacLight kit in which membrane integrity and associated injury of cells can be determined. The kit provides nucleic acid stains- green-fluorescing SYTO9 which permeates and stains all cells in a sample, and red-fluorescing propidium iodide (PI) which enters cells which are injured or dead due to their damaged cytoplasmic membranes (Berney et al., 2007). Likewise, nucleic acid stains such as thiazole orange (TO) would also act in the same manner as green-fluorescing SYTO9 here, and can be used in combination with PI. Previous work carried out by Davey and Hexley (2011) established that a subpopulation of *Saccharomyces cerevisiae* cells exposed to stress, took up PI during and immediately after such an exposure, but a short incubation period allowed for the cells to repair

their damaged membranes thus no longer enabling the permeation of PI when the stain was subsequently added. Such a finding suggests that the red-fluorescing PI stain needs careful attention when assigning a subpopulation of cells as PI-positive or dead synonymously (Davey and Hexley, 2011). Therefore, it is further exemplified that the cell stages from life to death and so determining a cell's viability status, is indeed more complicated when cells have shown a capacity to repair their membrane barriers and resuscitate themselves.

Another cytochemical assay previously used on aquatic and marine environmental samples, but not supraglacial, is 5-Cyano-2,3-ditolyl tetrazolium chloride (CTC). This particular compound is colourless and membrane-permeable, but once reduced by the electron transport system (ETS) of a cell, the red-fluorescing precipitate formazan is produced inside the cell (Créach et al., 2003). CTC has been used for the detection and quantification of microbial cells which are actively respiring thus showing cell-specific metabolic activity (Schaule et al., 1993). In previous studies, CTC has been successfully used to quantify the single-cell metabolic status of sea ice bacteria from melted ice cores from the Antarctic (Martin et al., 2008). Here, it was found that an average of 32 % of the bacterial cells were actively respiring showing that sea ice is included as one of the most productive microbial habitats, and that CTC is favoured for ascertaining a real-time response from the bacterial cells found in the marine ice ecosystem (Martin et al., 2008). However, another study showed how CTC reduction is a good indicator of cell viability alone rather than cell activity, as the bacterial cells in this particular study were in the stationary phase but still maintained enough energy for CTC reduction, despite respiratory activity and CO_2 levels having decreased (López-Amorós et al., 1995; Créach et al., 2003). In this example, the cells have simply been deemed as viable/alive because they are reducing CTC, and not because they are metabolically active/respiring- which in this instance, they were lacking anyway. This particular finding therefore reiterates how cells can have differing physiological states and still show viability, and that cytochemical assays are more equipped to assess such states and assign viability statuses.

A further approach to determining metabolically active cells is through the use of bioorthogonal noncanonical amino acid tagging (BONCAT) whereby the translational activity of a cell is measured through the incorporation of synthetic amino acids into proteins (Emerson et al., 2017). Upon incorporation of the synthetic amino acids, fluorescence can occur thus allowing detection due to click-chemistry, using copper-catalyse alkyne-azide (Sebastián and Gasol, 2019). When exploring the physiological status of bacteria in a marine setting, BONCAT has been shown as a powerful semi-quantitative and fast technique (Leizeaga et al., 2017). Similarly, another study has shown the application of BONCAT in order to ascertain the translational activity of marine microbial consortia which have been found to catalyse the anaerobic oxidation of methane; a gas stated as being a dominant sink in the ocean (Hatzenpichler et al., 2016). However, BONCAT is relatively new to being applied to microbial ecology studies and although not yet proven, broad applicability of the technique is presumed,

with minimal interference to the normal activity of the individual cell (Emerson et al., 2017). BONCAT is one such technique that when applied in environmental research, will help in determining the role that individual prokaryotes have in biogeochemical reactions; an essential finding in order to better understand the microbial processes occurring in the ocean (Sebastián and Gasol., 2019), or indeed other aquatic ecosystems, such as supraglacial streams.

It is clear that various approaches and cytochemical assays can aid in the determination of the viability statuses and activity levels of cell subpopulations; statuses of which are more complex than simply scoring cells as alive or dead. If such microbial cells possess the viability and vitality to thrive in their environments, such as in the supraglacial ecosystem, then the question remains as to what impact such viable microbes might have if liberated in glacial meltwater runoff and transported to proglacial environments. Therefore, the BD Cell Viability Kit (see Section 3.2.3 for this viability protocol) has been selected as the cytochemical dual-staining procedure of choice to assess the viability of supraglacial stream samples from two high-Arctic glacier locations.

6.3 Viability Dual-Staining Results

The viability dual-staining protocol as outlined in Section 3.2.3, was first carried out on the non-fixed Midtre Lovénbreen samples to act as a pilot experiment in order to preliminary assess the viability protocol. Here, it is important to reiterate that the analytical gates constructed in the BD Accuri C6 Plus software to distinguish the proportion of cells that were alive, dead or injured were based on the analyses carried out for the dual-staining of PI and TO on a laboratory sub-culture of the glacial isolate *Janthinobacterium* sp. (see Section 3.2.3). The results of the dual-staining of this laboratory sub-culture, and indeed later observed with the environmental samples, showed the dual-stain to not be working as expected here, so the classification of live, dead and injured gates are speculative given PI doesn't seem to be working in the manner published work suggests (Figure 3.3).

6.3.1 Midtre Lovénbreen

Preliminary assessment of the viability statuses of cells within the Midtre Lovénbreen supraglacial study stream samples, as well as the downstream samples, was carried out. However, it was apparent that there was a need to separate such average relative percentage abundance viability results into three separate viability staining procedures for each supraglacial source including: sample aliquots dual-stained with PI and TO only; sample replicate aliquots heated to 60 ℃ for 1.5 hours (see Davey and Hexley (2011) for such an approach), and then stained with PI and TO, and finally, sample replicate aliquots 'killed' with filtered 2 % w/v final concentration of glutaraldehyde (fixation time of 30 minutes), and then stained with PI and TO. For the supraglacial study stream, replicates only stained with PI and TO have a higher average relative percentage abundance of cells that are gated as alive (39.93 %), with the lowest percentage as injured (Figure 6.1a). Likewise, the sample replicates that experienced heat treatment

before being stained with PI and TO also had a higher proportion of cells that were alive and so less were gated as dead, although the proportion of cells injured does increase with heat treatment, just not the proportion of dead cells (Figure 6.1a). However, Figure 6.1a also shows that sample replicates treated with glutaraldehyde before being stained with PI and TO, did increase in the proportion of cells that were dead compared to alive. Similar trends in a higher proportion of live cells (41.93 %) can be seen for the downstream replicates stained with PI and TO alone, but again more live cells than injured or dead cells for sample replicates treated with heat, and more dead cells than live cells for sample replicates fixed with glutaraldehyde before viability dual-staining analyses (Figure 6.1b).

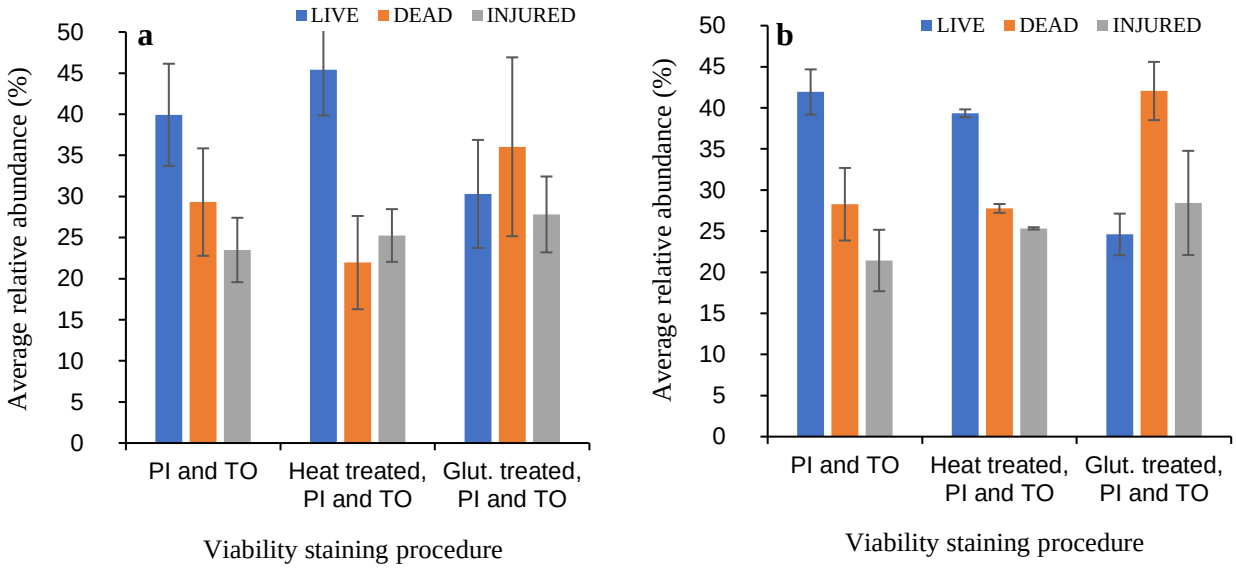

Figure 6.1. Bar chart showing the average relative percentage abundance of microbes from non-fixed Midtre Lovénbreen **(a)** supraglacial study stream samples and **(b)** downstream samples, enumerated in the different live, dead and injured viability gates. A comparison between the viability status of microbes is made for three different viability staining procedures: sample replicate aliquots stained with PI and TO (study stream n = 20 and downstream n = 5); sample replicate aliquots heated to 60 °C for 1.5 hours, and then stained with PI and TO (study stream n = 7 and downstream n = 2), and finally, sample replicate aliquots 'killed' with filtered 2 % w/v final concentration of glutaraldehyde (fixation time of 30 minutes), and then stained with PI and TO (study stream n = 7 and downstream n = 2). Standard deviation shown as error bars at ± 1 SD.

Furthermore, looking closely at the proportion of cells that are gated as live and dead across the study period which were not treated with heat or glutaraldehyde, and shown as their relative percentage abundances for the Midtre Lovénbreen supraglacial study stream, it is apparent that the live relative percentage abundance of cells across the entire study period are higher (Figure 6.2a) compared to that of the dead cells (Figure 6.2b).

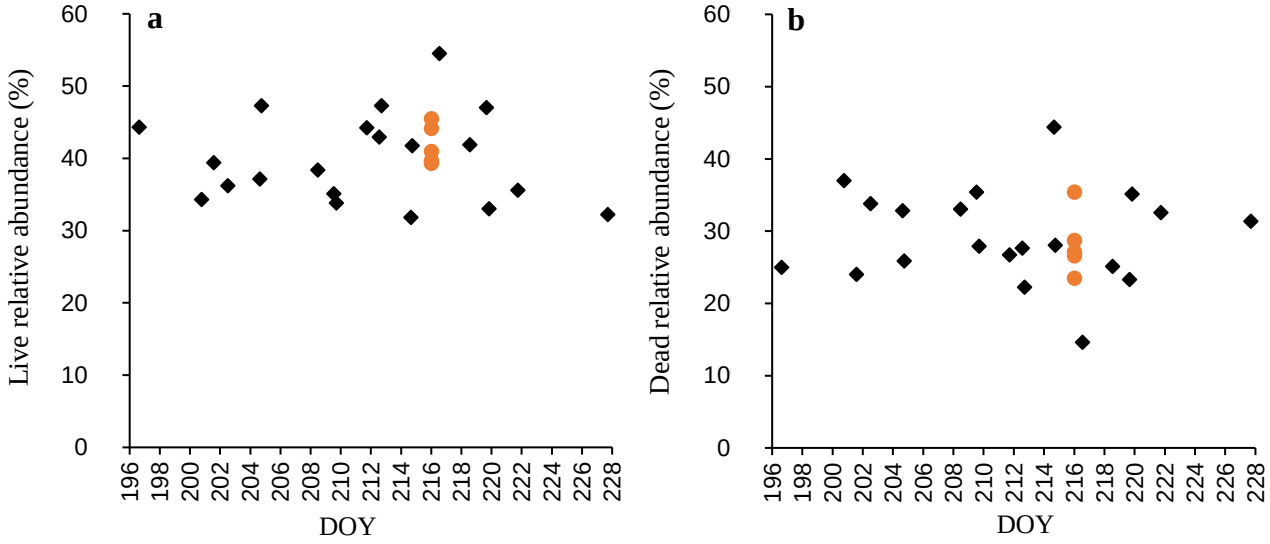

Figure 6.2. Time-series showing the dual-stained relative percentage abundance of microbes that have been gated as **(a)** live and **(b)** dead, across the study period in the study stream, with additional red dots representing downstream transect meltwater samples for comparison from Midtre Lovénbreen.

6.3.2 Foxfonna Glacier

Assessment of the viability statuses of cells within the Foxfonna Glacier supraglacial study stream samples, as well as the additional opportunistic supraglacial stream meltwater samples, was carried out based on the same viability analytical gates to distinguish the proportion of cells that were alive, dead or injured. Again, the average relative percentage abundances were separated based on the three separate viability staining procedures for each supraglacial source. For the supraglacial study stream and other opportunistic stream samples, it can be seen that the sample replicates stained with PI and TO alone, as well as the replicates treated with heat prior to dual-staining, produced similar average relative percentage abundances whereby there are more live cells than that of dead or injured, again showing the heat treatment in this investigation as ineffective in producing a 'killed' control (Figure 6.3a and b). However, as expected, the glutaraldehyde fixed sample replicates resulted in a higher average relative percentage abundance of cells that were gated as dead in both supraglacial stream sources (Figure 6.3a and b).

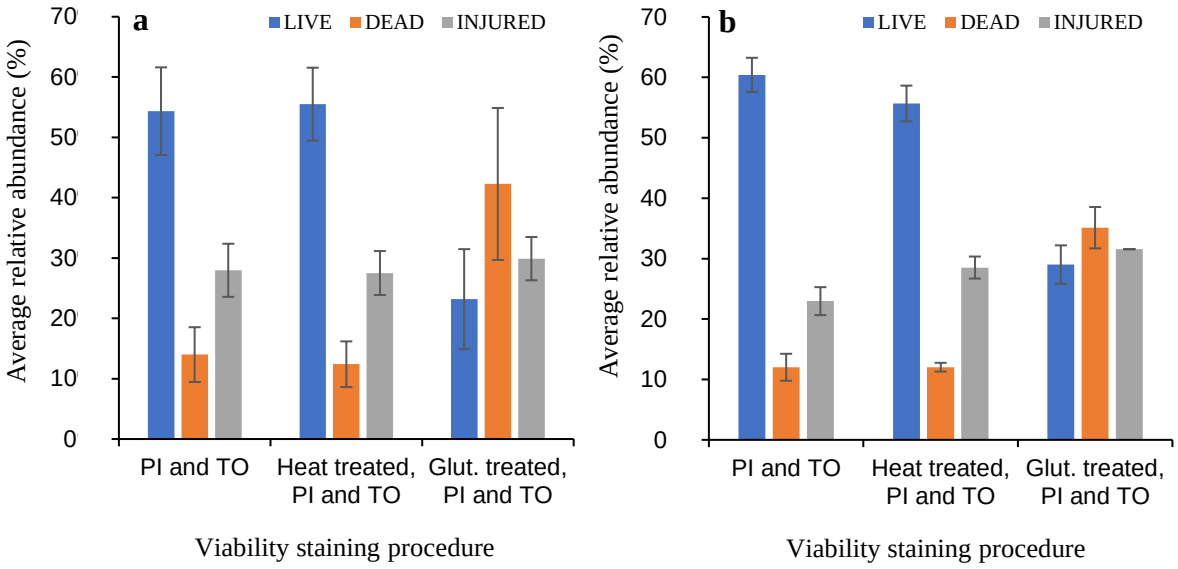

Figure 6.3. Bar chart showing the average relative percentage abundance of microbes from non-fixed Foxfonna Glacier **(a)** supraglacial study stream samples and **(b)** additional opportunistic supraglacial stream meltwater samples, enumerated in the different live, dead and injured viability gates. A comparison between the viability status of microbes is made for three different viability staining procedures: sample replicate aliquots stained with PI and TO (study stream n = 44 and downstream n = 11); sample replicate aliquots heated to 60 ℃ for 1.5 hours, and then stained with PI and TO (study stream n = 10 and downstream n = 2), and finally, sample replicate aliquots 'killed' with filtered 2 % w/v final concentration of glutaraldehyde (fixation time of 30 minutes), and then stained with PI and TO (study stream n = 10 and downstream n = 2). Standard deviation shown as error bars at ± 1 SD.

Furthermore, looking closely at the proportion of cells gated as live and dead across the Foxfonna Glacier study period; not treated with heat or glutaraldehyde and shown with relative percentage abundance within the supraglacial study stream, it is very clear that the live relative percentage abundance of cells across the entire study period are higher (Figure 6.4a) compared to that of the dead cells (Figure 6.4b). It could even be said that the live cells appear to increase in relative percentage abundance from DOY 213 to the end of the study period DOY 228, and so potentially coinciding with estimated melt as shown in Figure 5.7e which appears to present lower melt estimates in this time period.

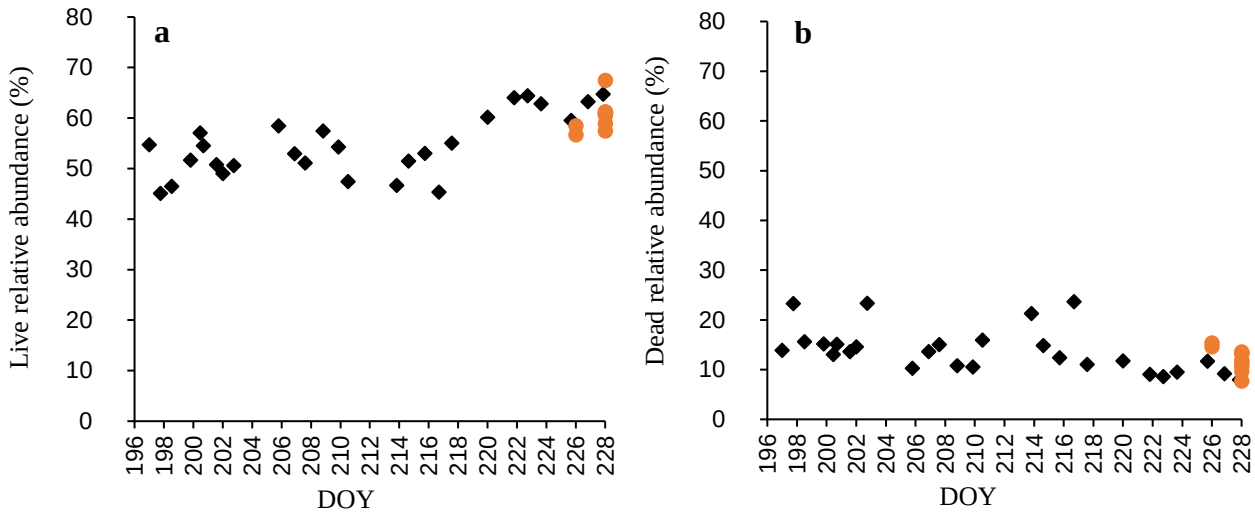

Figure 6.4. Time-series showing the dual-stained relative percentage abundance of microbes that have been gated as **(a)** live and **(b)** dead, across the study period in the study stream, with additional red dots representing the opportunistic supraglacial stream meltwater samples for comparison from Foxfonna Glacier.

6.3.3 Additional Validation Calculations

As previously shown in Section 3.2.3, in order to construct the necessary viability gates for the determination of cells as being live, dead or injured, *Janthinobacterium* sp. was used and dual-stained with PI and TO, whereby FL3-A fluorescence was represented by PerCP-A for PI uptake of damaged/dead cells, and FL1-A fluorescence was represented by FITC-A for TO staining of all cells on the density plot axes in this investigation (see Figure 3.3). However, a vertical shift in PerCP fluorescence which would be expected of live cells having been fixed by glutaraldehyde and so 'dead' thus allowing the intake of PI, did not occur in this viability protocol investigation but instead resulted in unusual rightward horizontal shifts in FITC thiazole orange fluorescence. Since a clear issue has been revealed by the interesting increased uptake of TO rather than PI in fixed cells, additional validation calculations were carried out to assess whether the dual-staining with the TO stain was indeed working in the way it would be expected to, such as staining all of the cells (total cells include live, dead and injured) while the PI just stains injured and dead cells. As TO is also a nucleic acid stain like that of SYBR Gold, then they would be expected to work in the same way and stain all cells in the sample replicates, and so a correlation would be expected between the total cells stained by SYBR Gold and all the cells stained by TO with the presence of PI, for the same sample replicates, thus showing that TO is in fact working appropriately in the dual-staining viability protocol in the presence of PI, to enumerate all cells in the sample. Such a validation assessment and correlation would instead suggest that another factor is therefore resulting in the unusual rightward FITC shift in fixed cells when stained with TO and PI, and not an expected vertical shift in PerCP.

For Midtre Lovénbreen and Foxfonna Glacier, the distributions of the total SYBR Gold stained cells found in the study streams (from the protocol outlined in Section 3.2.2, and shown in Chapter 5) and the dual-stained TO total cells in the presence of PI (live, dead, and injured cells) (from the protocol in Section 3.2.3) were determined and based on the events per mL, and the Anderson Darling normality test carried out with the knowledge that data with a significance level of more than 0.05 are classed as normally distributed. As a result of the normality testing, the appropriate non-parametric statistical test of Spearman's Rank Correlation Coefficient was selected as both the data sets were non-normally distributed. The individual location correlations tested for Midtre Lovénbreen and Foxfonna Glacier between their total SYBR Gold stained cell numbers and the dual-stained TO total cells in the presence of PI, resulted in statistically significant positive associations of $r_s = 0.562$, $p = 0.010$, and $r_s = 0.605$, $p < 0.001$, respectively. Therefore, it is clear that the total cells enumerated with the SYBR Gold nucleic stain and that of the TO in the dual-stain with PI, resulted in significantly correlated cell enumerations, and so it can be suggested that the unusual rightward shift in TO fluorescence when sample replicates were fixed with glutaraldehyde, and so instead of an expected vertical shift in PI fluorescence, is likely due to other factors and so will be discussed in Section 6.4. However, although the dual-staining total cell counts correlated with the SYBR Gold total counts, an estimated mean microbial cell flux for Foxfonna Glacier study stream using the dual-staining total cell counts in events per mL was also calculated, along with an estimate for the mean microbial flux of living cells through the supraglacial study stream, thus allowing for a proportion of the live cell flux to be estimated and shown to be discharged downstream to proglacial ecosystems. Therefore, using the dual-stain derived total cell counts, the estimated mean microbial flux of 1.04×10^{13} cells h^{-1} in the Foxfonna Glacier supraglacial study stream was calculated, again adopting the method previously described by Irvine-Fynn et al. (2012) (following Tranter et al., 2002), and so constructing a linear regression model between discharge and cell flux (see Appendix 5), with the mean estimated discharge of 0.188 $m^3 s^{-1}$. The same process was carried out for the cell abundances within the live gate from the dual-staining sample replicate analyses (see Appendix 6), and so an estimated mean microbial flux of live cells within the Foxfonna study stream was found as 5.70×10^{12} cells h^{-1}. Therefore, it is estimated that approximately 54.65 % of the microbes exported from the glacier ice surface and in supraglacial stream meltwater are alive, and ultimately delivered to downstream ecosystems.

6.3.4 Compiled Foxfonna Hydrometeorological and Viability Data Associations

The key hydrometeorological data from Foxfonna Glacier were correlated against the live and dead relative percentage abundance of microbes found within the supraglacial study stream. Anderson Darling normality testing identified the need for Spearman's Rank and Pearson's R correlation testing to be carried out where appropriate depending on which hydrometeorological data variables were or were not normally distributed. After correlation testing, it was found that only a statistically significant negative relationship was present between the relative percentage abundance of live cells and melt, with

the r_s value as -0.311 (p = 0.043) (Figure 6.5). Therefore, it is clear that melt is a factor which appears to decrease the proportion of live cells in the supraglacial study stream as melt increases.

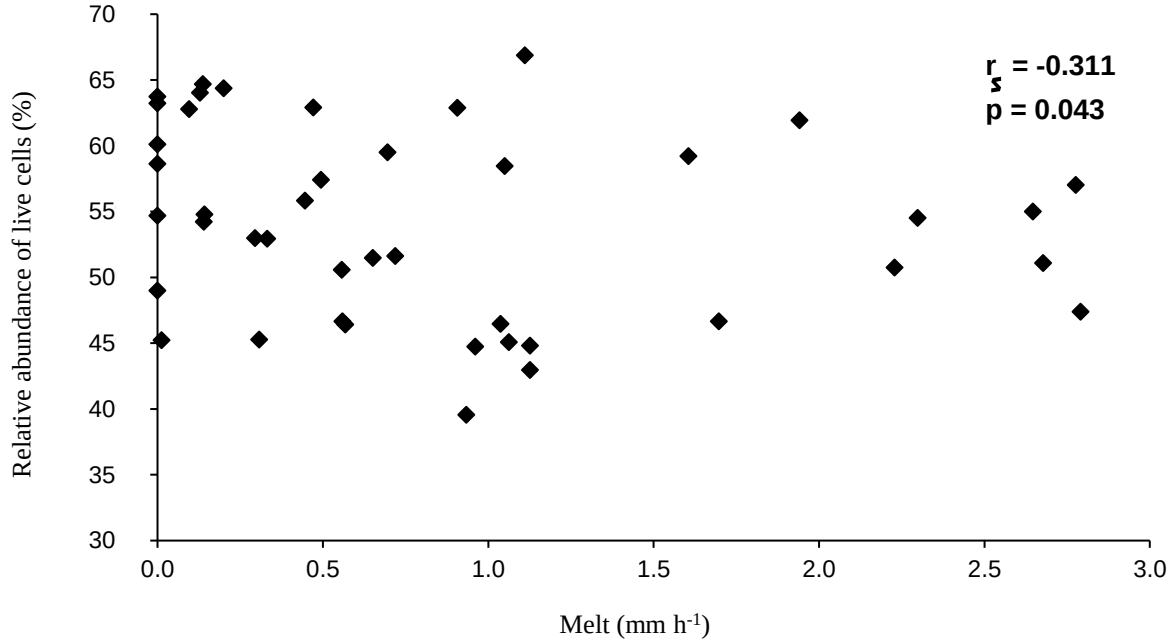

Figure 6.5. Scatter plot showing the negative association between melt and the relative percentage abundance of live microbes from the non-fixed Foxfonna Glacier supraglacial study stream samples.

6.4 Interpretation and Discussion

During this investigation with the environmental study samples, and in preliminary viability gate construction using sub-cultured *Janthinobacterium* sp. (see Section 3.2.3), it was revealed that the only shift in fluorescence observed when cell samples were fixed with glutaraldehyde and dual-stained, and so 'dead', was that of a rightward shift in FITC TO fluorescence. Existing literature and technical bulletins instead present how a vertical shift in PI fluorescence for 'killed' samples would be the expected outcome. However, for this investigation, viability determination was based on the unusual rightward shift in TO fluorescence since it was the only distinguishable difference between non-fixed and fixed, dual-stained sample replicates. However, the observed higher intake of TO by cells and subsequent increased FITC fluorescence when expectantly 'killed' with glutaraldehyde, could suggest a problem with TO uptake as it would be expected that cells with damaged DNA and so 'dead' would have less uptake of TO as there is less DNA for the TO to intercalate with, and so a higher intake of PI and PerCP fluorescence would be expected instead. However, it is tempting to speculate that this unexpected observation could be explained by the presence of the lipopolysaccharide (LPS) layer on the surface of Gram-negative bacterial cells; bacteria like that of the *Janthinobacterium* sp. used in the initial viability gating procedure, as well as other Gram-negative glacial microbes likely to be in the Midtre Lovénbreen and Foxfonna Glacier environmental samples. It has previously been stated how the LPS layer on the surface of Gram-negative bacteria can indeed interfere with the uptake of TO (BD

Biosciences, 2002). Therefore, the permeable TO in this investigation may have only been able to penetrate the supraglacial cells to a certain extent in the first instance due to the presence of the thick protective outer-membrane of the LPS layer on such cells, and so preventing any further uptake. However, when glutaraldehyde is added in order to fix cell sample replicate aliquots, the LPS layer may have been damaged and removed as a result. This assumption can be supported by a previous study whereby glutaraldehyde fixation has been shown to induce permeabilisation of cell membranes which allowed for an influx of a visible tracer into the cell as a result of the addition of such a fixative at the same time as, and before, the tracer addition (see Harper, 1986). Therefore, in this investigation more TO uptake could have occurred as the stain was able to permeate the cells better than seen previously with the non-fixed cell sample replicate aliquots, and so resulting in the subsequent rightward shift in increased FITC fluorescence due to the addition of glutaraldehyde. However, in order to overcome the interference of this LPS layer, the inclusion of 1 mM EDTA in a staining buffer has been reported to remove the LPS layer from Gram-negative bacteria (BD Biosciences, 2002), meaning that TO uptake is less likely to be prevented in such a manner as observed in the non-fixed sample replicates compared to when they are fixed as seen in this investigation, and so a less distinctive rightward shift in FITC fluorescence. Alternatively, using 50 % v/v ethanol for 30 minutes (see Davey and Hexley (2011) for ethanol addition method) as a 'killed' control instead of fixative, may result in a clearer vertical PerCP PI fluorescence for 'dead' cells, as fixative is also known to change the morphology and autofluorescence of cells, and so this alone could have impacted on the dual-staining viability results of more TO staining observed, and less intake of PI in fixed sample replicates. Furthermore, due to the non-fixed high-Arctic glacier samples having experienced long-term storage in a freezer and then being thawed before analyses, such a process may have resulted in the lysis of cells and breakdown of their cell membranes thus resulting in the release of DNA fragments in the samples instead of remaining as whole cells. As a result, this could also mean that when the dual-stain of TO and PI is added to the replicates of such samples, that the TO is able to stain the DNA fragments but the PI has less damaged cell membranes to actually permeate as some may have completely broken down in the freeze-thaw cycle, thus resulting in a stronger FITC TO than PerCP PI fluorescence in this way also. Finally, looking back at the viability dual-staining protocol outlined in Section 3.2.3, it was stated how a PI and TO dual-staining incubation time of 10 minutes before analyses was selected, however due to the number of sample aliquots being analysed in each particular batch run, it could have meant that this incubation time was longer than 10 minutes, albeit every effort was made to ensure timely analyses of the viability replicates after dual-staining. Here, it could have been that the maximum intensity of the TO staining was experienced since it was stated in BD Biosciences (2002) that at least 15 minutes allows TO to achieve maximum intensity. Subsequently, the observed higher intake of TO over PI in fixed sample replicates could also have been as a result of TO reaching this maximum intensity compared to PI. Finally, the higher intake of TO may also have been as a result of actively dividing cells thus presenting more ribosomes and so RNA content used for making proteins, which the TO will have intercalated

with. However, due to the age of the samples and the fact that cell activity is not directly assessed here, such an explanation is limited.

For both Midtre Lovénbreen and Foxfonna Glacier, the dual-stained viability sample replicates with PI and TO, but not treated prior to staining with heat or fixative, presented high relative percentage abundances of live cells compared to injured or dead cells. However, it is apparent that the heat treatment of 60 ℃ for 1.5 hours prior to the dual-staining of the aliquot replicates, did not produce a higher proportion of dead cells in this investigation but instead live cells, albeit with a slight increase in injured cells, thus suggesting that a higher temperature could be explored in future investigations in order to 'kill' cells. The heat treatment used in this investigation may have injured the cells in the sample replicates prior to dual-staining, and while every effort was made to ensure rapid staining of the sample aliquots straight after heat treatment, it could be suggested that such cells may have repaired themselves before dual-staining and so resulted in less uptake of PI, and so resulting cells being gated as live rather than dead or injured. Such a phenomenon has been observed in a study using *Saccharomyces cerevisiae* yeast cells, whereby the cells were exposed to a heat stress of 50 ℃ for 1 hour, already in the presence of PI, and resulted in a proportion of 23 % of the cells taking in PI, but after time was allowed for an equivalent population of cells which experienced the same heat treatment to recover after such a stress and so before the addition of PI, it was found that only a proportion of 14.5 % of cells now took in the PI, thus showing the ability of cells to repair their membranes after such a stress (Davey and Hexley, 2011). Additionally, it can therefore be suggested that the heat treatment for this investigation was ineffective in creating 'kille2ed' aliquot controls like that originally intended and outlined in Section 3.2.3 of the viability protocol. Instead, to obtain 'killed' aliquot controls to allow for an identification of dead cells, a protocol whereby cell replicates are 'killed' with ethanol stress may be more appropriate before the addition of the PI and TO stains as seen previously, whereby 50 % v/v of ethanol after 30 minutes led to the complete loss of viability of yeast cells (Davey and Hexley, 2011). Interestingly, it was also clear that for both glacier location sample replicates, the addition of glutaraldehyde fixative didn't effectively result in 'dead only' cells which would be expected, but did nonetheless, show the proportion of dead cells to increase with fixative treatment before dual-staining compared to the live or injured cells present. However, as stated by Kamiya et al. (2007), samples will be composed of different physiological and taxonomic microbes, and so the effect that fixation has on such cells may vary.

Additional validation calculations were used to assess whether the viability dual-staining protocol with the TO stain was indeed working in the way it would be expected, since an unusual rightward shift in FITC TO fluorescence was observed when sample replicates had been treated with glutaraldehyde, rather than an expected vertical shift in PerCP PI fluorescence. Therefore, correlations were carried out to test whether the original SYBR Gold total cell enumerations from Chapter 5 for both high-Arctic glacier locations were statistically significantly correlated to that of the total cells enumerated using the

viability dual-stain of TO in the presence of PI. Here, it was found that such total cell abundances positively correlated with one another, and for both locations, thus meaning that the nucleic acid stain of TO was staining all cells (live, dead and injured) appropriately, like that also observed of the SYBR Gold stain. However, it is important to note that although correlation testing was carried out between the SYBR Gold and dual-stained total cell enumerations, and positive associations observed, there is an uncertainty in assuming that SYBR Gold and TO nucleic acid stains will present the same microbe enumerations in FCM on the basis of their common modes of action in staining nucleic acids of cells. It would therefore be more appropriate to suggest that SYBR Gold and TO stains approximately result in similar total microbe enumerations, and that no one stain is the 'gold standard' for total cell enumerations as there is no systematic comparison of a broad range of such stains in the current literature. However, it is clear that the total cells enumerated with the SYBR Gold nucleic stain and that of the TO in the dual-stain with PI, resulted in significantly similar cell enumerations, and so suggests that the unusual rightward shift in TO fluorescence observed in the presence of glutaraldehyde, and instead of an expected vertical shift in PI fluorescence, is the result of other factors like those previously discussed.

Despite the positive correlation observed between the dual-stained total cell counts and the original SYBR Gold total counts presented in Chapter 5, an estimated mean microbial cell flux for Foxfonna Glacier study stream was calculated, but this time using the dual-stained total cell counts in events per mL. This meant that consistency was established in calculations, especially since replicates of the same samples from the SYBR Gold analyses compared to dual-staining did not produce the exact same total cell counts, albeit were similar as shown in the correlation analyses discussed previously. Furthermore, the mean microbe flux of living cells through the supraglacial study stream was also estimated, and so the live cell counts in events per mL from the dual-staining analyses were also used. Therefore, an estimated mean microbial flux of 1.04×10^{13} cells h^{-1} in the Foxfonna Glacier supraglacial study stream was found, with an estimated mean microbial flux of live cells of 5.70×10^{12} cells h^{-1}. Subsequently, it is estimated that approximately 54.65 % of the cells exported in this supraglacial study stream per hour are alive, potentially active, and delivered to proglacial environments- a surprising result for such cells to still be 'live' considering the samples have been in long-term storage at -80 °C for over 10 years. However, as shown in Section 5.4.4, freezer storage conditions over increased storage time periods did not show microbial abundance to significantly decrease in the non-fixed Foxfonna Glacier sample replicates (Figure 5.13). Additionally, the Foxfonna Glacier samples were less disturbed before FCM analyses in this investigation as they had always been frozen and never previously thawed, thus likely resulting in more live cells. In comparison, the Midtre Lovénbreen samples, experienced a relocation from an original storage and then were instead refrozen elsewhere meaning likely freeze-thaw cycling of the samples were experienced, thus presenting a stress on the cells within the samples and so less live cells enumerated in dual-staining compared to Foxfonna Glacier. Here, the previously stated 54.65 %

estimate of live cells transported through the supraglacial study stream per hour on Foxfonna means that such cells have the potential to interact with glacier-fed aquatic ecosystems once delivered there, such as shifting the already existing species distributions and microbial diversity, thus providing a potential threat to such ecosystems (Liu et al., 2021). Therefore, with rapidly receding glaciers worldwide with climatic global warming, and longer summer ablation, more meltwater will be discharged to such downstream ecosystems and with it, as shown in this chapter, live cells which may become dominant in such downstream habitats with their influx (Liu et al., 2021), and so displace other microbiota and disturb food webs. The result is the homogenisation of such exported, live microbial communities to these downstream glacier-fed environments where they are then able to carry out biogeochemical reactions and cycling of nutrients. However, it is important to note here that the statuses of 'live' and 'dead' in this chapter are generalised and it cannot be certain as to what stage of 'live' or 'dead' these cells may be at. As previously stated, it is difficult to define viability due to the different stages of a cell's life (see Davey, 2011) and physiological states (Davey and Guyout, 2020); such a detailed identification of microbe viability statuses was beyond the scope of this exploratory chapter, and so other viability stains and protocols may need to be adopted in order to identify this.

A statistically significant negative association was however found between the relative percentage abundance of live cells and melt for the supraglacial study stream on Foxfonna Glacier, thus suggesting that as melt increases, the proportion of live cells decreases, and so that of which are transported to downstream ecosystems. Therefore, this finding may suggest how increased melt from climatic global warming, and longer summer ablation periods, may indeed impact on the viability of microbes liberated from the weathering crust and discharged into nearby supraglacial streams. However, this association could be explained with the knowledge that short-wave incident radiation significantly correlates with driving melt (as established in Chapter 5), and so this solar radiation may cause photolysis of cells at the ice surface which are then liberated in melt and discharged into nearby supraglacial streams, thus accounting for the decrease in live cells with melt. Additionally, such an observation could instead be explained by the fact that when the abundance of microbes is increased during melt and transferred to nearby supraglacial streams; a finding also previously evidenced with the observed statistically significant positive association between melt and microbe abundance in Chapter 5 for Fountain Glacier, then various microbes- ancient and modern genotypes, are able to mix (Rogers et al., 2004). Such mixing may indeed impact on the various characteristics of the liberated glacial microorganisms such as fitness, mutation rates, survival, and pathogenicity (Rogers et al., 2004), especially in a supraglacial stream were microbes are all being channelled in one direction to downstream ecosystems, and so the viability of cells may be reduced this way within melt, and so revealing less cells to be alive. Therefore, if microbes are also not able to metabolise optimally with increased melt and potential impact of other liberated microbes, then reduced biogeochemical reactions will occur and subsequent decrease in by-products will be exported to downstream ecosystems, and so could impact on the bioavailability of such nutrients

for use by existing microbial communities in downstream glacier-fed environments. For example, less nutrients and DOC available from such glacial meltwater means that the micro- and macroscopic communities living in benthic zones of glacier-fed downstream ecosystems receive less support (Hotaling et al., 2017), and so could affect the bio-productivity of proglacial ecosystems with less live microbes from increased ice melt. However, it is also important to understand that such microbes may in fact already be dead on the ice surface prior to being liberated in ice melt, and then the process of melt results in 'killed' or 'injured' cells transported downstream, and so this could be why melt presents a decreased proportion of live cells within this supraglacial study stream on Foxfonna Glacier. As described previously in Chapter 4 and 5, microbes can be rejected to the ice surface during superimposed ice formation, and then liberated in such surface superimposed ice melt and transported into nearby supraglacial streams. Here, cells could potentially experience damage from the mechanical process of cells being expelled to the ice surface from ice crystals during superimposed ice formation, and so when melt increases and subsequent cells transferred to supraglacial streams, then this may suggest the reason for an observed decreased proportion of live cells with increased ice melt. Alternatively, the cells may be alive and active within ice crystals on the glacier ice surface, but when liberated during ice melt, the cells may experience lysis due to freeze-thaw cycling or even the biochemical damage due to eluted solutes from the surrounding snowmelt also being transferred in such surface ice melt along with the cells, and so resulting in the lysis of such cells due to rapid changes in osmotic pressure, and so a decreased proportion of live cells with increased ice melt.

Due to doubts in the accuracy of the dual-staining protocol as a result of the unusual rightward FITC TO fluorescence shifts when cells were fixed prior to dual-staining, future research using supraglacial cell samples may look toward alternative staining combinations for viability determination, such as using cell permeable fluorescein diacetate (FDA) and PI, instead of TO. FDA is an esterase-substrate which is a non-fluorescent dye until the point at which it enters a cell and non-specific esterase de-acetylate the dye molecule, thus converting it into a green fluorescing fluorescein (Boyd et al., 2008). Previous work has observed the use of PI and FDA as a dual-staining method for viability determination in which viable cells with strong esterase metabolic activity fluoresce green, compared to dead or dying cells with no or little activity (Boyd et al., 2008). However, this combination still possesses potential for complication in determining dead cells as such cells may still present residual activity of esterase (Boyd et al., 2008). Therefore, it is apparent that other combinations of dual-stains for viability determination of cells, and in the context of this thesis investigation- supraglacial cells, present their own limitations in the detection of cells as viable/live or dead. However, it has also been observed that a limitation in such a viability determination using FDA, and that of which could be the case as seen in this research investigation viability protocol with TO whereby TO fluorescence was stronger than PI in dead cell samples, is that too high a concentration of FDA compared to red fluorescing PI, causes an extension of the green emission peak of the FDA into the red spectrum of emission thus potentially representing dead

cells as green even if they are not fluorescing from the PI stains (Boyd et al., 2008). Therefore, a similar scenario may have occurred in this investigation whereby the concentration of TO was too high for the viability stain combination of PI and TO, thus resulting in the strong shifts in FITC TO fluorescence potentially masking the PerCP PI fluorescence for glutaraldehyde fixed samples of dead cells. Such a phenomenon can further be supported as it is stated that a dead cell stain is usually provided in a higher molar excess to ensure that the 'live' stain used is displaced from the nucleic acids in the dead cells to allow for improved discrimination (Boyd et al., 2008). Therefore, it is possible that the concentration of PI was not high enough in this thesis investigation to displace the potentially already high concentration of TO in the dead cells. Therefore, future research would be advised to further assess differing concentrations for the viability dual-stain combination of TO and PI, or even FDA and PI, and include appropriate colour compensation in the applied imaging software, in order to further optimise the staining approach, however this was beyond the scope of the research presented in this investigation.

Finally, it is important to take into account that the fresh laboratory sub-cultured glacial isolate of *Janthinobacterium* sp. used for this investigation's construction of viability gates, will present differences in viability compared to that of the environmental cells present in the Midtre Lovénbreen and Foxfonna, non-fixed, archived samples. The fresh laboratory sub-cultured *Janthinobacterium* sp. was used to represent the most likely outcome for viability staining of such glacial bacteria, especially since *Janthinobacterium* sp. is a common bacteria found in both Midtre Lovénbreen and Foxfonna glacier environments. Ultimately, a laboratory liquid sub-culture, archived environmental samples, and fresh environmental samples of the same bacteria, will all have been subject to different growing and living conditions, and so produce different viability results. Therefore, freshly collected environmental samples containing such glacial bacteria would be the desired samples to use in a pilot investigation to establish the optimum concentrations of TO and PI, or FDA and PI; allowing for a construction of the live, dead and injured gates, with an expected vertical shift in PerCP fluorescence for fixed environmental samples which will have had the expected 'live' glacial cells. Ultimately, there is a diverse range of bacterial cells in the supraglacial samples analysed in this chapter and so this alone will mean that the viability staining results will vary depending on the contents of each sample.

6.5 Summary

This exploratory chapter has reported the first quantification of the proportion of live, dead and injured cells found within high-Arctic supraglacial streams using the dual-staining analyses of PI and TO for viability determination. The dual-staining viability protocol did however produce unusual fluorescent shifts in FITC TO fluorescence rather than an expected vertical PerCP PI fluorescence for cell samples that had been 'killed', like that exemplified in existing literature, thus presenting doubts in the dual-staining combination of PI and TO of the LIVE/DEAD BD Cell Viability dual-staining kit for supraglacial cell sample viability analyses. Therefore, such a finding and the knowledge that the storage

length experienced by the sample sets may have potentially impacted on the viability status of such cells, means that the first hypothesised objective of this chapter cannot be confidently accepted. However, this investigation serves as a benchmark for viability analyses in the field of supraglacial eco-hydrology, and invites further investigation and refinement of the viability assessment dual-staining protocol used in this chapter. From this chapter's results, it was found that for the Foxfonna Glacier supraglacial study stream over half of the microbe flux through the stream per hour were classed as alive through this study's viability determination analyses, and so presenting microbes with the potential to impact the existing microbial diversity in downstream ecosystems. Furthermore, this exploratory chapter revealed a negative correlation between the proportion of live cells against melt, thus suggesting that the viability of cells found at the glacier ice surface and discharged into supraglacial stream meltwater, and ultimately exported to downstream glacier-fed environments, is affected by the melt season. However, it is not certain as to whether such cells liberated from the glacier surface and discharged in supraglacial meltwaters, are indeed dead before mobilisation in melt or die during such a process. The impact of live and dead cells on downstream ecosystems is still unknown.

7 THESIS SYNTHESIS AND CONCLUSION

7.1 Review of Research Aim and Objectives

During a time of ongoing climatic global warming, it is important to better understand and contribute to current knowledge of the eco-hydrology of declining mountain and Arctic glacier environments, and so improve predictions of how connected ecosystems may respond to such ice mass loss. The underlying interest in this research is the eco-hydrology of the supraglacial ecosystem including the microbial liberation, flux, and viability of such supraglacial cells within supraglacial streams. Ultimately, the near-surface weathering crust occupies substantially more of a glacier surface area than supraglacial channels and has been shown in this thesis to feed such supraglacial channels with meltwater and associated liberated microbial cells since no significant differences were found between such abundances for the weathering crust and supraglacial stream environments. However, the variation in microbe fluxes subsequently exported to downstream ecosystems, and the associated viability of those microbes, needed further examination. The research aim for this investigation was to assess the variability in the abundance of microbes liberated in supraglacial stream fluxes, and their viability status, using previously archived meltwater samples drawn from four Arctic valley glacier environments.

Chapter 3 allowed for the refinement of an FCM SOP for the reliable enumeration of supraglacial microbes, and so achieved Objective 1 outlined in Section 1.2 of this investigation. Such steps outlined in this methodological chapter to optimise the flow cytometer settings and the SYBR Gold staining protocol itself, meant that microbe enumerations revealed in Chapters 4 and 5 were comparable with microbe abundances observed in existing literature. In Chapter 4, it was revealed that mean microbe abundance ranged from 1.47 to 10.78 × 10^4 cells mL^{-1} for five different ice types with rill ice presenting the lowest mean abundance, followed by glacier coarse bubbly ice, coarse clear, fine ice, and then finally superimposed ice with the highest mean microbe abundance on the surface of Storglaciären. Estimated mean cellular carbon content in the bulk ice density ranged from 2.70 × 10^{-7} kg C m^{-3} of ice to 1.98 × 10^{-6} kg C m^{-3} of ice (2.95 × 10^{-7} to 2.16 × 10^{-6} kg C m^{-3} meltwater equivalent (w.e.), respectively), thus further evidencing how the glacier ice surface acts as a carbon sink and source for metabolically and biogeochemically active microbes. The high mean abundance revealed for superimposed ice suggests that the mechanism of superimposed ice formation and melt presents a likely process for cell liberation at the glacier ice surface, and so with potential to then be exported in meltwater runoff into nearby supraglacial streams. Chapter 5 also saw the application of the refined FCM protocol to enumerate supraglacial microbes and respective size fraction distributions. For Fountain Glacier, a mean microbe abundance of 1.16 × 10^4 cells mL^{-1}, an estimated mean cellular carbon content of 2.32 × 10^{-7} kg C m^{-3} w.e., and a mean microbial flux of 5.46 × 10^{11} cells h^{-1} through the supraglacial study stream were found. However, the weathering crust environment presented a higher mean microbe abundance of 1.77 × 10^4 cells mL^{-1}, with an estimated mean cellular carbon content of 3.53 × 10^{-7} kg C m^{-3} w.e. found. No

statistically significant difference was found between the microbe abundance within the supraglacial stream and weathering crust environment, and so supporting the assumption that cells liberated on the glacier surface are discharged into nearby supraglacial channels. For Foxfonna Glacier, a mean microbe abundance of 0.72×10^4 cells mL^{-1}, an estimated mean cellular carbon content of 1.43×10^{-7} kg C m^{-3} w.e., and a mean microbial flux of 4.81×10^{12} cells h^{-1} through the supraglacial study stream here were revealed. Such glacier locations also allowed for Objective 3 to be achieved by assessing the associations between key hydrometeorological variables and microbe abundance. For Fountain Glacier, positive correlations were revealed for microbe abundance against short-wave incident radiation, melt, and discharge, thus presenting environmental controlling factors of microbial fluxes. However, for Foxfonna Glacier, a positive correlation was revealed between microbe abundance and EC, thus suggesting a potential process for cell liberation as identified in Chapter 4. Here, it is surmised that superimposed ice present on Foxfonna Glacier could have rejected cells and solutes to the ice surface during superimposed ice formation, whereby liberated cells and solutes can then be mobilised in such snow/ice melt and discharged into supraglacial streams, and resulting in a subsequent increase in the EC of the stream due to the increased presence of ice surface solutes. Such enumeration results here allowed for confidence in Chapter 3's refined FCM SOP and so is deemed as appropriate for the enumeration of supraglacial microbes in future research.

For Objective 2, the dual-staining protocol for viability determination did present particular challenges meaning that this staining protocol presents a less confident approach in identifying the viability status of supraglacial cells as 'live' or 'dead'. Chapter 6 allowed for the first application of Chapter 3's viability dual-staining protocol in order to identify the viability statuses of supraglacial cells as 'live' or 'dead', but only in the generalised sense as it has previously been established how the viability of a cell is more complex than simply being stated as 'live' or 'dead'. This exploratory chapter presents the first example in research to attempt to assess the viability of supraglacial microbes. However, it was found that during this dual-staining protocol, glutaraldehyde fixative did not produce all 'dead' cells that would be expected and that in such a presence with this fixative, cells experienced a higher uptake of TO compared to PI. Such observations in the results were not expected since previous literature and technical bulletins have shown that 'dead' cells should experience a higher uptake of PI in such instances and so a resulting vertical shift in PI fluorescence. However, the apparent rightward shift in TO fluorescence observed in this investigation makes it tempting to speculate that the presence of an LPS layer of Gram-negative bacteria may present a factor in the unusual uptakes of the stains, and in combination with the fixative which could present a permeabilising role to cell membranes. However, viability gates were still constructed on such observations, albeit not the usual gates that would be expected, in order to allow a basis and estimate of the proportion of 'live' and 'dead' cells in the samples to be made. For Foxfonna Glacier, it was estimated that approximately 54.65 % of the microbes exported from the glacier ice surface and in supraglacial meltwater flux are alive, and so ultimately delivered to downstream

ecosystems with the potential to be active and interact with such ecosystems. Furthermore, again achieving Objective 3, a significant negative association was found between live cells and melt, thus suggesting increased melt is a controlling factor of microbial viability. However, explanations for such a decrease in live cells with increased melt are speculative, such as mechanical damage to cells caused by ice formation; a result of cells experiencing freeze-thaw cycles; lysis of cells, or even the mixing with other microbes in melt that may 'harm' other microbes.

7.2 Potential Directions for Future Research

Microbe abundance analyses were carried out on previously archived samples; storage of over 10 years for some sample sets. However, it is encouraged to use fresh supraglacial microbial samples (collected straight from the field if the required facilities for analyses and equipment are available, or within a few months of collection back at a laboratory when time allows) in future research with the same FCM protocols outlined in this thesis for the enumeration of supraglacial microbes, but also to be able to test the viability dual-staining SOP more accurately. Additionally, the results presented for the storage experiments were limited since the samples had themselves already been subject to long-term storage and freeze-thaw stress and so again, fresh samples would be suggested in order to carry out similar storage experimental analyses in the future. Therefore, a hypothesis in this context could test the impact of storage length and condition on cell samples in the first instance of being stored after sample collection, and before sample analyses. For example, fresh samples could be collected and represent 0 hours if able to carry out FCM analyses during the study period of sample collection in the field, with then the preceding 1, 4, 11 and 14 days later of FCM analyses also. Therefore, the storage impact on the fresh samples' microbe abundances, as well as quantifying the proportion of 'live' and 'dead' cells, and so how these results change from the 0 hour analyses to 14 days, could be analysed more accurately.

As a result of the unexpected observations in fluorescence when using the viability dual-staining combination of TO and PI, it is also encouraged that the individual staining of TO and PI should be tested, as well as varying the concentrations, and so not in combination with each other but instead assessing the individual responses of the stains. Such an approach was beyond the scope of this thesis but would allow for a clearer assessment as to how the stains individually work on the supraglacial cells, and to hopefully observe the expected vertical shift in PI fluorescence for dead cells as shown in existing literature. Also, the addition of EDTA is suggested to reduce the influence from the LPS layer of bacteria, and instead the use of ethanol in cell samples to produce 'dead' controls rather than fixative, since glutaraldehyde may have impacted on the permeability of the cells. Therefore, a hypothesis should be tested to ascertain whether the LIVE/DEAD BD Cell Viability dual-staining kit in FCM can indeed allow for reliable proportions of live and dead supraglacial cells from fresh samples to be determined accurately, and with only expected shifts in propidium iodide fluorescence for 'dead' cells. Furthermore, other viability staining combinations, such as PI and FDA are encouraged to be explored for the

determination of viability in supraglacial cells. Additionally, since only a generalised categorisation of cells as being either 'live' or 'dead' was made in this investigation, staining techniques could be applied to show a clearer identification as to the stage of viability in a cell. The 'live' cells presented in this investigation could have been viable but not culturable, or dormant. However, with the use of stains such as CTC, it would instead allow for the specific identification of the proportion of cells that are actively respiring and so showing cell-specific metabolic activity. Thus, in the wider context, the contribution of such cells to downstream proglacial ecosystems would be easier to determine by knowing the cells' actual stages of viability and so test the hypothesis as to whether supraglacial microbes exported downstream and carrying out metabolic reactions ultimately impact on their surrounding environment- information that is unknown in current literature.

Finally, it is known that microbes in the supraglacial ecosystem are active and can change the ice surface, such as filamentous cyanobacteria which form cryoconite granules by combining microbes and dust using EPS. However, future research could also involve looking at microbes as ecosystem engineers within the weathering crust. Therefore, rather than just enumerating the microbes inhabiting such a porous ice matrix, research could investigate whether such microbes are alive and so determine whether they have the potential to change the weathering crust environment to sustain themselves, such as interacting with the structure of the weathering crust. Hitherto, there is no evidence which describes how microbes might change the structure of this porous near-surface, or the association of given microbial taxa with changes in weathering crust development. Therefore, sampling of the weathering crust and so the microbial taxa present, abundance, and viability during different stages of development, such as in daylight hours when the weathering crust is highly saturated compared to at night when the weathering crust is drained and so less saturated, could be made. Thus, an assessment could be carried out as to the association between the different microbes found in the weathering crust against the various stages of development of this near-surface ice matrix, and the role they may play in changing the weathering crust structure in order to survive during such development in this environment. Additionally, since a negative association was observed between melt and the proportion of live cells present in a supraglacial stream in this investigation, it could be suggested that longer assessments could be made and so compare the proportion of live cells at the start, middle and end of the summer ablation season to see how this seasonal temporal change may impact microbial viability with ice melt.

7.3 Research Synthesis

This investigation has revealed an eco-hydrological narrative whereby microbial abundances enumerated from supraglacial streams are inherently supplied by the weathering crust of glaciers. Cell liberation occurs at the ice surface as a likely result of ice formation mechanisms which expel such cells to the surface and allow them to be mobilised and discharged into nearby supraglacial streams as dictated by hydrometeorological environmental controls. Subsequent microbes exported to glacier-fed

downstream environments have the potential to impact on their surrounding environment, but their actual contribution is still unknown and cellular viability is complex with a need to define more viability statuses of cells other than ‘live’ or ‘dead’. However, this investigation has presented the first estimation in current literature using dual-staining in FCM for ‘live’ and ‘dead’ cells within a supraglacial environment, and found that the proportion of ‘live’ cells within a high-Arctic supraglacial meltwater channel may be influenced by melt seasons, but additional research is encouraged to support this finding further.

REFERENCES

Alexander, A., Kruusmaa, M., Tuhtan, J.A., Hodson, A.J., Schuler, T.V. and Kääb, A. (2020). Pressure and inertia sensing drifters for glacial hydrology flow path measurements. *The Cryosphere*, 14(3), 1009-1023.

Alsharif, R. and Godfrey, W. (2002). *Microbial Cytometry Application Note: Bacterial Detection and Live/Dead Discrimination by Flow Cytometry*. BD Biosciences, Immunocytometry Systems, San Jose, CA, 6pp.

Amato, P., Hennebelle, R., Magand, O., Sancelme, M., Delort, A-M., Barbante, C., Boutron, C. and Ferrari, C. (2007). Bacterial characterization of the snow cover at Spitzberg, Svalbard. *FEMS Microbiology Ecology*, 59(2), 255–264.

Anesio, A.M., Lutz, S., Chrismas, N.A.M. and Benning, L.G. (2017). The microbiome of glaciers and ice sheets. *Biofilms and Microbiomes*, 3(10), 1-11.

Anesio, A.M., Sattler, B., Foreman, C., Telling, J., Hodson, A., Tranter, M. and Psenner, R. (2010). Carbon fluxes through bacterial communities on glacier surfaces. *Annals of Glaciology*, 51(56), 32-40.

Battin, T.J., Wille, A., Psenner, R. and Richter, A. (2004). Large-scale environmental controls on microbial biofilms in high-alpine streams. *Biogeosciences*, 1(2), 159-171.

BD Biosciences. (2002). Application Note: Bacterial Detection and Live/Dead Discrimination by Flow Cytometry. https://www.bdbiosciences.com/content/dam/bdb/marketing-documents/Bacterial_Deetection_Live_Dead.pdf [Accessed: 18th January 2022].

BD Biosciences. (2012). Technical Bulletin: Threshold and Analysis of Small Particles on the BD Accuri® C6 Flow Cytometer. https://static.bdbiosciences.com/documents/accuri/Accuri-TB-Threshold-and-Analysis-of-Particles.pdf [Accessed: 12th March 2021].

BD Biosciences. (2016). BD Accuri™ C6 Plus System User's Guide. https://static.bdbiosciences.com/documents/BD-Accuri-C6-Plus-Users-Guide.pdf [Accessed: 12th March 2021].

Berney, M., Hammes, F., Bosshard, F., Weilenmann, H.-U. and Egli, T. (2007). Assessment and Interpretation of Bacterial Viability by Using the LIVE/DEAD BacLight Kit in Combination with Flow Cytometry. *Applied and Environmental Microbiology*, 73(10), 3283-3290.

Bhatia, M., Sharp, M. and Foght, J. (2006). Distinct Bacterial Communities Exist beneath a High Arctic Polythermal Glacier. *Applied and Environmental Microbiology*, 72(9), 5838-5845.

Bingham, R.G., Nienow, P.W. and Sharp, M.J. (2003). Intra-annual and intra-seasonal flow dynamics of a High Arctic polythermal valley glacier. *Annals of Glaciology*, 37, 181-188.

Blatter, H. and Hutter, K. (1991). Polythermal conditions in Arctic glaciers. *Journal of Glaciology*, 37(126), 261-269.

Boetius, A., Anesio, A.M., Deming, J.W., Mikucki, J.A. and Rapp, J.Z. (2015). Microbial ecology of the cryosphere: sea ice and glacial habitats. *Nature Reviews*, 13, 677-690.

Boyd, V., Cholewa, O.M. and Papas, K.K. (2008). Limitations in the Use of Fluorescein Diacetate/Propidium Iodide (FDA/PI) and Cell Permeable Nucleic Acid Stains for Viability Measurements of Isolated Islets of Langerhans. *Current Trends in Biotechnology and Pharmacy*, 2(2), 66-84.

Brock, B.W. and Arnold, N.S. (2000). A spreadsheet-based (Microsoft Excel) point surface energy balance model for glacier and snow melt studies. *Earth Surface Processes and Landforms*, 25(6), 649-658.

Brock, B.W., Willis, I.C. and Sharp, M.J. (2006). Measurement and parameterization of aerodynamic roughness length variations at Haut Glacier d'Arolla, Switzerland. *Journal of Glaciology*, 52(177), 1-17.

Brussaard, C.P.D. (2004). Optimization of Procedures for Counting Viruses by Flow Cytometry. *Applied and Environmental Microbiology*, 70(3), 1506-1513.

Carter, N.P. and Ormerod, M.G. (2000). *Flow Cytometry Third Edition: A Practical Approach*. Oxford University Press, Surrey, UK, 276pp.

Cauvy-Fraunié, S. and Dangles, O. (2019). A global synthesis of biodiversity responses to glacier retreat. *Nature Ecology & Evolution*, 3(12), 1675-1685.

Christner, B.C., Lavender, H.F., Davis, C.L., Oliver, E.E., Neuhaus, S.U., Myers, K.F., Hagedorn, B., Tulaczyk, S.M., Doran, P.T. and Stone, W.C. (2018). Microbial processes in the weathering crust aquifer of a temperate glacier. *The Cryosphere*, 12, 3653-3669.

Cook, J.M., Hodson, A.J. and Irvine-Fynn, T.D.L. (2016a). Supraglacial weathering crust dynamics inferred from cryoconite hole hydrology. *Hydrological Processes*, 30, 433-446.

Cook, J.M., Edwards, A., Takeuchi, N. and Irvine-Fynn, T.D.L. (2016b). Cryoconite: The dark biological secret of the cryosphere. *Progress in Physical Geography*, 40(1), 66-111.

Créach, V., Baudoux, A.-C., Bertru, G. and Rouzic, B.L. (2003). Direct estimate of active bacteria: CTC use and limitations. *Journal of Microbiological Methods*, 52(1), 19-28.

Dancer, S.J., Shears, P. and Platt, D.J. (1997). Isolation and characterization of coliforms from glacial ice and water in Canada's High Arctic. *Journal of Applied Microbiology*, 82, 597-609.

Darcy, H. (1856). *Les fontaines publiques de la ville de Dijon: exposition et application*. Victor Dalmont, Paris, 647pp.

Davey, H. (2011). Life, Death, and In-Between: Meanings and Methods in Microbiology. *Applied and Environmental Microbiology*, 77(16), 5571-5576.

Davey, H. and Guyot, S. (2020). Estimation of microbial viability using flow cytometry. *Current Protocols in Cytometry*, 93(72), 1-13.

Davey, H. and Hexley, P. (2011). Red but not dead? Membranes of stressed *Saccharomyces cerevisiae* are permeable to propidium iodide. *Environmental Microbiology*, 13(1), 163-171.

DeWalle, D.R. and Rango, A. (2008). *Principles of snow hydrology*. Cambridge University Press, UK, 410pp.

Emerson, J.B., Adams, R.I., Román, C.M.B., Brooks, B., Coil, D.A., Dahlhausen, K., Ganz, H.H., Hartmann, E.M., Hsu, T., Justice, N.B., Paulino-Lima, I.G., Luongo, J.C., Lymperopoulou, D.S., Gomez-Silvan, C., Rothschild-Mancinelli, B., Balk, M., Huttenhower, C., Nocker, A., Vaishampayan, P. and Rothschild, L.J. (2017). Schrödinger's microbes: tools for distinguishing the living from the dead in microbial ecosystems. *Microbiome*, 5(86), 1-23.

Ewing, K.J. (1970). Supraglacial streams of the Kaskawulsh Glacier. In: Bushnell, V.C. and Ragle, R.H. (Editors) *Icefield Ranges Research Project*: *Scientific Results*. New York, American Geographical Society, 153-162.

Fair, H., Smiley Jr, P.C. and Qiao, L. (2020). Physical, chemical, and biological characteristics of supraglacial pools on a debris-covered glacier in Mt. Gongga, Tibetan Plateau. *Arctic, Antarctic, and Alpine Research*, 52(1), 635-649.

Foreman, C.M., Cory, R.M., Morris, C.E., SanClements, M.D., Smith, H.J., Lisle, J.T., Miller, P.L., Chin, Y.-P. and McKnight, D.M. (2013). Microbial growth under humic-free conditions in a supraglacial stream system on the Cotton Glacier, Antarctica. *Environmental Research Letters*, 8, 1-11.

Franzetti, A., Navarra, F., Tagliaferri, I., Gandolfi, I., Bestetti, G., Minora, U., Azzoni, R.S., Diolaiuti, G., Smiraglia, C. and Ambrosini, R. (2017). Potential sources of bacteria colonizing the cryoconite of an Alpine glacier. *PLoS One*, 12(3), 1-13.

Fyffe, C.L., Brock, B.W., Kirkbride, M.P., Mair, D.W.F., Arnold, N.S., Smiraglia, C., Diolaiuti, G. and Diotri, F. (2019). Do debris-covered glaciers demonstrate distinctive hydrological behaviour compared to clean glaciers? *Journal of Hydrology*, 570, 584-597.

Gerdel, R.W. and Drouet, F. (1960). The Cryoconite of the Thule Area, Greenland. *American Microscopical Society*, 79(3), 256-272.

Glasser, N.F., Hambrey, M.J., Etienne, J.L., Jansson, P. and Pettersson, R. (2003). The origin and significance of debris-charged ridges at the surface of Storglaciären, northern Sweden. *Geografiska Annaler*, 85A(2), 127–147.

Goelles, T. and Bøggild, C.E. (2017). Albedo reduction of ice caused by dust and black carbon accumulation: a model applied to the K-transect, West Greenland. *Journal of Glaciology*, 63(242), 1063-1076.

Gokul, J.K., Hodson, A.J., Saetnan, E.R., Irvine-Fynn, T.D.L., Westall, P.J., Detheridge, A.P., Takeuchi, N., Bussel, J., Mur, L.A.J. and Edwards, A. (2016). Taxon interactions control the distributions of cryoconite bacteria colonizing a High Arctic ice cap. *Molecular Ecology*, 25(15), 3752-3767.

Goto-Azuma, K., Nakawo, M., Jiankang, H., Watanabe, O. and Azuma, N. (1994). Melt-induced relocation of ions in glaciers and in a seasonal snowpack. *Snow and Ice Covers: Interactions with the Atmosphere and Ecosystems*, 223, 287-297.

Gusmeroli, A., Jansson, P., Pettersson, R. and Murray, T. (2012). Twenty years of cold surface layer thinning at Storglacia¨ren, sub-Arctic Sweden, 1989–2009. *Journal of Glaciology*, 58(207), 3-10.

Han, T., Li, X., Gao, M., Sillanpää, M., Pu, H. and Lu, C. (2015). Electrical Conductivity during the Ablation Process of the Glacier No. 1 at the Headwaters of the Urumqi River in the Tianshan Mountains. *Arctic, Antarctic, and Alpine Research*, 47(2), 327-334.

Harper, I.S. (1986). Glutaraldehyde-induced permeabilization of cell membranes. *Journal of Microscopy*, 141(2), RP3-RP4.

Hatzenpichler, R., Connon, S.A., Goudeau, D., Malmstrom, R.R., Woyke, T. and Orphan, V.J. (2016). Visualizing in situ translational activity for identifying and sorting slow-growing archaeal−bacterial consortia. *PNAS*, 113(28), E4069-E4078.

Hinlo, R., Gleeson, D., Lintermans, M. and Furlan, E. (2017). Methods to maximise recovery of environmental DNA from water samples. *PLoS ONE*, 12(6), 1-22.

Hock, R. (2005). Glacier melt: a review of processes and their modelling. *Progress in Physical Geography*, 29(3), 362-391.

Hodson, A., Paterson, H., Westwood, K., Cameron, K. and Laybourn-Parry, J. (2013). A blue-ice ecosystem on the margins of the East Antarctic ice sheet. *Journal of Glaciology*, 59(214), 255-268.

Hodson, A., Anesio, A.M., Tranter, M., Fountain, A., Osborn, M., Priscu, J., Laybourn-Parry, J. and Sattler, B. (2008). Glacial Ecosystems. *Ecological Monographs*, 78(1), 41-67.

Hoffman, M.J., Fountain, A.G. and Liston, G.E. (2014). Near-surface internal melting: a substantial mass loss on Antarctic Dry Valley glaciers. *Journal of Glaciology*, 60(220), 361-374.

Holmlund, E.S. and Holmlund, P. (2019). Constraining 135 years of mass balance with historic structure-from-motion photogrammetry on Storglaciären, Sweden. *Geografiska Annaler: Series A, Physical Geography*, 101(3), 195-210.

Hood, E., Fellman, J., Spencer, R.G.M., Hernes, P.J., Edwards, R., D'Amore, D. and Scott, D. (2009). Glaciers as a source of ancient and labile organic matter to the marine environment. *Nature*, 462, 1044-1047.

Hotaling, S., Hood, E. and Hamilton, T.L. (2017). Microbial ecology of mountain glacier ecosystems: biodiversity, ecological connections and implications of a warming climate. *Environmental Microbiology*, 19(8), 2935-2948.

Hotaling, S., Wimberger, P.H., Kelley, J.L. and Watts, H.E. (2020). Macroinvertebrates on glaciers: a key resource for terrestrial food webs? *Ecology*, 101(4), 1-3.

Hubbard, B. and Glasser, N. (2005). *Field Techniques in Glaciology and Glacial Geomorphology*. Centre for Glaciology, University of Wales, Aberystwyth, John Wiley & Sons Ltd, England, 400pp.

Huss, M. and Hock, R. (2018). Global-scale hydrological response to future glacier mass loss. *Nature Climate Change*, 8, 135-140.

IPCC. (2019). Summary for Policymakers. In: Pörtner, H.-O., Roberts, D.C., Masson-Delmotte, V., Zhai, P., Tignor, M., Poloczanska, E., Mintenbeck, K., Nicolai, M., Okem, A., Petzold, J., Rama, B. and Weyer, N. (Editors) *IPCC Special Report on the Ocean and Cryosphere in a Changing Climate.* In press, 1-42.

Irvine-Fynn, T.D.L. and Edwards, A. (2014). A Frozen Asset: The Potential of Flow Cytometry in Constraining the Glacial Biome. *Cytometry Part A*, 85(1), 3-7.

Irvine-Fynn, T.D.L. and Hubbard, B. (2017). Glacier Hydrology and Runoff. In: Richardson, D., Castree, N., Goodchild, M.F., Kobayashi, A., Liu, W. and Marston, R.A. (Editors) *The International Encyclopedia of Geography*. John Wiley & Sons, 1-18.

Irvine-Fynn, T.D.L., Hodson, A.J., Moorman, B.J., Vatne, G. and Hubbard, A.L. (2011). Polythermal Glacier Hydrology: A Review. *Reviews of Geophysics*, 49(4), 1-37.

Irvine-Fynn, T.D.L., Hanna, E., Barrand, N.E., Porter, P.R., Kohler, J. and Hodson, A.J. (2014). Examination of a physically based, high-resolution, distributed Arctic temperature-index melt model, on Midtre Lovénbreen, Svalbard. Hydrological Processes, 28(1), 134-149.

Irvine-Fynn, T.D.L., Holt, T.O., James, T.D., Smith, M.W., Rutter, N., Porter, P.R. and Hodson, A.J. (2022). Time-lapse photogrammetry reveals hydrological controls of fine-scale High-Arctic glacier surface roughness evolution. *Earth Surface Processes and Landforms*, 1-18.

Irvine-Fynn, T.D.L., Edwards, A., Newton, S., Langford, H., Rassner, S.M., Telling, J., Anesio, A.M. and Hodson, A.J. (2012). Microbial cell budgets of an Arctic glacier surface quantified using flow cytometry. *Environmental microbiology*, 14(11), 2998-3012.

Irvine-Fynn, T.D.L., Edwards, A., Stevens, I.T., Mitchell, A.C., Bunting, P., Box, J.E., Cameron, K.A., Cook, J.M., Naegeli, K., Rassner, S.M.E., Ryan, J.C., Stibal, M., Williamson, C.J. and Hubbard, A. (2021). Storage and export of microbial biomass across the western Greenland Ice Sheet. *Nature Communications*, 12(3960), 1-11.

Jennings, S.J.A. and Hambrey, M.J. (2021). Structures and Deformation in Glaciers and Ice Sheets. *Reviews of Geophysics*, 59(3), 1-135.

Kamiya, E., Izumiyama, S., Nishimura, M., Mitchell, J.G. and Kogure, K. (2007). Effects of Fixation and Storage on Flow Cytometric Analysis of Marine Bacteria. *Journal of Oceanography*, 63, 101-112.

Koziol, K.A., Moggridge, H.L., Cook, J.M. and Hodson, A.J. (2019). Organic carbon fluxes of a glacier surface: A case study of Foxfonna, a small Arctic glacier. *Earth Surface Processes and Landforms*, 44(2), 405-416.

Krainer, K. and Mostler, W. (2002). Hydrology of Active Rock Glaciers: Examples from the Austrian Alps. *Arctic, Antarctic, and Alpine Research*, 34(2), 142-149.

Leizeaga, A., Estrany, M., Forn, I. and Sebastián, M. (2017). Using Click-Chemistry for Visualizing *in Situ* Changes of Translational Activity in Planktonic Marine Bacteria. *Frontiers in Microbiology*, 8(2360), 1-11.

Li, T., Wang, S., Fu, B. and Feng, X. (2020). Frequency analyses of peak discharge and suspended sediment concentration in the United States. *Journal of Soils and Sediments*, 20(2), 1157-1168.

Liu, Y., Yao, T., Jiao, N., Kang, S., Zeng, Y. and Liu, X. (2009). Abundance and diversity of snow bacteria in two glaciers at the Tibetan Plateau. *Frontiers of Earth Science in China*, 3(1), 80-90.

Liu, K., Liu, Y., Hu, A., Wang, F., Zhang, Z., Yan, Q., Ji, M. and Vick-Majors, T.J. (2021). Fate of glacier surface snow-originating bacteria in the glacier-fed hydrologic continuums. *Environmental Microbiology*, 23(11), 6450-6462.

Lliboutry, L. (1996). Temperate ice permeability, stability of water veins and percolation of internal meltwater. *Journal of Glaciology*, 42(141), 201-211.

López-Amorós, R., Mason, D.J. and Lloyd, D. (1995). Use of two oxonols and a fluorescent tetrazolium dye to monitor starvation of Escherichia coli in seawater by flow cytometry. *Journal of Microbiological Methods*, 22, 165-176.

Lund, M., Stiegler, C., Abermann, J., Citterio, M., Hansen, B.U. and Van As, D. (2017). Spatiotemporal variability in surface energy balance across tundra, snow and ice in Greenland. *Ambio*, 46, 81-93.

MacDonell, S. and Fitzsimons, S. (2008). The formation and hydrological significance of cryoconite holes. *Progress in Physical Geography*, 32(6), 595-610.

Mader, H.M., Pettitt, M.E., Wadham, J.L., Wolff, E.W. and Parkes, R.J. (2006). Subsurface ice as a microbial habitat. *Geology*, 34(3), 169-172.

Mantelli, E., Camporeale, C. and Ridolfi, L. (2015). Supraglacial channel inception: Modelling and processes. *Water Resources Research*, 51, 7044-7063.

Martin, A., Hall., J.A., O'Toole, R., Davy, S.K. and Ryan, K.G. (2008). High single-cell metabolic activity in Antarctic sea ice bacteria. *Aquatic Microbial Ecology*, 52, 25-31.

McIntyre, N.F. (1984). Cryoconite hole thermodynamics. *Canadian Journal of Earth Sciences*, 21(2), 152-156.

Metcalf, R.C. (1984). Instruments & Methods: Field pH determinations in glacial meltwaters. *Journal of Glaciology*, 30(104), 106-111.

Milner, A.M., Brown, L.E. and Hannah, D.M. (2009). Hydroecological response of river systems to shrinking glaciers. *Hydrological Processes*, 23(1), 62-77.

Milner, A.M., Khamis, K., Battin, T.J., Brittain, J.E., Barrand, N.E., Füreder, L., Cauvy-Fraunié, S., Gíslason, G.M., Jacobsen, D., Hannah, D.M., Hodson, A.J., Hood, E., Lencioni, V., Ólafsson, J.S., Robinson, C.T., Tranter, M. and Brown, L.E. (2017). Glacier shrinkage driving global changes in downstream systems. *PNAS*, 114(37), 9770-9778.

Mindl, B., Anesio, A.M., Meirer, K., Hodson, A.J., Laybourn-Parry, J., Sommaruga, R. and Sattler, B. (2007). Factors influencing bacterial dynamics along a transect from supraglacial runoff to proglacial lakes of a high Arctic glacieri. *FEMS Microbiology Ecology*, 59(2), 307-317.

Miner, K.R., D'Andrilli, J., Mackelprang, R., Edwards, A., Malaska, M.J., Waldrop, M.P. and Miller, C.E. (2021). Emergent biogeochemical risks from Arctic permafrost degradation. *Nature Climate Change*, 11, 809-819.

Miteva, V. (2008). Bacteria in Snow and Glacier Ice. In: Margesin, R., Schinner, F., Marx, J-C. and Gerday, C. (Editors) *Psychrophiles: From Biodiversity to Biotechnology*. Springer, Berlin, Heidelberg, 31-50.

Molecular Probes. (2003). Flow Cytometry Size Calibration Kit Product Information. https://www.thermofisher.com/order/catalog/product/F13838 [Accessed: 12th March 2021].

Monz, M.E., Hudleston, P.J., Prior, D.J., Michels, Z., Fan, S., Negrini, M., Langhorne, P.J. and Qi, C. (2021). Full crystallographic orientation (c and a axes) of warm, coarse-grained ice in a shear-dominated setting: a case study, Storglaciären, Sweden. *The Cryosphere*, 15, 303-324.

Müller, F. and Keeler, C.M. (1969). Errors in short-term ablation measurements on melting ice surfacers. *Journal of Glaciology*, 8(52), 91-105.

Munro, D.S. (2011). Delays of supraglacial runoff from differently defined microbasin areas on the Peyto Glacier. *Hydrological Processes*, 25, 2983-2994.

Oerlemans, J., Giesen, R.H. and Van den Broeke, M.R. (2009). Retreating alpine glaciers: increased melt rates due to accumulation of dust (Vadret da Morteratsch, Switzerland). *Journal of Glaciology*, 55(192), 729-736.

Oke, T.R. (1987). *Boundary Layer Climates- Second Edition*. Routledge Press, London, 464pp.

Paterson, W.S.B. (1994). *The Physics of Glaciers (Third Edition)*. Butterworth-Heinemann, Oxford, 481pp.

Pellicciotti, F., Carenzo, M., Helbing, J., Rimkus, S. and Burlando, P. (2009). On the role of subsurface heat conduction in glacier energy-balance modelling. *Annals of Glaciology*, 50(50), 16-24.

Pettersson, R. and Jansson, P. (2004). Spatial variability in water content at the cold-temperate transition surface of the polythermal Storglaciären, Sweden. *Journal of Geophysical Research*, 109, 1-12.

Pettersson, R., Jansson, P. and Holmlund, P. (2003). Cold surface layer thinning on Storglaciären, Sweden, observed by repeated ground penetrating radar surveys. *Journal of Geophysical Research*, 108(F1), 5.1-5.9.

Pitcher, L.H. and Smith, L.C. (2019). Supraglacial Streams and Rivers. *Annual Review of Earth and Planetary Sciences*, 47, 421-452.

Postgate, J.R. (1969). Chapter XVIII viable counts and Viability. *Methods in Microbiology*, 1, 611-628.

Rassner, S.M.E., Anesio, A.M., Girdwood, S.E., Hell, K., Gokul, J.K., Whitworth, D.E. and Edwards, A. (2016). Can the Bacterial Community of a High Arctic Glacier Surface Escape Viral Control? *Frontiers in Microbiology*, 7(956), 1-16.

Remias, D., Holzinger, A., Aigner, S. and Lütz, C. (2012). Ecophysiology and ultrastructure of Ancylonema nordenskio¨ldii (Zygnematales, Streptophyta), causing brown ice on glaciers in Svalbard (high arctic). *Polar Biology*, 35, 899-908.

Rime, T., Hartmann, M. and Frey, B. (2016). Potential sources of microbial colonizers in an initial soil ecosystem after retreat of an alpine glacier. *The ISME Journal*, 10, 1625-1641.

Rogers, S.O., Starmer, W.T. and Castello, J.D. (2004). Recycling of pathogenic microbes through survival in ice. *Medical Hypotheses*, 63(5), 773-777.

Rutter, N., Hodson, A., Irvine-Fynn, T.D.L. and Solås, M.K. (2011). Hydrology and hydrochemistry of a deglaciating high-Arctic catchment, Svalbard. *Journal of Hydrology*, 410(1-2), 39-50.

Santibanez, P.A., McConnell, J.R. and Priscu, J.C. (2016). A flow cytometric method to measure prokaryotic records in ice cores: an example from the West Antarctic Ice Sheet Divide drilling site. *Journal of Glaciology*, 62(234), 655-673.

Schaule, G., Flemming, H.C. and Ridgway, H.F. (1993). Use of 5-Cyano-2,3-Ditolyl Tetrazolium Chloride for Quantifying Planktonic and Sessile Respiring Bacteria in Drinking Water. *Applied and Environmental Microbiology*, 59(11), 3850-3857.

Schuler, T.V., Kohler, J., Elagina, N., Hagen, J.O.M., Hodson, A.J., Jania, J.A., Kääb, A.M., Luks, B., Małecki, J., Moholdt, G., Pohjola, V.A., Sobota, I. and Van Pelt, W.J.J. (2020). Reconciling Svalbard Glacier Mass Balance. *Frontiers in Earth Science*, 8(156), 1-16.

Scott, D., Hood, E. and Nassry, M. (2010). In-stream uptake and retention of C, N and P in a supraglacial stream. *Annals of Glaciology*, 51(56), 80-86.

Sebastián, M. and Gasol, J.M. (2019). Visualization is crucial for understanding microbial processes in the ocean. *Philosophical Transactions B*, 374, 1-7.

Seligman, G. (1949). The Growth of the Glacier Crystal. *Journal of Glaciology*, 1(5), 254-268.

Sheridan, P.P., Miteva, V.I. and Brenchley, J.E. (2003). Phylogenetic Analysis of Anaerobic Psychrophilic Enrichment Cultures Obtained from a Greenland Glacier Ice Core. *Applied and Environmental Microbiology*, 69(4), 2153-2160.

Shibata, A., Goto, Y., Saito, H., Kikuchi, T., Toda, T. and Taguchi, S. (2006). Comparison of SYBR Green I and SYBR Gold stains for enumerating bacteria and viruses by epifluorescence microscopy. *Aquatic Microbial Ecology*, 43, 223-231.

Shiklomanov, I.A. (1998). *World Water Resources*. United Nations Educational, Scientific and Cultural Organization, Paris, 40pp.

Singer, G. A., Fasching, C., Wilhelm, L., Niggemann, J., Steier, P., Dittmar, T. and Battin, T. J. (2012). Biogeochemically diverse organic matter in Alpine glaciers and its downstream fate. *Nature Geoscience*, 5(10), 710-714.

Smith, H.J., Schmit, A., Foster, R., Littman, S., Kuypers, M.M.M. and Foreman, C.M. (2016). Biofilms on glacial surfaces: hotspots for biological activity. *NPJ Biofilms and Microbiomes*, 2(16008), 1-4.

Smith, H.J., Foster, R.A., McKnight, D.M., Lisle, J.T., Littmann, S., Kuypers, M.M.M. and Foreman, C.M. (2017). Microbial formation of labile organic carbon in Antarctic glacial environments. *Nature Geoscience*, 10, 1-6.

Smith, L.C., Chu, V.W., Yang, K., Gleason, C.J., Pitcher, L.H., Rennermalm, A.K., Legleiter, C.J., Behar, A.E., Overstreet, B.T., Moustafa, S.E. and Tedesco, M. (2015). Efficient meltwater drainage through supraglacial streams and rivers on the southwest Greenland Ice Sheet. *Proceedings of the National Academy of Sciences*, 112(4), 1001-1006.

Sobota, I. (2009). The near-surface ice thermal structure of the Waldemarbreen, Svalbard. *Polish Polar Research*, 30(4), 317-338.

Stevens, I.T. (2019). *The Eco-Hydrology of Glacier Surfaces*. PhD Thesis, Aberystwyth University, 192pp.

Stevens, I.T., Irvine-Fynn, T.D.L., Porter, P.R., Cook, J.M., Edwards, A., Smart, M., Moorman, B.J., Hodson, A.J. and Mitchell, A.C. (2018). Near-surface hydraulic conductivity of northern hemisphere glaciers. *Hydrological Processes*, 32, 850-865.

Stevens, I.T., Irvine-Fynn, T.D.L., Edwards, A., Porter, P., Cook, J., Holt, T., Moorman, B., Hodson, A. and Mitchell, A. (2020). Microbial abundance and transport in glacial near-surface meltwater. *EGU General Assembly 2020*, https://doi.org/10.5194/egusphere-egu2020-16998 [Accessed: 6th October 2020].

St Germain, S.L. and Moorman, B.J. (2016). The development of a pulsating supraglacial stream. *Annals of Glaciology*, 57(72), 31-38.

St Germain, S.L. and Moorman, B.J. (2019). Long-term observations of supraglacial streams on an Arctic glacier. *Journal of Glaciology*, 65(254), 900-911.

Stibal, M., Šabacká, M. and Žárský, J. (2012). Biological processes on glacier and ice sheet surfaces. *Nature Geoscience*, 5(11), 771-774.

Stibal, M., Gözdereliler, E., Cameron, K.A., Box, J.E., Stevens, I.T., Gokul, J.K., Schostag, M., Zarsky, J.D., Edwards, A., Irvine-Fynn, T.D.L. and Jacobsen, C.S. (2015). Microbial abundance in surface ice on the Greenland Ice Sheet. *Frontiers in Microbiology*, 6(225), 1-12.

Stibal, M., Bradley, J.A., Edwards, A., Hotaling, S., Zawierucha, K., Rosvold, J., Lutz, S., Cameron, K.A., Mikucki, J.A., Kohler, T.J., Šabacká, M. and Anesio, A.M. (2020). Glacial ecosystems are essential to understanding biodiversity responses to glacier retreat. *Nature Ecology & Evolution*, 4, 686-687.

Takeuchi, N. (2011). Glacial Ecosystems. In: Singh, V.P., Singh, P. and Haritashya, U.K. (Editors) *Encyclopedia of Snow, Ice and Glaciers*. Springer, Berlin, 330-331.

Takeuchi, N., Tanaka, S., Konno, Y., Irvine-Fynn, T.D.L., Rassner, S.M.E. and Edwards, A. (2019). Variations in Phototroph Communities on the Ablating Bare-Ice Surface of Glaciers on Brøggerhalvøya, Svalbard. *Frontiers in Earth Science*, 7(4), 1-10.

Tedstone, A.J., Bamber, J.L., Cook, J.M., Williamson, C.J., Fettweis, X., Hodson, A.J. and Tranter, M. (2017). Dark ice dynamics of the south-west Greenland Ice Sheet. *The Cryosphere*, 11(6), 2491-2506.

Tranter, M., Huybrechts, P., Munhoven, G., Sharp, M.J., Brown, G.H., Jones, I.W., Hodson, A.J., Hodgkins, R. and Wadham, J.L. (2002). Direct effect of ice sheets on terrestrial bicarbonate, sulphate and base cation fluxes during the last glacial cycle: minimal impact on atmospheric CO2 concentrations. *Chemical Geology*, 190, 33-44.

Trivedi, C.B., Lau, G.E., Grasby, S.E., Templeton, A.S. and Spear, J.R. (2018). Low-Temperature Sulfidic-Ice Microbial Communities, Borup Fiord Pass, Canadian High Arctic. *Frontiers in Microbiology*, 9(1622), 1-16.

Turley, C.M. and Hughes, D.J. (1992). Effects of storage on direct estimates of bacterial numbers of preserved seawater samples. *Deep Sea Research Part A. Oceanographic Research Papers*, 39(3-4), 375-394.

Van den Broeke, M. and Giesen, R. (2021). Mass Balance. In: Fowler, A. and Ng, F. (Editors) *Glaciers and Ice Sheets in the Climate System.* Springer, Switzerland, 161-184.

Varliero, G., Holland, A., Barker, G.L.A., Yallop, M.L., Fountain, A.G. and Anesio, A.M. (2021). Glacier clear ice bands indicate englacial channel microbial distribution. *Journal of Glaciology*, 67(265), 811-823.

Wadham, J.L. and Nuttall, A-M. (2002). Multiphase formation of superimposed ice during a mass-balance year at a maritime high-Arctic glacier. *Journal of Glaciology*, 48(163), 545-551.

Wainstein, P., Moorman, B. and Whitehead, K. (2008). Importance of Glacier-Permafrost Interactions in the Preservation of a Proglacial Icing: Fountain Glacier, Bylot Island, Canada. In: Kane, D. L. and Hinkel, K. M. (Editors) *Ninth International Conference on Permafrost*. 1881-1886.

Wainstein, P., Moorman, B. and Whitehead, K. (2010). Hydro-physical conditions of an Arctic proglacial valley, Bylot Island. In: *Proceedings 63rd Canadian Geotechnical Conference & 6th Canadian Permafrost Conference*. Calgary, Alberta, 1525-1532.

Whitehead, K., Moorman, B.J. and Hugenholtz, C.H. (2013). Brief Communication: Low-cost, on-demand aerial photogrammetry for glaciological measurement. *The Cryosphere*, 7, 1879-1884.

Whitman, W.B., Coleman, D.C. and Wiebe, W.J. (1998). Prokaryotes: the unseen majority. *Proceedings of the National Academy of Sciences*, 95(12), 6578-6583.

Williamson, C.J., Anesio, A.M., Cook, J., Tedstone, A., Poniecka, E., Holland, A., Fagan, D., Tranter, M. and Yallop, M.L. (2018). Ice algal bloom development on the surface of the Greenland Ice Sheet. *FEMS Microbiology Ecology*, 94(3), 1-10.

Williamson, C.J., Cook, J., Tedstone, A., Yallop, M., McCutcheon, J., Poniecka, E., Campbell, D., Irvine-Fynn, T.D.L., McQuaid, J., Tranter, M., Perkins, R. and Anesio, A. (2020). Algal photophysiology drives darkening and melt of the Greenland Ice Sheet. *PNAS*, 117(11), 5694-5705.

Wilson, N.J., Flowers, G.E. and Mingo, L. (2013). Comparison of thermal structure and evolution between neighboring subarctic glaciers. *Journal of Geophysical Research: Earth Surface*, 118, 1443-1459.

Yang, K., Smith, L.C., Karlstrom, L., Cooper, M.G., Tedesco, M., Van As, D., Cheng, X., Chen, Z. and Li, M. (2018). A new surface meltwater routing model for use on the Greenland Ice Sheet Surface. *The Cryosphere*, 12, 3791-3811.

APPENDICES

Appendix 1. A scatter graph showing the linear transformation between the events per mL results of the Storglaciären optimised protocol (FSC-H threshold of 40,000) against the events per mL for the initial protocol (FSC-H threshold of 64,000).

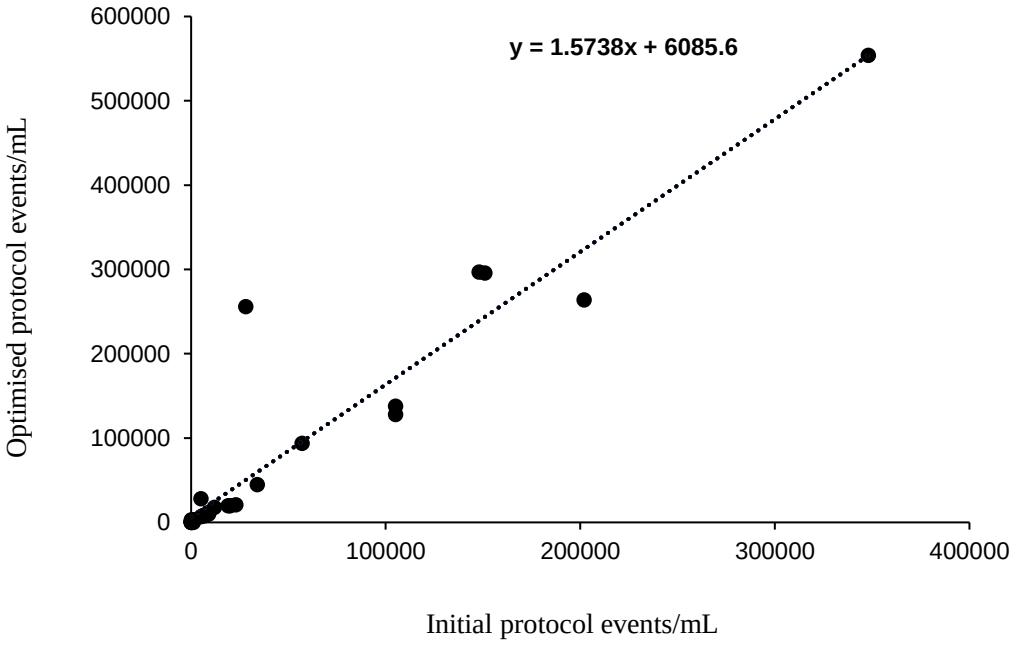

Appendix 2. Scatter plot associations showing the microbial cell abundance against the specific perimeters of such ice crystal for: **(a)** CC; **(b)** FI; **(c)** RI; **(d)** CB, and **(e)** SI. No association was able to be calculated for RI due to only two data points, and so there is an absence of accompanying correlation statistics.

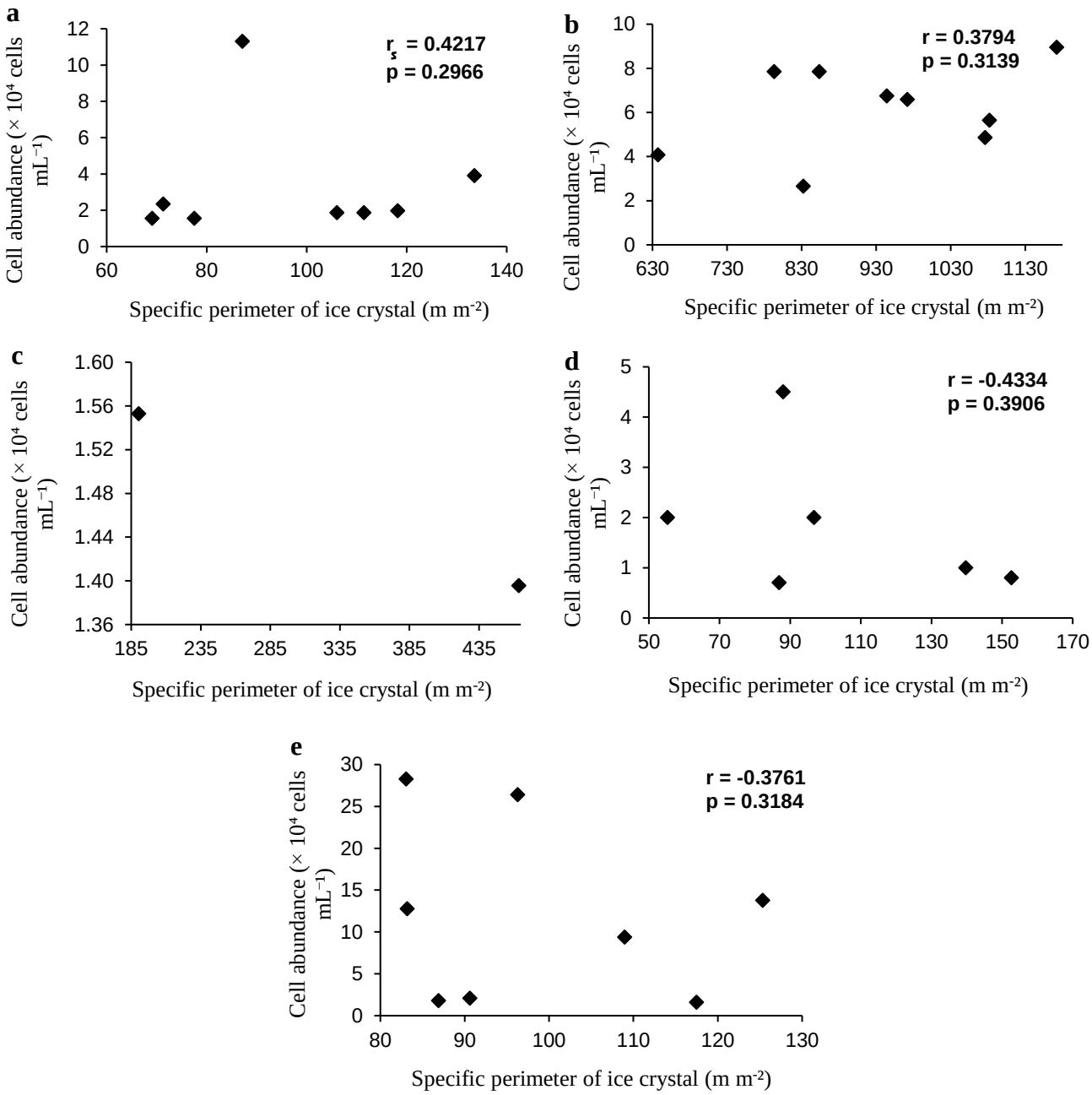

Appendix 3. Regression **s**catter plot used to derive microbial flux for Fountain Glacier supraglacial study stream after Irvine-Fynn et al. (2012) (following Tranter et al., 2002).

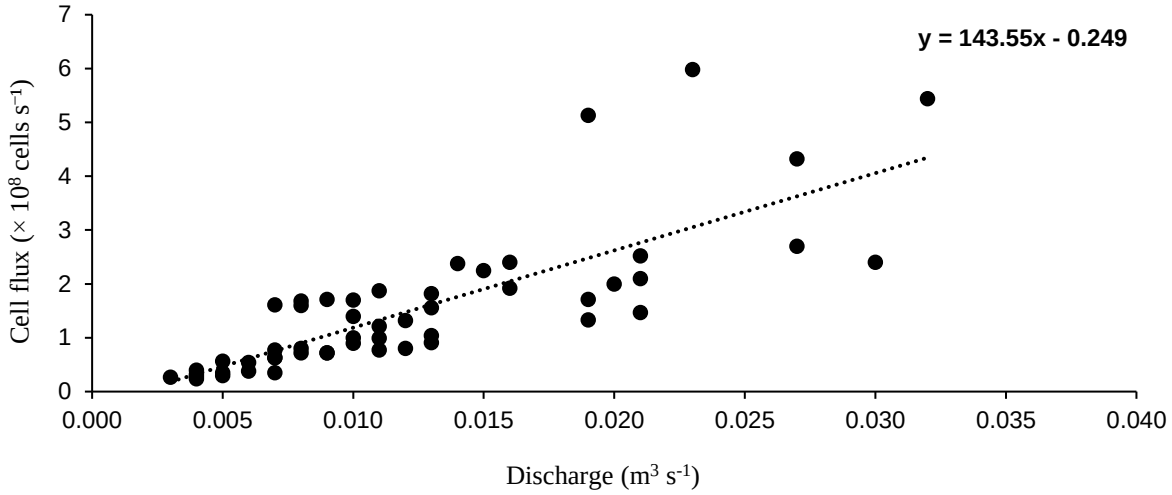

Appendix 4. Regression **s**catter plot used to derive microbial flux for Foxfonna Glacier supraglacial study stream after Irvine-Fynn et al. (2012) (following Tranter et al., 2002).

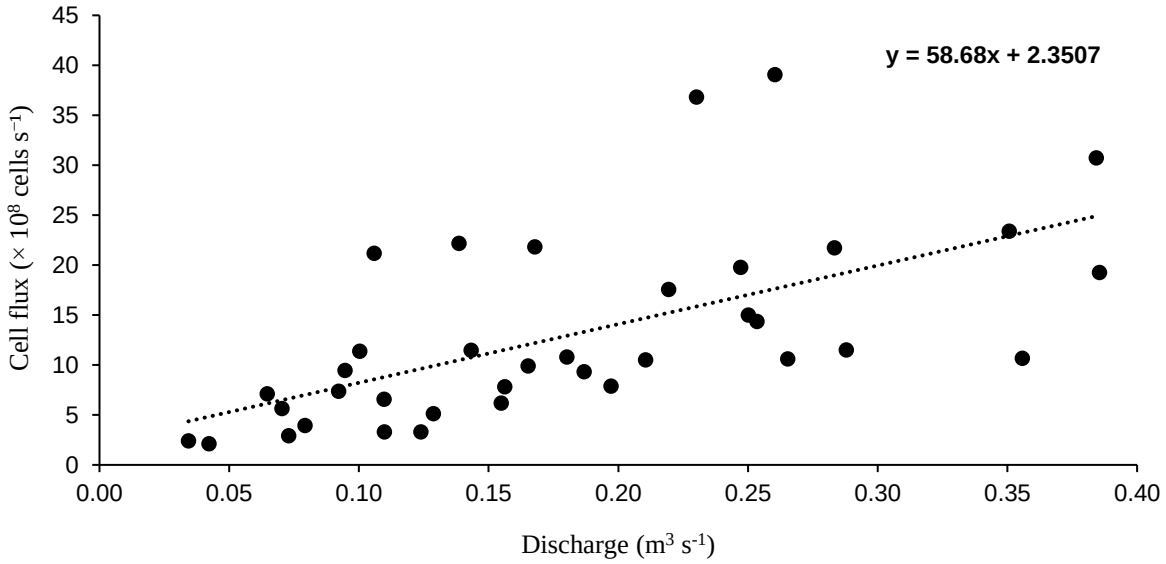

Appendix 5. Regression **s**catter plot used to derive microbial flux for Foxfonna Glacier supraglacial study stream after Irvine-Fynn et al. (2012) (following Tranter et al., 2002), but using the viability dual-stain enumerated total cells.

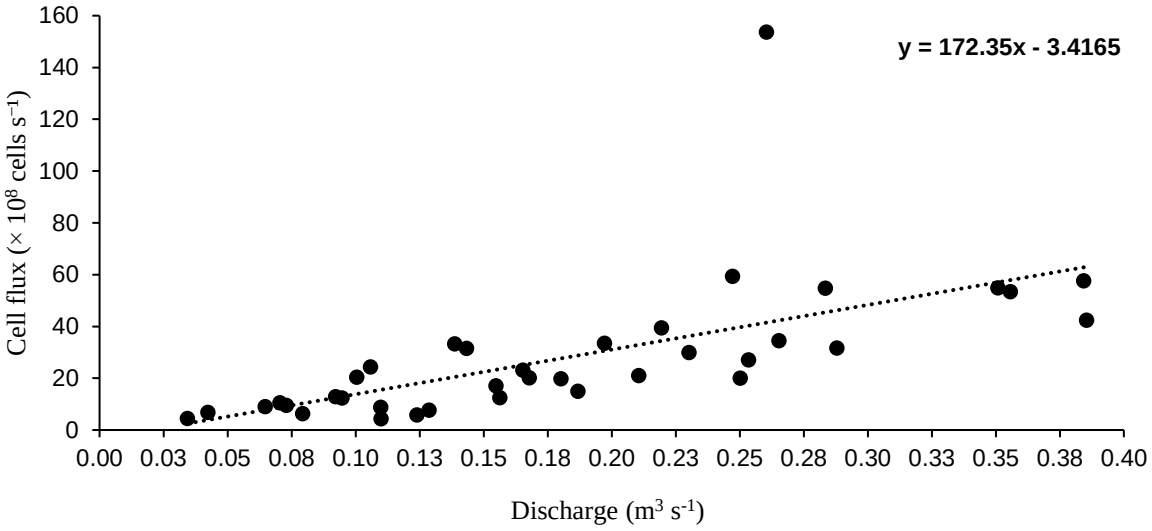

Appendix 6. Regression **s**catter plot used to derive the live microbial flux for Foxfonna Glacier supraglacial study stream after Irvine-Fynn et al. (2012) (following Tranter et al., 2002), from the viability dual-stain analyses.